# MODELLING AND CONTROL OF SATELLITE FORMATIONS

A Dissertation

by

VEERA VENKATA SESHA SAI VADDI

Submitted to the Office of Graduate Studies of
Texas A&M University
in partial fulfillment of the requirements for the degree of

DOCTOR OF PHILOSOPHY

May 2003

Major Subject: Aerospace Engineering

MODELLING AND CONTROL OF SATELLITE FORMATIONS

A Dissertation

by

VEERA VENKATA SESHA SAI VADDI

Submitted to Texas A&M University
in partial fulfillment of the requirements
for the degree of

DOCTOR OF PHILOSOPHY

Approved as to style and content by:

| | |
|---|---|
| Srinivas Rao Vadali<br>(Chair of Committee) | |
| Kyle T. Alfriend<br>(Member) | John L. Junkins<br>(Member) |
| Darbha Swaroop<br>(Member) | Ramesh Talreja<br>(Head of Department) |

May 2003

Major Subject: Aerospace Engineering

## ABSTRACT

Modelling and Control of Satellite Formations. (May 2003)
Veera Venkata Sesha Sai Vaddi, B.Tech., R. E. C. Calicut;
M.S., I. I. Sc Bangalore
Chair of Advisory Committee: Dr. Srinivas R. Vadali

Formation flying is a new paradigm in space mission design, aimed at replacing large satellites with multiple small satellites. Some of the proposed benefits of formation flying satellites are: (i) Reduced mission costs and (ii) Multi mission capabilities, achieved through the reconfiguration of formations. This dissertation addresses the problems of initiatialization, maintenance and reconfiguration of satellite formations in Earth orbits. Achieving the objectives of maintenance and reconfiguration, with the least amount of fuel is the key to the success of the mission. Therefore, understanding and utilizing the dynamics of relative motion, is of significant importance.

The simplest known model for the relative motion between two satellites is described using the Hill-Clohessy-Wiltshire(HCW) equations. The HCW equations offer periodic solutions that are of particular interest to formation flying. However, these solutions may not be realistic. In this dissertation, bounded relative orbit solutions are obtained, for models, more sophisticated than that given by the HCW equations. The effect of the nonlinear terms, eccentricity of the reference orbit, and the oblate Earth perturbation, are analyzed in this dissertation, as a perturbation to the HCW solutions. A methodology is presented to obtain initial conditions for formation establishment that leads to minimal maintenance effort.

A controller is required to stabilize the desired relative orbit solutions in the presence of disturbances and against initial condition errors. The tradeoff between stability and fuel optimality has been analyzed for different controllers. An innovative controller which drives the dynamics of relative motion to control-free natural solutions by matching the periods of the two satellites has been developed under the assumption of spherical Earth. A disturbance accommodating controller which significantly brings down the fuel consumption has been designed and implemented on a full fledged oblate Earth simulation. A formation rotation concept is introduced and implemented to homogenize the fuel consumption among different satellites in a formation.

To achieve the various mission objectives it is necessary for a formation to reconfigure itself periodically. An analytical impulsive control scheme has been developed for this purpose. This control scheme has the distinct advantage of not requiring extensive online optimization and the cost incurred compares well with the cost incurred by the optimal schemes.

To Amma

## ACKNOWLEDGMENTS

I feel the best way to influence a young mind is by leading an exemplary life. My advisors Dr. Srinivas R. Vadali and Dr. Kyle T. Alfriend, did exactly the same. Their commitment, dedication to work, and relentless pursuit of the goal, have often been my source of inspiration. I would first like to thank them both, for all the time they spent with me on my research, and for funding my graduate studies at A&M. I would also like to thank Dr. Junkins, and Dr. Swaroop for serving on my Ph.D. committee, and the education they imparted to me through course work, and otherwise.

Discussions and technical interactions with my colleagues Kamesh, Amit, Puneet, Monish, and Prasenjit have contributed a lot to my own intellectual enhancement. My friends Maruthi Akella, Narayanan Ramakrishnan, Sriram Shankar and Ashutosh Redkar have often been a source of support and encouragement during my doctoral studies. Other than research, my life at TAMU was a pleasant experience due to some good friends. I shall carry with me indelible memories of some of the great times I had with my close friends Anup, Raghavendran, Sangeeta, Hemant, Radhika and Ruchi. I also feel sad for the loss of my great friend Kishore who died in an accident in December 2002. A special thanks goes to Karen Knabe and Andrea Loggins who often helped with the administrative paperwork. My involvement with the starting of the Association for India's Development at TAMU is a proud achievement that I will cherish. It not only gave me a chance to do something for my country but also a chance to meet some committed people like Vinod Srinivasan.

Nothing would have been possible without the love and affection of my mother and

two brothers Phani and Ravi. This dissertation is a tribute to my mother's love and her dedicated efforts towards raising her kids after my father expired. Life took a pleasant turn after I met my wife Lavanya. Her love and patience while I was finishing my dissertation deserves a special mention.

# TABLE OF CONTENTS

CHAPTER Page

# LIST OF FIGURES

FIGURE Page

FIGURE Page

FIGURE Page

# LIST OF TABLES

# CHAPTER I

# INTRODUCTION

Formation flying of satellites is an emerging technology for next generation space systems. The cost of launching a satellite depends on the size of the satellite. It becomes prohibitively expensive to launch large satellites. Formation flying technology aims at creating a "virtual satellite" by a network of co-orbiting small satellites. The virtual satellite thus created, is expected to perform the functions of a large satellite at a much lower cost. Another advantage of formation flying is achieving multi mission capabilities, through the reconfiguration of the formation. Some of the applications of formation flying satellites are space-based radar, ground-based terrestrial laser communication system, Earth surveillance, remote sensing, stellar imaging, and astrometry. Terrestrial Planet Finder(TPF), Laser Interferometer Space Antenna(LISA), Stellar Imager, Planet Imager, TechSat-21, and Earth Observer-1 are some of the proposed formation flying missions. We focus our attention on formations that consist of a central chief satellite, surrounded by multiple deputy satellites. In some formations a central chief satellite may not physically exist. However, an imaginary chief satellite may be assumed, in order to provide a reference point for the formation. The chief satellite could be in a heliocentric orbit, geocentric orbit or the $L_2$ libration point, depending on the application. In this dissertation, we addresses the issues of establishment, maintenance and reconfiguration of formations in Earth orbits.

The relative orbit between the satellites dictates the shape of the formation. A bounded relative orbit between the chief and the deputies is necessary for simulating

---

The journal model is *AIAA Journal of Guidance, Control, and Dynamics.*

the functions of a monolithic satellite. Fuel is a scarce commodity on the spacecraft. Therefore, it is desirable to spend minimum fuel for the purposes of maintenance and reconfiguration of the formations. In the absence of disturbances, formations in naturally occurring relative orbits need zero external controls for maintenance. Hence, a naturally occurring bounded relative orbit is a judicious choice for the shape of a formation. Such natural solutions are explored by modelling and studying the dynamics of spacecraft relative motion.

Modelling the dynamics of relative motion for nearby spacecraft had been of interest for the spacecraft rendezvous problem, as discussed in Refs.1 and 2. Models can be developed with varying levels of sophistication. Drag, oblateness of the Earth and solar radiation are significant perturbations to the two-body problem that may need to be modelled depending on the parameters of a specific formation flying mission. The aerodynamic characteristics of different satellites in a formation are expected to be the same, hence, it is assumed that the differential drag will be negligible. In this dissertation, the oblateness of the Earth is modelled by $J_2$, the first harmonic in the gravitational potential expansion.

Models for spacecraft relative motion can be developed using different choices of relative motion coordinates and reference frames. A geocentric inertial frame of reference and a chief centered local vertical local horizontal (LVLH) frame are the two choices of reference frames. Shown in Fig.(1.1) are the inertial and LVLH reference frames.

The motion along $x, y$, and $z$ will also be referred to as radial, along-track, and out-of-plane motion, respectively.

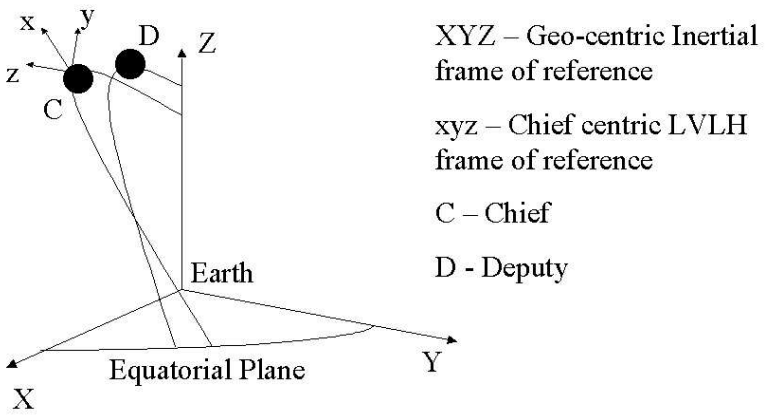


**Fig. 1.1:** Reference frames

The choices for the coordinates are inertial Cartesian coordinates, LVLH Cartesian coordinates and orbital elements. Each choice of coordinates offers certain advantages as will be seen in this dissertation. Inertial Cartesian coordinates, $X, Y$, and $Z$ in Fig.(1.1), are preferable for oblate Earth simulations and are amenable to conversion from orbital elements and vice-versa. LVLH Cartesian coordinates, $x, y$, and $z$ in Fig.(1.1), are the best choice for visualizing the relative orbits. Relative motion models developed using LVLH Cartesian coordinates are also useful for designing feedback controllers and formation flying reference trajectories. The choice of orbital elements as coordinates offers useful insight into the design of bounded relative orbits and their geometry. It is also easier to design impulsive control laws using orbital element models.

## 1.1 Inertial Coordinates

The equations of motion of a satellite in inertial coordinates, under the influence of gravitational effects is given below:

$$\ddot{\mathbf{r}} = -\phi_r \tag{1.1}$$

where, $\mathbf{r} = [X\ Y\ Z]^T$, is the inertial position vector, $\phi$, is the gravitational potential, and $\phi_r$, is its gradient. The gravitational potential and its gradient are :

$$\phi = -\frac{\mu}{r}\left[1 - \frac{J_2}{2}\left(\frac{R_e}{r}\right)^2\left(3\frac{Z^2}{r^2} - 1\right)\right] \tag{1.2}$$

$$\phi_r = \frac{\mu}{r^3}\mathbf{r} + \frac{J_2\mu R_e^2}{2}\left[\frac{6Z}{r^5}\hat{\mathbf{n}} + \left(\frac{3}{r^5} - \frac{15Z^2}{r^7}\right)\mathbf{r}\right] \tag{1.3}$$

where $r = ||\mathbf{r}||$, $\hat{\mathbf{n}}$ is the unit vector in the inertial $Z$ direction, $\mu$ is the gravitational constant, $J_2$ represents the gravitational contribution from the oblate portion of the Earth, and $R_e$ is the radius of the Earth.

As mentioned earlier, inertial coordinates are suitable for simulating the oblate Earth perturbation. Furthermore, initial conditions obtained using orbital elements can be transformed to initial conditions in inertial coordinate space. The relative motion between two satellites can be simulated by integrating two sets of Eqn.(1.1), one for the chief and one for the deputy. The inertial relative displacement and relative velocity vectors, respectively, are defined as follows:

$$\delta\ \mathbf{r} = \mathbf{r_d} - \mathbf{r_c} \tag{1.4}$$

$$\delta\ \mathbf{v} = \mathbf{v_d} - \mathbf{v_c} \tag{1.5}$$

Herein, the subscript,"c" is used to denote the chief. Any variable connected with a deputy is denoted by the subscript,"d". The relative motion between the two satellites

can be transformed to the LVLH frame as follows:

$$x = \frac{\delta\ \mathbf{r}^T \mathbf{r}_c}{r_c} \tag{1.6}$$

$$y = \frac{\delta\ \mathbf{r}^T (\mathbf{H}_c \times \mathbf{r}_c)}{|\mathbf{H}_c \times \mathbf{r}_c|} \tag{1.7}$$

$$z = \frac{\delta\ \mathbf{r}^T \mathbf{H}_c}{H_c} \tag{1.8}$$

where, $\mathbf{H_c} = \mathbf{r_c} \times \mathbf{v_c}$ is the angular momentum. The coordinates, $x, y,$ and $z$ are, respectively, the LVLH Cartesian coordinates of relative motion. The relative velocities in this frame are given below:

$$\dot{x} = \frac{\delta\ \mathbf{v^T r_c} + \delta\ \mathbf{r^T v_c}}{r_c} - \frac{(\delta\ \mathbf{r^T} \mathbf{r}_c)(\ \mathbf{r_c^T} \mathbf{v}_c)}{r_c^3} \tag{1.9}$$

$$\dot{y} = \frac{\delta\ \mathbf{v^T}(\mathbf{H_c} \times \mathbf{r_c}) + \delta\ \mathbf{r^T}(\dot{\mathbf{H}}_\mathbf{c} \times \mathbf{r_c} + \mathbf{H_c} \times \mathbf{v_c})}{|\mathbf{H_c} \times \mathbf{r_c}|} - \frac{\delta\ \mathbf{r^T}(\mathbf{H_c} \times \mathbf{r_c})(\mathbf{H_c} \times \mathbf{r_c})^\mathbf{T}(\dot{\mathbf{H}}_\mathbf{c} \times \mathbf{r_c} + \mathbf{H_c} \times \mathbf{v_c})}{|\mathbf{H_c} \times \mathbf{r_c}|^\mathbf{3}} \tag{1.10}$$

$$\dot{z} = \frac{\delta\ \mathbf{v^T H_c} + \delta\ \mathbf{r^T} \dot{\mathbf{H}}_c}{H_c} - \frac{\delta\ \mathbf{r^T H_c}(\mathbf{H_c^T} \dot{\mathbf{H}}_\mathbf{c})}{H_c^3} \tag{1.11}$$

## 1.2 LVLH Coordinates

Relative orbits of interest for formation flying are described in a rotating frame of reference attached to the chief satellite. Hence, it is desirable to write down the relative motion dynamics in this frame of reference. A brief survey of relative motion models in LVLH coordinates and results thus obtained are given in this section.

Kechichian[3] has derived in LVLH Cartesian coordinates the most comprehensive set of relative motion equations modelling drag and oblate Earth perturbations. Integrating these equations is equivalent to integrating two sets of Eqn.(1.1), one set for the chief and one for the deputy, with equivalent initial conditions. Kechichian's equations constitute a set of twelve nonlinear ordinary differential equations. On the other hand, the Hill-Clohessy-Wiltshire (HCW) equations Eqs.(1.12) are the simplest set of equations in LVLH coordinates. A derivation of the HCW equations is available in Ref.4. They are obtained for a circular chief orbit by making the assumption of and spherical Earth, and linearizing the differential gravity accelerations, and neglecting all other perturbations to the two-body problem. The HCW equations constitute a system of sixth-order constant coefficient linear ordinary differential equations.

$$\begin{aligned} \ddot{x} - 2n\dot{y} - 3n^2 x &= 0 \\ \ddot{y} + 2n\dot{x} &= 0 \\ \ddot{z} + n^2 z &= 0 \end{aligned} \tag{1.12}$$

where $n = \sqrt{\frac{\mu}{a^3}}$ the mean motion of the chief, and $a$ is the semi-major axis of the chief's orbit.

The HCW equations admit bounded periodic solutions given by Eqs.(1.13-1.18) which are suitable for formation flying missions. These solutions, referred to as HCW solutions, are as follows:

$$x = \frac{c_1}{2}\sin(nt + \alpha_0) \tag{1.13}$$

$$y = c_1 \cos(nt + \alpha_0) + c_3 \tag{1.14}$$

$$z = c_2 \sin(nt + \beta_0) \tag{1.15}$$

$$\dot{x} = \frac{c_1}{2} n \cos(nt + \alpha_0) \tag{1.16}$$

$$\dot{y} = -c_1 n \sin(nt + \alpha_0) \tag{1.17}$$

$$\dot{z} = c_2 n \cos(nt + \beta_0) \tag{1.18}$$

where $c_1, c_2, c_3, \alpha_0$ and $\beta_0$ are constants that are determined by initial conditions. These solutions are isolated periodic orbits in an otherwise unstable system. The solutions are obtained by satisfying the following constraint on initial conditions:

$$\dot{y_0} + 2nx_0 = 0 \tag{1.19}$$

Initial conditions which satisfy Eqn.(1.19) will be referred to as HCW initial conditions. The HCW initial conditions are obtained by substituting $t = 0$ in Eqs.(1.13-1.18):

$$x_0 = \frac{c_1}{2} \sin \alpha_0 \tag{1.20}$$

$$y_0 = c_1 \cos \alpha_0 + c_3 \tag{1.21}$$

$$z_0 = c_2 \sin \beta_0 \tag{1.22}$$

$$\dot{x_0} = \frac{c_1}{2} n \cos \alpha_0 \tag{1.23}$$

$$\dot{y_0} = -c_1 n \sin \alpha_0 \tag{1.24}$$

$$\dot{z_0} = c_2 n \cos \beta_0 \tag{1.25}$$

Bounded relative orbits of various shapes and sizes can be obtained by choosing arbitrary values for $c_1, c_2, c_3, \alpha_0$ and $\beta_0$. The relative orbit that is obtained by choosing $c_1 = c_2 = \rho$, $c_3 = 0$ and $\alpha_0 = \beta_0$ is known as the projected circular orbit(PCO),

because the relative orbit is circular when projected onto the local horizontal plane, i.e., the $y-z$ plane:

$$x = \frac{\rho}{2}\sin(nt+\alpha_0) \tag{1.26}$$

$$y = \rho\cos(nt+\alpha_0) \tag{1.27}$$

$$z = \rho\sin(nt+\alpha_0) \tag{1.28}$$

Therefore,

$$y^2 + z^2 = \rho^2 \tag{1.29}$$

which represents a circle in the $y-z$ plane with radius $\rho$. $\alpha_0$ characterizes the position of the deputies along the circumference of the circle. $\rho$ is a measure of the size of the formation and will be referred to as disc size throughout this dissertation. The PCO is an attractive option for formation flying. It can serve as an antenna for space based radar.

There exists another circular orbit of interest for the choice of $c_1 = \rho, c_2 = \frac{\sqrt{3}}{2}\rho, c_3 = 0$ and $\alpha_0 = \beta_0$. This results in a circle(section of a sphere through the center) in the three dimensional space.

$$x = \frac{\rho}{2}\sin(nt+\alpha_0) \tag{1.30}$$

$$y = \rho\cos(nt+\alpha_0) \tag{1.31}$$

$$z = \frac{\sqrt{3}}{2}\rho\sin(nt+\alpha_0) \tag{1.32}$$

which results in

$$x^2 + y^2 + z^2 = \rho^2 \tag{1.33}$$

a circle in the three dimensional space. This relative orbit is known as the general circular orbit(GCO). The GCO is also an useful option for formation flying and can be used to simulate a large satellite with a circular geometry.

Choosing $c_1 = 0, c_2 = 0$ and $c_3 = d$ yields $x = 0, y = d, z = 0$ which results in constant along-track separation. This is known as the leader follower configuration(LFC) because, the deputies either lead or follow the chief by a constant distance in the along-track direction. A long slender satellite can be simulated by the straight line formation that results from the LFC.

The initial conditions corresponding to the projected circular orbit, general circular orbit and the leader follower configuration will be referred to as PCO initial conditions, GCO initial conditions and LFC initial conditions, respectively. It should be noted that the projected circular orbit, general circular orbit and the leader follower configuration, are three particular cases of the HCW solutions resulting from the PCO, GCO and LFC initial conditions respectively. As these particular solutions are of special interest to formation flying, they are chosen for further analysis and simulations in this dissertation.

The assumptions leading to the HCW equations are highly restrictive. Kechichian's equations, when integrated with HCW initial conditions, result in unbounded solutions for large formations, and elliptic chief orbits. Therefore, it is necessary to incorporate the effects of nonlinear differential gravity accelerations, eccentricity of the chief orbit and $J_2$ in the search for bounded relative orbit solutions. For the sake of brevity, the above mentioned effects will be referred to as simply nonlinearity, eccentricity and $J_2$ respectively, for the rest of the dissertation. Unbounded solutions

resulting from HCW initial conditions on models more realistic than HCW equations, will be referred to as "the breakdown of HCW solutions" in this dissertation. We seek to obtain bounded relative orbit solutions, that are close to HCW solutions, on more realistic models. In that pursuit, a next level of sophistication to HCW equations is obtained by modelling the effect of eccentricity. The resulting equations, while retaining all other assumptions of the HCW equations, are given in Eqn.(1.34).

$$\begin{aligned}
&\ddot{x} - 2\dot{\theta}\dot{y} - \ddot{\theta}y - \dot{\theta}^2 x - 2\frac{\mu}{{r_c}^3}x = 0 \\
&\ddot{y} + 2\dot{\theta}\dot{x} + \ddot{\theta}x - \dot{\theta}^2 y + \frac{\mu}{{r_c}^3}y = 0 \\
&\ddot{z} + \frac{\mu}{{r_c}^3}z = 0 \\
&\ddot{r}_c = r_c\dot{\theta}^2 - \frac{\mu}{r_c^2} \\
&\ddot{\theta} = -\frac{2\dot{r}_c\dot{\theta}}{r_c}
\end{aligned} \tag{1.34}$$

where $r_c$ is the radius of the chief from the center of the earth and $\theta$ is the latitude angle of the chief satellite.

Solutions to these equations are more realistic than the HCW equations. Several researchers have addressed the problem of solving these equations using different approaches in Refs. 5–7. However, bounded solutions were not investigated. A comprehensive compilation of all the work done in solving these equations is available in Ref.8. Tschauner and Hempel[9] derived simpler version of Eqs.(1.34) by using non-dimensional relative motion coordinates and using true anomaly as the independent variable. Carter[10] derived an analytical solution to these equations in terms of arbitrary constants. Inalhan et al.[11] derived a criterion for bounded solutions using Carter's analytical solution. The integration constants have been further related to

the relative motion initial conditions. Melton[12] derived an approximate time-explicit, series solution in powers of eccentricity, to Eqs.(1.34). Though it is the only solution explicit in time and initial conditions, it has the problem of unexplained secular terms appearing in the radial direction. The effect of nonlinearities were studied in Refs. 1, 2, 13, 14. In this dissertation, we seek the following desirable features for representing bounded relative orbit solutions, that are relevant to the formation flying problem:

- The solution should be analytical and yield the desired accuracy.
- The solution should be time-explicit so that secular terms be easily identified. Time-explicit solution also obviates the need to solving Kepler's equation.
- The solution should be explicit in initial conditions. This helps choosing initial conditions appropriate for a desired relative orbit.
- The solution should be in the actual LVLH Cartesian coordinates, instead of non-dimensional coordinates.

Most of the earlier research, discussed in the previous paragraph, lacks one or more of the above mentioned features.

Few researchers, other than Kechichian,[3] have modelled the effect of $J_2$ on relative motion models using LVLH coordinates. Though Kechichian's equations model the all the relevant perturbations, exactly, they are very complicated and not amenable to analysis. Schweighart and Sedwick[15] developed a linearized $J_2$ model. The model consists of a set of constant coefficient, linear differential equations similar to HCW equations. This model is restricted to low eccentricity orbits and is specific to certain set of initial conditions. Vadali et al.[16] have also derived a modified set of Hill's

equations using a mean, precessing, circular ghost orbit as a reference, in the presence of $J_2$. Vadali's model qualitatively captures the effect of $J_2$ on the out-of-plane dynamics, but the effect of $J_2$ on the in-plane dynamics is not completely addressed. A simplified set of equations modelling the effect of $J_2$ for all initial conditions and elliptic chief orbits, remains elusive, till date.

### 1.3 Orbital Elements

Formation flying problems can also be modelled using the orbital element differences between two satellites. In this section, a brief description of orbital elements, orbital element models, and a survey of previous results obtained using orbital elements, are presented.

The classical set of orbital elements for a two body problem are semi-major axis($a$), eccentricity($e$), inclination($i$), longitude of ascending node($\Omega$), argument of perigee($\omega$) and the mean anomaly($M$). In the absence of $J_2$, the first five of these elements are constant and the mean anomaly varies linearly with time. Gauss's equations model the influence of external controls on orbital elements. These equations are given below:

$$\frac{di}{dt} = \frac{r\cos\theta}{h}u_h \tag{1.35}$$

$$\frac{d\Omega}{dt} = \frac{rsin\theta}{h\sin i}u_h \tag{1.36}$$

$$\frac{da}{dt} = \frac{2a^2}{h}(e\sin f u_r + \frac{p}{r}u_t) \tag{1.37}$$

$$\frac{de}{dt} = \frac{1}{h}(p \sin f u_r + [(p+r)\cos f + re]u_t) \tag{1.38}$$

$$\frac{d\omega}{dt} = \frac{1}{he}[-p\cos f u_r + (p+r)\sin f u_t] - \frac{r\sin\theta\cos i}{h\sin i}u_h \tag{1.39}$$

$$\frac{dM}{dt} = n + \frac{\eta}{he}[(p\cos f - 2re)u_r - (p+r)\sin f u_t] \tag{1.40}$$

where $p = a(1-e^2)$, is the semi-latus rectum, $\eta = \sqrt{1-e^2}$, $r = \frac{p}{1+e\cos f}$, is the radius of the spacecraft from the center of the earth, $f$ is the true anomaly, $h = \sqrt{\mu p}$ is the angular momentum, $u_r, u_t$ and $u_h$ are the external accelerations in the radial, tangential, and out- of-plane directions, respectively. It can be clearly seen from the above equations that the first five orbital elements are constant when $u_r = 0, u_t = 0$ and $u_h = 0$.

The orbital elements are no longer constant in the presence of $J_2$. $J_2$ introduces perturbation accelerations[3] through $u_r, u_t$ and $u_h$. A new set of orbital elements can be defined by averaging out the short and long period oscillations due to these perturbations. These elements are known as mean elements, in contrast to osculating elements which contain the short and long period oscillations. The mean semi-major axis, mean eccentricity, and mean inclination are constant. The other three mean elements vary linearly with time, at rates that are functions of mean semi-major axis, mean eccentricity and mean inclination only. The osculating elements are obtained by converting the inertial position and velocity at each instant to orbital elements. The mean elements are then extracted from them using Brouwer's theory.[17]

In the absence of any perturbations, two satellites in Keplerian orbits, can have

bounded relative motion only when they have the same period. The period of a satellite depends only on the semi-major axis, hence it is essential that $\delta a = 0$. In the presence of $J_2$, this condition is no more valid. Schaub and Alfriend[18] used mean elements to derive conditions for $J_2$ invariant orbits. The conditions are expressed in terms of mean element differences. Hence, it is useful to map orbital element differences to relative motion Cartesian coordinates, in a LVLH frame of reference. Alfriend et al.[19] used the geometry of the orbits to obtain the following transformation:

$$\mathbf{X} = \mathbf{A}(\mathbf{e})\delta\mathbf{e} \tag{1.41}$$

where $\mathbf{X} = [x\ y\ z\ \dot{x}\ \dot{y}\ \dot{z}]$ is the relative motion coordinate vector, $\mathbf{e} = [a\ \theta\ i\ q_1\ q_2\ \Omega]$ is the orbital element vector, and $q_1 = e\cos\omega$, and $q_2 = e\sin\omega$. The following geometric relations are found to be useful in deriving the above transformation:

$$x \approx \delta R \tag{1.42}$$

$$y \approx R_c(\delta\theta + \delta\Omega\cos i_c) \tag{1.43}$$

$$z \approx R_c(-\cos\theta_c \sin i_c \delta\Omega + \sin i_c \delta i) \tag{1.44}$$

where $R_c$ is the radius of the chief satellite from the center of the earth, $\theta_c$ is the latitude angle of the chief, $i_c$ is the inclination and $\Omega$ the longitude of the ascending node. Gim and Alfriend[20] obtained a state transition matrix solution to the linearized relative motion dynamics in the presence of $J_2$, starting with the above transformation. Alfriend et al.[21] have characterized different relative orbits suitable for formation flying, in terms of orbital element differences. Vadali[22] has obtained an analytical solution for relative motion of satellites by using a unit sphere for the description of motion. The solution is written in terms of mean elements, and their differences

using a geometric approach. The resulting solution is very accurate and can be used for faster propagation of relative orbits, in contrast to numerical integration of the exact differential equations.

## 1.4 Control

A control scheme is required to stabilize the formation in the presence of disturbances and initial condition errors. Control algorithms are also necessary, for establishing and reconfiguring formations. Continuous time control is more suitable for tracking the desired relative orbits, that may or may not be natural solutions to the relative motion dynamics. Continuous time control seeks to establish zero tracking errors at all times. On the other hand impulsive control can only keep errors within a threshold. Traditionally, impulsive control has been found to be more suitable for orbit corrections, and is done on a periodic basis.

### *1.4.1 Continuous Control*

Schaub and Alfriend[23] developed feedback control laws using Cartesian coordinates as well as orbital elements. Yedavalli and Sparks[24] used a theoretical framework called 'ultimate boundedness analysis of switched systems'. In their work they use HCW equations and keep the errors bounded within a threshold ellipsoid. Starin et al.[25] developed a LQR with no radial axis inputs. Simulations from their work show that by not using radial thrusting the fuel consumption for maintenance can be reduced. Mitchell and Richardson[26] provide an active nonlinear controller which retains the relative motion dynamics close to invariant manifolds defined through various system Hamiltonians. The application of this work is restricted to circular orbit and spherical Earth assumption scenarios. de Queiroz et al.[27] developed a Lyapunov based

nonlinear adaptive control law. The control law adapts for varying spacecraft masses, disturbances and gravity forces. Nonlinearities and disturbances are explicitly cancelled in their control law and the vital issue of optimality is not addressed. Naasz et al.[28] compare the performance of LQR and optimal controllers. Middour[29] developed a Kalman filter to estimate the initial conditions and mean motion parameters of the HCW equations in order to compute the average along track separation and drift between two neighboring satellites. Fumin and Krishnaprasad[30] developed asymptotically stable control laws in the absence of $J_2$, by defining a Lyapunov function in the space of the angular momentum vector and the Laplace vector. In their work, both the satellites in a formation are controlled and steady state dynamics is forced to naturally occurring solutions that need zero steady-state external controls. Vadali et al.[31] have obtained control laws by projecting the relative motion on a unit sphere and expressing the inter satellite range vector in terms of Euler parameters.

### *1.4.2 Impulsive Control*

Orbital element models are more suitable for designing impulsive control laws. Gauss's equations can be used to relate the magnitude of the impulses to the corresponding orbital element differences created. Schaub and Alfriend[32] developed an analytical, impulsive, feedback control law for establishing a desired set of mean element differences. In this dissertation, an improved version of the same, will be developed, for establishing and reconfiguring formations. Vadali et al.[33] have also dealt with impulsive orbit correction schemes in the presence of $J_2$. A numerical approach is used in their work, for solving the nonlinear optimization problem that results from the maintenance problem. It should be noted that numerical optimization techniques may not be suitable for online implementation, as they are not always guaranteed to

converge. Ahn and Spencer[34] studied the optimal reconfiguration of a formation flying satellite constellation following the failure of a constellation member, using impulsive control. Again, numerical optimization techniques were used in their work. Tillerson et al.[35] present fuel and time optimal control algorithms using linear and integer programming techniques, for formation reconfiguration, using linearized equations of relative motion dynamics. Since, the methodology is numerical in nature, not much insight is obtained into the solution. It should be noted that all the impulsive control laws discussed above, other than that of Tillerson et al., use Gauss's equations for designing the impulse components.

A globally optimal, analytical, impulsive control scheme, suitable for the purposes of maintenance and reconfiguration, still remains to be developed.

### 1.5 Goals

The goals of this dissertation are to analyze the following issues of importance to formation flying:

- Perturbations - In this dissertation we study the effect of the three most significant perturbations to the solutions of the HCW equations. They are (i) nonlinearity of the differential gravity terms (ii) eccentricity of the chief's orbit and (iii) oblateness of the Earth.

- Initiation - Naturally occurring relative motion trajectories are the most economical ones to maintain. Initial conditions that result in bounded relative orbit solutions, for more realistic models than the HCW equations, will be explored in this dissertation.

- Maintenance - The tradeoff between stability and optimality of different continuous time control laws is studied in the context of the formation flying maintenance problem.

- Reconfiguration - This dissertation seeks to develop analytical reconfiguration schemes that are easy to implement and incur control costs that are close to the corresponding costs incurred by the optimal solutions obtained by numerical optimization.

Given below is a brief description of each chapter in this dissertation.

### 1.6 Nonlinearity and Eccentricity Perturbations

In this chapter, we first review various LVLH Cartesian coordinate models of relative motion dynamics in the absence of $J_2$. The effect of nonlinearity and eccentricity on the HCW solutions is studied using perturbation methods. Initial conditions that minimize the secular growth in the along-track direction, are obtained in LVLH Cartesian coordinates. A time-explicit bounded relative orbit representation is also obtained. LVLH Cartesian coordinates and models will be used for analysis and simulation throughout this chapter.

### 1.7 Linear and Nonlinear Controllers for Formation Flying

In this chapter, we analyze different control schemes for formation maintenance in the absence of $J_2$. LVLH coordinates and models will be used for analysis and simulation throughout this chapter. The objective is to devise control strategies that can stabilize large formations optimally. Three types of controllers will be studied in this

chapter: (i) Lyapunov stabilized controller, (ii) LQR controllers, and (iii) Period-matching controllers. The Lyapunov and LQR controllers are tracking controllers that are designed to track a desired relative orbit. The period-matching controller exploits the existence of naturally occurring bounded solutions to the relative motion dynamics. Bounded relative orbits that require zero steady state controls can be generated using the period-matching controller.

### 1.8 $J_2$, Modelling and Control

In this chapter we analyze the $J_2$ perturbation. Relative orbits are modelled using mean elements and the geometry of the orbits. Initial conditions that minimize the secular growth in the along-track direction, are obtained using the geometric model. An intelligent control concept that maintains equal, average fuel consumption for each satellite, is presented. The concept is implemented using a novel, disturbance accommodating control design process. Inertial coordinate models are used for numerical simulations.

### 1.9 Formation Establishment and Reconfiguration

In this chapter we address the problems of optimal formation establishment and reconfiguration. Formations are characterized in terms of orbital element element differences. Gauss's equations are used to design a sub-optimal, analytical, impulsive control scheme for establishing the desired orbital element differences. The control scheme is validated by simulations conducted using the inertial coordinate models.

# CHAPTER II

# NONLINEARITY AND ECCENTRICITY PERTUBATIONS

## 2.1 Abstract

In this chapter we study the equations of relative motion dynamics in the absence of $J_2$. The Hill-Clohessy-Wiltshire equations describe the relative motion of a satellite with respect to another in a circular reference orbit. Initial conditions that generate periodic solutions to these equations have to be corrected in order to obtain bounded solutions in the presence of nonlinearity of the differential gravitational acceleration model and eccentricity of the reference orbit. The corrections to the initial conditions due to quadratic terms in the differential gravitational acceleration for circular reference orbits are established first by using a perturbation approach. These corrections are related to the period matching constraint required for bounded relative motion. Next, a solution and bounded relative orbit criterion are obtained for the linearized problem, with the chief in an eccentric orbit. The two solutions obtained are combined to produce an asymptotic solution for the quadratic, eccentricity problem. The effects of nonlinearity and eccentricity on the relative orbits are characterized as functions of their initial position in the formation.

## 2.2 Introduction

The problem of relative motion dynamics of satellites has been of interest since the 1960's. Much of the work has been performed in the context of the rendezvous problem. Accurate modeling of the relative motion dynamics for initial conditions close to the target is important for the rendezvous problem. Formation flying requires bounded relative motion. The solutions of interest are therefore restricted to

a certain set of initial conditions that lead to bounded relative motion. The Hill-Clohessy-Wiltshire (HCW) equations that model the relative motion dynamics under the assumption of a circular reference orbit, spherical Earth, and linearized differential gravitational acceleration, admit periodic solutions that are of interest for formation flying . Nonlinearity of the differential gravitational acceleration, eccentricity of the reference orbit, and the Earth's oblateness are the three most important perturbations that breakdown the periodic HCW solutions.

The developments in this chapter draw upon several previous studies. Melton[12] developed a state transition matrix solution for the linearized relative motion dynamics by incorporating the effect of eccentricity. Inalhan et al.[11] obtained the condition for bounded relative orbit solutions to the linearized problem with non-zero eccentricity. Alfriend et al.[19] used a geometric approach to map relative motion coordinates to orbital element differences.

In this chapter, we first review various models of relative motion dynamics. Nonlinearity and eccentricity are identified as the perturbations which breakdown the desired HCW solutions. The effects of these perturbations are first studied independently. Accordingly, in the next section we present a perturbation solution to the problem with nonlinearity and without eccentricity. The perturbation solution is used to generate a correction to the HCW initial conditions. This correction is also related to the period matching requirement for bounded relative motion between two satellites. Next, we study the linear relative motion model in the presence of eccentricity of the reference orbit. Conditions for bounded solutions developed in Ref.11 are used to generate another correction to HCW initial conditions. Melton's state transition matrix solution is utilized to obtain a time-explicit representation to the bounded

solutions of the linearized relative motion problem with eccentricity. A solution to the same problem is also available in Ref.11 but as a function of true anomaly rather than time. Melton's state transition matrix involves a series expansion in powers of the eccentricity. Hence, its accuracy is determined by the order of the highest power retained in the series solution. Melton's solution, derived until second order, has been extended to third order. The solution obtained has been further tailored to represent bounded relative orbits. This process leads to another correction to the HCW initial conditions. The two corrections obtained independently are finally combined to produce bounded relative orbit solutions to the nonlinear problem with non-zero eccentricity.

### 2.3 Relative Motion Dynamics

The relative motion dynamics for an eccentric reference orbit is modelled by the following set of nonlinear differential equations:

$$\begin{aligned}
&\ddot{x} - 2\dot{\theta}\dot{y} - \ddot{\theta}y - \dot{\theta}^2 x = -\frac{\mu(r_c+x)}{[(r_c+x)^2+y^2+z^2]^{\frac{3}{2}}} + \frac{\mu}{r_c^2} \\
&\ddot{y} + 2\dot{\theta}\dot{x} + \ddot{\theta}x - \dot{\theta}^2 y = -\frac{\mu y}{[(r_c+x)^2+y^2+z^2]^{\frac{3}{2}}} \\
&\ddot{z} = -\frac{\mu z}{[(r_c+x)^2+y^2+z^2]^{\frac{3}{2}}} \\
&\ddot{r}_c = r_c\dot{\theta}^2 - \frac{\mu}{r_c^2} \\
&\ddot{\theta} = -\frac{2\dot{r}_c\dot{\theta}}{r_c}
\end{aligned} \tag{2.1}$$

where $x$, $y$, $z$ are the relative motion co-ordinates of the deputy w. r. t the chief in the LVLH coordinate system, $r_c$ refers to the scalar radius of the chief from the center of the Earth,$\theta$ refers to the latitude angle of the chief, and$\mu$ is the gravitational parameter.

The system of equations presented above involves ten states and the full-fledged effects of both nonlinearity and eccentricity are accounted for. The effects of eccentricity of the reference orbit that influences the relative motion dynamics of the deputy are captured by the augmented fourth order dynamics of the chief. This model is referred to as the"true model" and the simulations conducted on this model are referred to as the"complete nonlinear simulations".

The relative motion equations for a circular reference orbit, which are also known as HCW equations, are given below:

$$\begin{aligned} \ddot{x} - 2n\dot{y} - 3n^2 x &= 0 \\ \ddot{y} + 2n\dot{x} &= 0 \\ \ddot{z} + n^2 z &= 0 \end{aligned} \tag{2.2}$$

where $n = \sqrt{\frac{\mu}{a_c^3}}$ and $a_c$ is the semi-major axis of the chief.

While Eqs.(2.1) are closest to reality, Eqs.(2.2) are the most amenable to analysis. But the HCW equations are based upon two approximations: (i) Linearization of the differential gravitational acceleration and (ii) Assumption of a circular reference orbit. These assumptions are found to be valid for small formations($\rho < 1$km) and values of eccentricity of the chief less than $1e-5$. But the desirable HCW solutions are not realizable in the complete nonlinear simulations for large formations and for higher eccentricity values of the chief's orbit. Shown in Figures (2.1) and (2.2) are the relative orbits obtained by integrating Eqs.(2.1) with the PCO initial conditions for 20 orbits, for a formation size of 10km and an eccentricity value of $e = 0.005$.

The objective in this chapter is to study the effects of nonlinearity and eccentricity

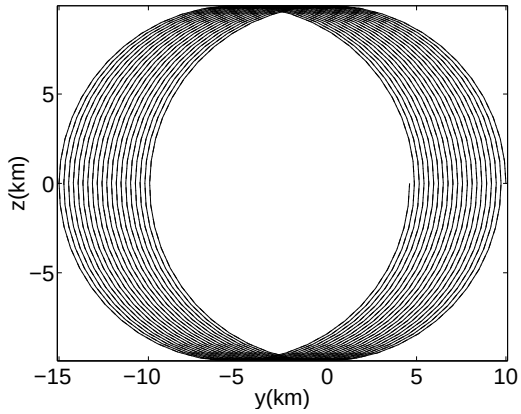


**Fig. 2.1:** Breakdown of projected circular orbit in complete nonlinear simulation, for $\alpha_0 = 0^o, \rho = 10$km and $e = 0.005$

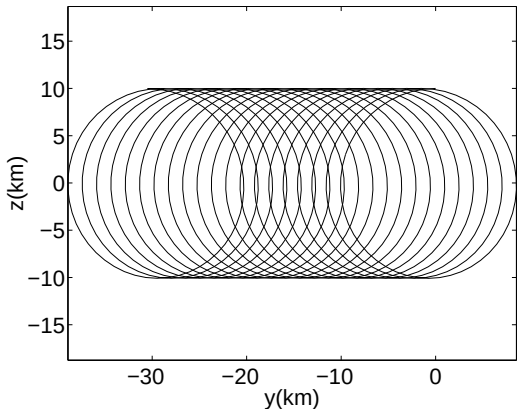


**Fig. 2.2:** Breakdown of projected circular orbit in complete nonlinear simulation, for $\alpha_0 = 90^o, \rho = 10$km and $e = 0.005$

perturbations on the HCW equations and determine approximate solutions to the complete nonlinear problem that are close to the HCW solutions. A primary requirement for such a solution is that it be bounded. Exciting those solutions that are bounded and close to the HCW solutions, will be beneficial since natural force-free solutions are the most economical to maintain. Every solution is characterized by an initial condition. Therefore, we seek to find those initial conditions that lead to bounded solutions, close to the HCW solutions.

A model that includes quadratic terms in the differential gravity field expansion is shown below. This model, in terms of accuracy, lies between the true model and the linear model (HCW equations).

$$
\begin{aligned}
&\ddot{x} - 2\dot{\theta}\dot{y} - \ddot{\theta}y - \dot{\theta}^2 x - \tfrac{2\mu x}{r_c^3} = \left(\tfrac{3\mu}{a^4}\right)\left[\tfrac{y^2}{2} + \tfrac{z^2}{2} - x^2\right] \\
&\ddot{y} + 2\dot{\theta}\dot{x} + \ddot{\theta}x - \dot{\theta}^2 y + \tfrac{\mu y}{r_c^3} = \left(\tfrac{3\mu}{a^4}\right) xy \\
&\ddot{z} + \tfrac{\mu z}{r_c^3} = \left(\tfrac{3\mu}{a^4}\right) xz \\
&\ddot{r}_c = r_c\dot{\theta}^2 - \tfrac{\mu}{r_c^2} \\
&\ddot{\theta} = -\tfrac{2\dot{r}_c\dot{\theta}}{r_c}
\end{aligned}
\tag{2.3}
$$

The analytical results presented in this paper are based on the above model, but the solutions are evaluated on the true model.

## 2.4 Nonlinearity Without Eccentricity

In this section, we study the effect of nonlinearity on relative motion dynamics for a circular reference orbit. The governing differential equations are given below:

$$
\begin{aligned}
&\ddot{x} - 2n\dot{y} - n^2 x = \tfrac{-\mu(a+x)}{[(a+x)^2+y^2+z^2]^{\frac{3}{2}}} + \tfrac{\mu}{a^2} \\
&\ddot{y} + 2n\dot{x} + n^2 x = \tfrac{-\mu y}{[(a+x)^2+y^2+z^2]^{\frac{3}{2}}} \\
&\ddot{z} = \tfrac{-\mu z}{[(a+x)^2+y^2+z^2]^{\frac{3}{2}}}
\end{aligned}
\tag{2.4}
$$

where $a$ is the semi-major axis of the chief and $n = \sqrt{\frac{\mu}{a^3}}$is the mean motion of the chief. A Taylor's series expansion of the RHS of Eqs.(2.4), retaining quadratic terms, leads to the following model:

$$
\begin{aligned}
&\ddot{x} - 2n\dot{y} - 3n^2 x = \left(\tfrac{3\mu}{a^4}\right)\left[\tfrac{y^2}{2} + \tfrac{z^2}{2} - x^2\right] \\
&\ddot{y} + 2n\dot{x} = \left(\tfrac{3\mu}{a^4}\right) xy \\
&\ddot{z} + n^2 z = \left(\tfrac{3\mu}{a^4}\right) xz
\end{aligned}
\tag{2.5}
$$

The above model can be considered as perturbed HCW equations with $\varepsilon = \frac{3\mu}{a^4}$, being the perturbation parameter.

Let $x_h$, $y_h$, and $z_h$be the solutions to the HCW equations, the unperturbed problem. We assume the solution to Eqs.(2.5) to be of the following form:

$$\begin{aligned} x = x_h + \varepsilon x_p \Rightarrow \dot{x} = \dot{x}_h + \varepsilon \dot{x}_p \Rightarrow \ddot{x} = \ddot{x}_h + \varepsilon \ddot{x}_p \\ y = y_h + \varepsilon y_1 \Rightarrow \dot{y} = \dot{y}_h + \varepsilon \dot{y}_p \Rightarrow \ddot{y} = \ddot{y}_h + \varepsilon \ddot{y}_p \\ z = z_h + \varepsilon z_p \Rightarrow \dot{z} = \dot{z}_h + \varepsilon \dot{z}_p \Rightarrow \ddot{z} = \ddot{z}_h + \varepsilon \ddot{z}_p \end{aligned} \tag{2.6}$$

The subscript $h$ in the above equations refers to the solutions to the HCW equations and the subscript $p$ refers to the perturbation. The variables with the subscript $p$ are also referred to as the perturbation variables.

The HCW state vector and its initial value are represented as shown below:

$$\begin{aligned} \mathbf{X_h}(t) &= [x_h(t)\ y_h(t)\ z_h(t)\ \dot{x}_h(t)\ \dot{y}_h(t)\ \dot{z}_h(t)]^T \\ \mathbf{X_h}(0) &= [x_h(0)\ y_h(0)\ z_h(0)\ \dot{x}_h(0)\ \dot{y}_h(0)\ \dot{z}_h(0)]^T \end{aligned} \tag{2.7}$$

The unperturbed solution, linear solution, as well as the HCW solution are completely equivalent in the present context. We choose the HCW solution as shown in the previous chapter as $\mathbf{X}_h(t)$:

$$\begin{aligned} x_h(t) &= \tfrac{c_1}{2}\sin(nt + \alpha_0) \\ y_h(t) &= c_1 \cos(nt + \alpha_0) + c_3 \\ z_h(t) &= c_2 \sin(nt + \beta_0) \\ \dot{x}_h(t) &= \tfrac{c_1}{2} n \cos(nt + \alpha_0) \\ \dot{y}_h(t) &= -c_1 n \sin(nt + \alpha_0) \\ \dot{z}_h(t) &= c_2 n \cos(nt + \beta_0) \end{aligned} \tag{2.8}$$

The corresponding HCW initial conditions are:

$$
\begin{aligned}
x_h(0) &= \tfrac{c_1}{2}\sin\alpha_0 \\
y_h(0) &= c_1\cos\alpha_0 + c_3 \\
z_h(0) &= c_2\sin\beta_0 \\
\dot{x_h}(0) &= \tfrac{c_1}{2}n\cos\alpha_0 \\
\dot{y_h}(0) &= -c_1 n\sin\alpha_0 \\
\dot{z_h}(0) &= c_2 n\cos\beta_0
\end{aligned}
\tag{2.9}
$$

The perturbation variables and their initial conditions are represented as shown in Eqs.(2.10):

$$
\begin{aligned}
\mathbf{X}_p(t) &= [x_p(t)\ y_p(t)\ z_p(t)\ \dot{x}_p(t)\ \dot{y}_p(t)\ \dot{z}_p(t)]^T \\
\mathbf{X}_p(0) &= [x_p(0)\ y_p(0)\ z_p(0)\ \dot{x}_p(0)\ \dot{y}_p(0)\ \dot{z}_p(0)]^T
\end{aligned}
\tag{2.10}
$$

The initial conditions to the complete solution are

$$
\mathbf{X}(0) = \mathbf{X}_h(0) + \varepsilon\mathbf{X}_p(0) \tag{2.11}
$$

While the initial conditions for the HCW solution $\mathbf{X_h}(0)$, are predetermined, the initial conditions on the perturbation variables $\mathbf{X_p}(0)$, are free to be chosen. The objective in this section is to show that the initial conditions on the perturbation variables can be chosen to prevent the breakdown of the total solution.

The following equations are obtained for the perturbation variables after substituting Eqs.(2.6) into Eqs.(2.5) and equating the coefficient of $\varepsilon$ on both sides:

$$
\begin{aligned}
\ddot{x}_p - 2n\dot{y}_p - 3n^2 x_p &= \tfrac{y_h^2 + z_h^2 - 2x_h^2}{2} \\
\ddot{y}_p + 2n\dot{x}_p &= x_h y_h \\
\ddot{z}_p + n^2 z_p &= x_h z_h
\end{aligned}
\tag{2.12}
$$

Substitution of Eqs.(2.8) into Eqs.(2.12) results in the following set of equations:

$$\begin{aligned}
&\ddot{x}_p - 2n\dot{y}_p - 3n^2 x_p = \tfrac{1}{2}[c_1\cos(nt+\alpha_0)+c_3]^2 + \tfrac{1}{2}{c_2}^2\sin^2(nt+\beta_0) - \tfrac{1}{4}{c_1}^2\sin^2(nt+\alpha_0)\\
&\ddot{y}_p + 2n\dot{x}_p = \tfrac{1}{2}c_1\sin(nt+\alpha_0)[c_1\cos(nt+\alpha_0)+c_3]\\
&\ddot{z}_p + n^2 z_p = \tfrac{1}{2}c_1\sin(nt+\alpha_0)c_2\cos(nt+\beta_0)
\end{aligned} \tag{2.13}$$

The above equations can be written in the following form:

$$\dot{\mathbf{X}}_p = A_h\mathbf{X}_p + B\mathbf{u}_h \tag{2.14}$$

where,

$$A_h = \begin{bmatrix} 0 & 0 & 0 & 1 & 0 & 0\\ 0 & 0 & 0 & 0 & 1 & 0\\ 0 & 0 & 0 & 0 & 0 & 1\\ 3n^2 & 0 & 0 & 2n & 0 & 0\\ 0 & 0 & -2n & 0 & 0 & 0\\ 0 & 0 & 0 & 0 & 0 & -n^2 \end{bmatrix} \quad \mathbf{X_p} = \begin{bmatrix} x_p\\ y_p\\ z_p\\ \dot{x}_p\\ \dot{y}_p\\ \dot{z}_p \end{bmatrix} \quad B = \begin{bmatrix} 0 & 0 & 0\\ 0 & 0 & 0\\ 0 & 0 & 0\\ 1 & 0 & 0\\ 0 & 1 & 0\\ 0 & 0 & 1 \end{bmatrix}$$

$$\mathbf{u}_\mathrm{h} = \begin{bmatrix} \tfrac{1}{2}[c_1\cos(nt+\alpha_0)+c_3]^2 + \tfrac{1}{2}{c_2}^2\sin^2(nt+\beta_0) - \tfrac{1}{4}{c_1}^2\sin^2(nt+\alpha_0)\\ \tfrac{1}{2}c_1\sin(nt+\alpha_0)[c_1\cos(nt+\alpha_0)+c_3]\\ \tfrac{1}{2}c_1\sin(nt+\alpha_0)c_2\cos(nt+\beta_0) \end{bmatrix} \tag{2.15}$$

Eqs.(2.14) are a set of linear constant coefficient non-homogeneous ordinary differential equations. The state transition matrix for the homogeneous solution is same as the state transition matrix for the HCW equations, available in Ref.4:

$$\Phi_h(t) = \begin{bmatrix} 4-3c & 0 & 0 & \frac{s}{n} & \frac{2}{n}(1-c) & 0 \\ 6(s-nt) & 1 & 0 & \frac{-2}{n}(1-c) & \frac{4s-3nt}{n} & 0 \\ 0 & 0 & c & 0 & 0 & \frac{s}{n} \\ 3ns & 0 & 0 & c & 2s & 0 \\ -6n(1-c) & 0 & 0 & -2s & 4c-3 & 0 \\ 0 & 0 & -ns & 0 & 0 & c \end{bmatrix} \tag{2.16}$$

$c = \cos(nt), s = \sin(nt)$

The general solution to Eqs.(2.14) can be written as:

$$\mathbf{X_p}(t) = \Phi(t)\mathbf{X_p}(0) + \int_0^t \Phi(t-\tau)B\mathbf{u}(\tau)d\tau \tag{2.17}$$

from which the following results for the scalar position components of $\mathbf{X_p}(t)$ can be derived as shown below:

$$\begin{aligned} x_p(t) &= [4 - 3\cos nt]x_p(0) + \frac{\sin nt}{n}\dot{x}_p(0) + 2\frac{1-\cos nt}{n}\dot{y}_p(0) + \frac{1}{48n^2} \\ &[6{c_1}^2 + 24{c_3}^2 + 12{c_2}^2 - 2{c_1}^2\cos(2nt + 2\alpha_0) - 24c_1c_3\cos(nt + \alpha_0) + \\ &4c_2^2\cos(2nt + 2\beta_0) - 6\cos nt{c_1}^2 - 24\cos nt{c_3}^2 - 12\cos nt{c_2}^2 - \\ &7{c_1}^2\cos(nt - 2\alpha_0) - 3{c_1}^2\cos(nt + 2\alpha_0) - 24c_1c_3\cos(nt - \alpha_0) + \\ &2{c_2}^2\cos(nt - 2\beta_0) - 6{c_2}^2\cos(nt + 2\beta_0) + 12{c_1}^2\cos 2\alpha_0 + 48c_1c_3\cos 2\alpha_0] \end{aligned} \tag{2.18}$$

$$\begin{aligned} y_p(t) &= [6\sin nt - 6nt]x_p(0) + y_p(0) - 2\frac{1-\cos nt}{n}\dot{x}_p(0) + \frac{4\sin nt - 3nt}{n}\dot{y}_p(0) - \\ &\frac{1}{48n^2}[4{c_2}^2\sin(2nt + 2\beta_0) + {c_1}^2\sin(2nt + 2\alpha_0) \end{aligned}$$

$$
\begin{aligned}
&-24c_1c_3\sin(nt+\alpha_0)+12{c_1}^2nt+48{c_3}^2nt+\\
&24{c_2}^2nt+4{c_2}^2\sin(nt-2\beta_0)-6{c_1}^2\sin(nt+2\alpha_0)\\
&-14{c_1}^2\sin(nt-2\alpha_0)-12{c_2}^2\sin(nt+2\beta_0)-48c_1c_3\sin(nt-\alpha_0)\\
&+72c_1c_3nt\cos\alpha_0+12{c_2}^2\sin 2\beta_0-24c_1c_3\sin\alpha_0+\\
&18nt{c_1}^2\cos 2\alpha_0-12{c_1}^2\sin nt-48{c_3}^2\sin nt-24{c_2}^2\sin nt-9{c_1}^2\sin 2\alpha_0]
\end{aligned}
\tag{2.19}
$$

$$
\begin{aligned}
&z_p(t)=\cos ntz_p(0)+\frac{\sin nt}{n}\dot{z}_p(0)+\\
&\frac{c_1c_2}{24n^2}[6\cos(\alpha_0-\beta_0)+2\cos(2nt+\alpha_0+\beta_0)\\
&-3\cos(nt+\beta_0-\alpha_0)+\cos(nt-\alpha_0-\beta_0)\\
&-3\cos(nt+\alpha_0+\beta_0)-3\cos(nt+\alpha_0-\beta_0)]
\end{aligned}
\tag{2.20}
$$

It is clear from the above expressions that no choice of initial conditions will make all the perturbation variables vanish. There are three types of terms in the above expressions: (i) constant bias terms, (ii) secular terms, and (iii) harmonic terms. The secular terms are of serious concern as they can cause unbounded departure of the nonlinear solution from the HCW solutions. The secular terms only appear in the along-track direction ($y$). Therefore, a weak criterion for zero secular growth for the nonlinear problem is

$$
[-6nx_p(0)-3\dot{y}_p(0)-\frac{1}{48n}(12{c_1}^2+48{c_3}^3+24{c_2}^2+72c_1c_3\cos\alpha_0+18{c_1}^2\cos 2\alpha_0)]=0
\tag{2.21}
$$

The above is referred to as a weak criterion because it results from an approximate solution (first order perturbation solution) to an approximate model (with quadratic nonlinearities only) to the true nonlinear problem. The following arbitrary choice of

perturbation variable initial conditions satisfy the above criterion:

$$x_p(0) = 0 \; \dot{y}_p(0) = -\frac{1}{48n}(4{c_1}^2 + 16{c_3}^3 + 8{c_2}^2 + 24c_1c_3\cos\alpha_0 + 6{c_1}^2\cos 2\alpha_0) \quad (2.22)$$

It should be noted that the above choice is just one of the infinite combinations of $x_p(0)$ and $\dot{y}_p(0)$that satisfy the zero secular growth requirement. Therefore, the desired set of initial conditions are [HCW initial conditions + $\epsilon$(nonlinearity correction on $\dot{y}$)]. These initial conditions will be referred to as the nonlinearity corrected HCW initial conditions.

$$\mathbf{X}(0) = \begin{bmatrix} \frac{c_1}{2}\sin\alpha_0 \\ c_1\cos\alpha_0 + c_3 \\ c_2\sin\beta_0 \\ \frac{c_1}{2}n\cos\alpha_0 \\ -c_1n\sin\alpha_0 \\ c_2n\cos\beta_0 \end{bmatrix} + \epsilon \begin{bmatrix} 0 \\ 0 \\ 0 \\ 0 \\ \gamma \\ 0 \end{bmatrix}$$

where

$$\gamma = -\frac{1}{48n}(12{c_1}^2 + 48{c_3}^3 + 24{c_2}^2 + 72c_1c_3\cos\alpha_0 + 6{c_1}^2\cos 2\alpha_0) \quad (2.23)$$

The non-zero initial condition on $\dot{y}_p$, $\gamma$ is a correction to the HCW initial conditions, to accommodate the effect of quadratic nonlinear terms. This will be referred to as the "Circular nonlinearity correction" in the rest of the chapter, because this nonlinearity correction has been derived for circular chief orbits. This correction is necessary to eliminate secular growth resulting from the quadratic nonlinear terms. It should be noted that the initial conditions on the remaining perturbation variables

could also be chosen appropriately to eliminate some of the biases and the harmonic terms appearing in the $x_{qp}$ and $z_{qp}$ solutions. Shown in figures (2.3) and (2.4) are the evolutions of the LFC and GCO initial conditions on Eqs.(2.4), for 20 orbits with and without the nonlinearity correction. The solid lines represent the nonlinear simulation results with the nonlinearity correction and the broken line represents the nonlinear simulation without the nonlinearity correction. The figures amply demonstrate the effect of the nonlinearity correction in suppressing the secular growth in the along -track direction. Though the resulting relative orbits do not exactly conform to the prescription of the HCW solutions, they do remain close to them.

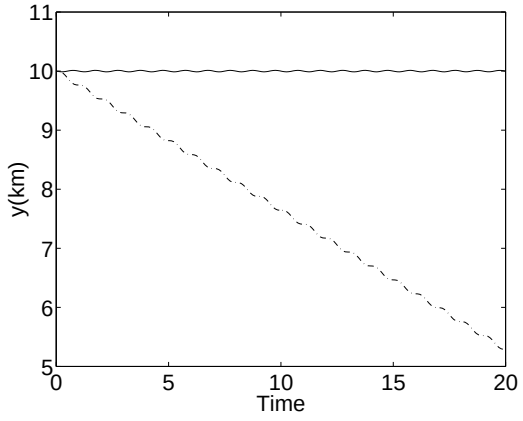


**Fig. 2.3:** Evolution of the leader follower configuration with and without the nonlinearity correction

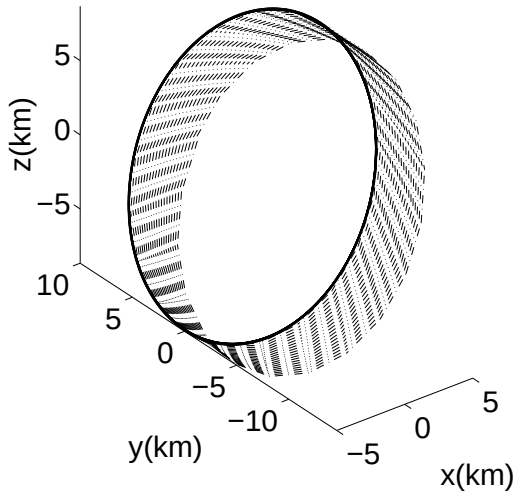


**Fig. 2.4:** Evolution of the general circular orbit formation with and without the nonlinearity correction

For the projected circular orbit $c_1 = c_2 = \rho$, $c_3 = 0$ and $\alpha_0 = \beta_0$ hence the nonlinearity

correction reduces to the following:

$$x_p(0) = 0 \; \dot{y}_{qp}(0) = -\frac{\rho^2}{48n}(12 + 6\cos 2\alpha_0) \tag{2.24}$$

Hence, the desired perturbation state vector for the PCO initial conditions is

$$\mathbf{X_p}(0) = [0 \;\; 0 \;\; 0 \;\; 0 \;\; \frac{-\rho^2}{48n}(12 + 6\cos 2\alpha_0) \;\; 0]^T \tag{2.25}$$

The effectiveness of this correction is tested on Eqs.(2.4). The plots in Figures (2.5) and (2.6) are the results of simulations conducted on Eqs.(2.4) with the parameters: $a_c = 8000$km, $\rho = 10$km, $\alpha_0 = 0^o, 90^o$, $e = 0$. Figures(2.5) and (2.6) respectively show the deviations from the HCW projected circular orbit solutions, with and without the non-linearity correction, for the $\alpha_0 = 0^0$deputy. It can be seen that the correction brings down to almost zero, an otherwise secular growth of 260m/orbit.

Shown in Figures (2.7) and (2.8) are similar plots for the $\alpha_0 = 90^0$satellite.

The complete solution to the perturbed problem is

$$\mathbf{X}(t) = \Phi(t)\mathbf{X_0}(0) + \varepsilon\Phi(t)\mathbf{X_1}(0) + \varepsilon \int_0^t \Phi(t-\tau)B\mathbf{u}(\tau)d\tau \tag{2.26}$$

The validity of the perturbation solution with the corrected initial conditions is shown in Figures (2.9) and (2.10), for the $0^0$ and the $90^0$ satellites, respectively. The deviations from the exact numerical results are bounded for both of the deputies. Figures (2.5) and (2.7) show small but constant offsets from the Hill's solutions in in the $x$ and $z$ directions. The perturbation solution captures the bias term in the $x$ direction partially but it captures the bias term in the $z$ direction very accurately, as can be seen from the figures (2.9) and (2.10).

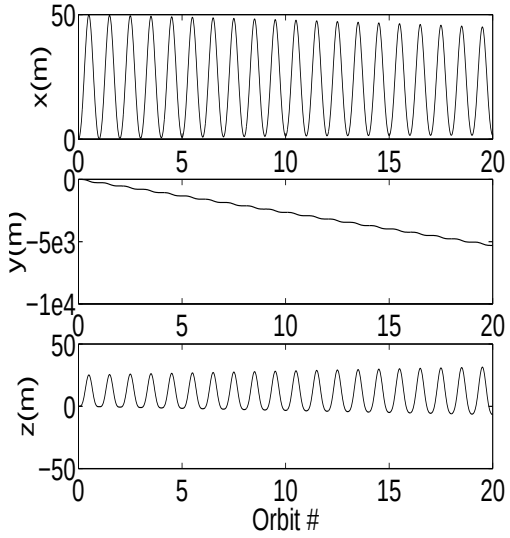


**Fig. 2.5:** Deviation of nonlinear simulation from the PCO solution, with PCO initial conditions for $\alpha_0 = 0^o$

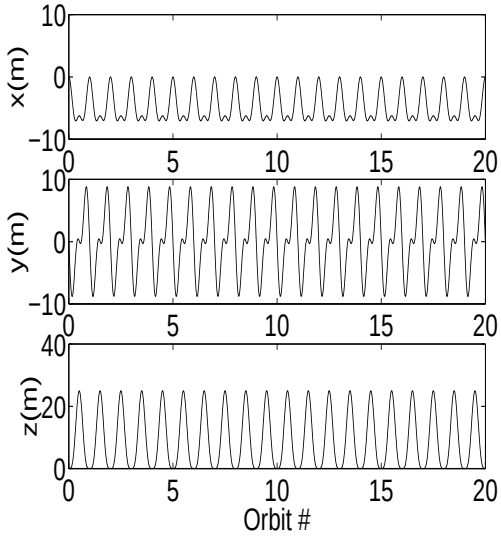


**Fig. 2.6:** Deviation of nonlinear simulation from PCO solution, with corrected PCO initial conditions for $\alpha_0 = 0^o$

### *2.4.1 Period Matching*

In the absence of any disturbances and perturbations, two satellites in Keplerian orbits can have bounded relative motion, only when their periods match. This requires the semi-major axes of both the satellites to be the same. The relative motion initial conditions, along with the chief's initial conditions, determine the orbital elements of the deputy. In this section, we shall relate the nonlinearity correction to the period matching requirement. The semi-major axis of the deputy is computed using the initial conditions of the chief and the relative motion initial conditions, with and without the correction. First, the relative motion initial conditions are transformed from the LVLH frame to the inertial frame. The transformed quantities are added to the inertial co-ordinates of the chief, to obtain the inertial co-ordinates of the deputy.

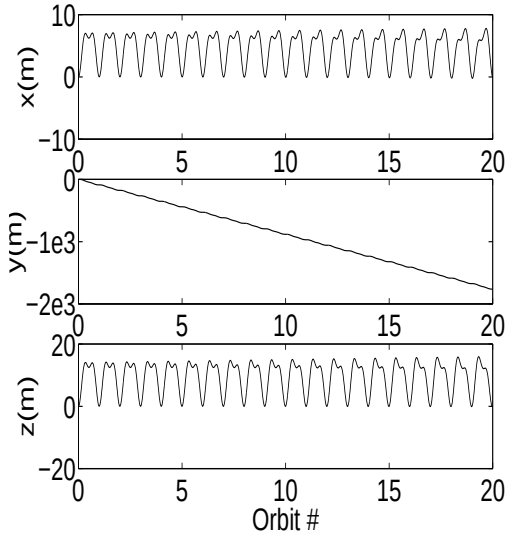


**Fig. 2.7:** Deviation of nonlinear simulation from the PCO solution, with PCO initial conditions for $\alpha_0 = 90^o$

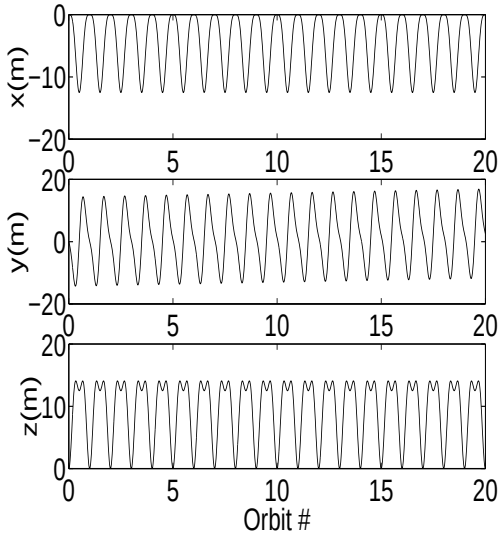


**Fig. 2.8:** Deviation of nonlinear simulation from the PCO solution, with corrected PCO initial conditions for $\alpha_0 = 90^o$

Then the semi-major axis of the deputy is obtained by converting the inertial coordinates of the deputy to its orbital elements. It can be shown that a semi-major axes difference of $\delta a$, results in approximately a secular drift of $-3\pi\delta a/orbit$. Shown in Figures (2.11) and (2.12), are the secular drift predictions based on $\delta a$ computation, with and without the circular nonlinearity correction, respectively. The secular drift is plotted as a function of $\alpha_0$ of the deputy. Figure (2.11) shows the secular growth predicted with PCO initial conditions, i.e., without the circular nonlinearity correction. The secular growth prediction varies from a maximum of 265m/orbit for the $\alpha_0 = 0^0$satellite, to a minimum of 85m/orbit for the $\alpha_0 = 90^0$deputy satellite. The plots in figures (2.5) and (2.6) confirm these predictions, both qualitatively and quantitatively. Also, the circular nonlinearity correction term, which is a function of $\alpha_0$, assumes a maximum value for $\alpha_0 = 0^0, 180^0$and a minimum value for $\alpha_0 = 90^0, 270^0$.

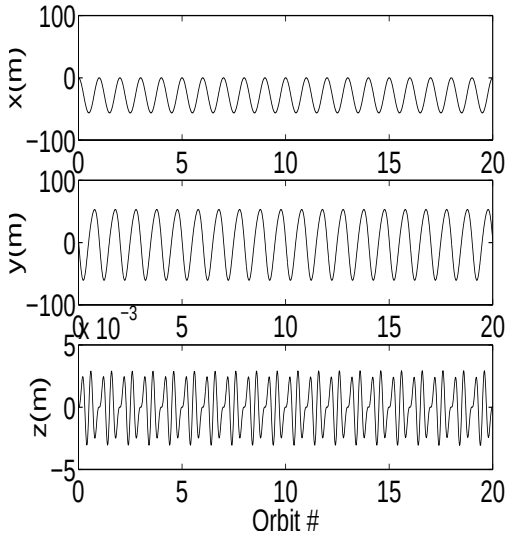


**Fig. 2.9:** Deviation of nonlinear simulation from the perturbation solution, with corrected initial conditions for $\alpha_0 = 0^o$

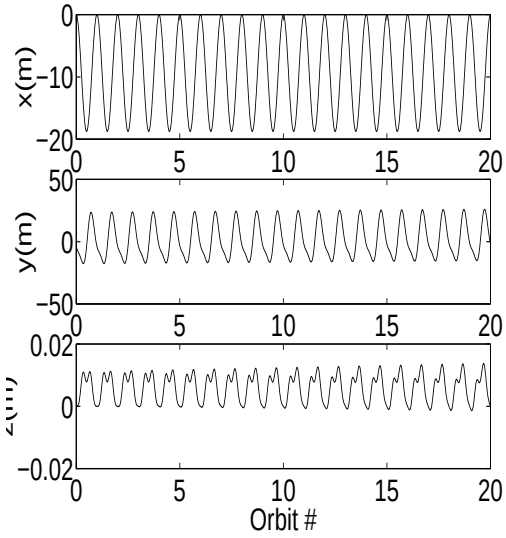


**Fig. 2.10:** Deviation of nonlinear simulation from the perturbation solution, with corrected initial conditions for $\alpha_0 = 90^o$

The secular drifts shown in Fig.(2.12) with the nonlinearity corrected PCO initial conditions, is much smaller than that of Fig.(2.11). It can be seen that the nonlinearity correction enforces the period matching requirement. Matching the periods is of cardinal importance for bounded relative motion. HCW initial conditions do not result in deputy orbits with the same semi-major axis as that of the chief. The nonlinearity corrected HCW initial conditions result in orbits with much smaller $\delta a$. Hence, they result in much smaller secular drifts. The secular growth resulting from the corrected initial conditions, is not exactly zero because the correction is made considering terms only up to first order and nonlinearities only up to quadratic terms.

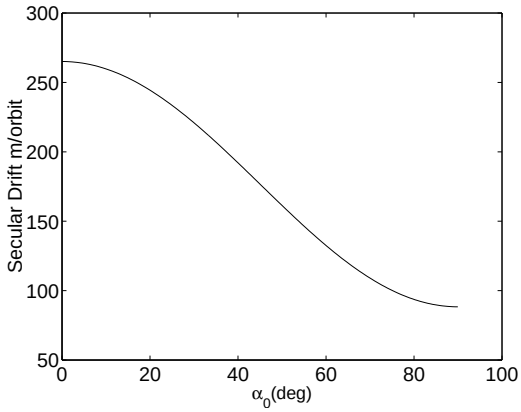


**Fig. 2.11:** Secular drift prediction based on $\delta a$ computation with PCO initial conditions

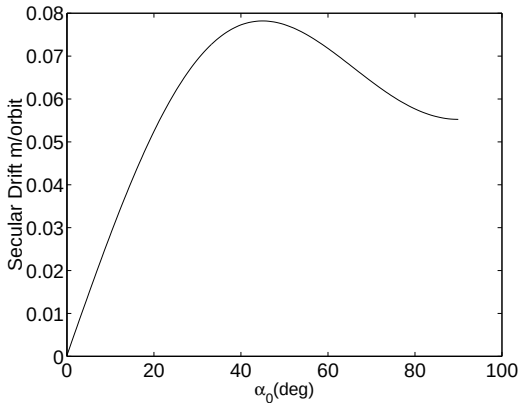


**Fig. 2.12:** Secular drift prediction based on $\delta a$ computation with nonlinearity corrected PCO initial conditions

## 2.5 Linearized Dynamics with Eccentricity Effects

In the previous section, we studied the effect of nonlinearity in the absence of eccentricity, using the HCW solutions. In this section, we study the effect of eccentricity on the HCW solutions, in the absence of nonlinearity. The governing differential equations are given in Eqs.(2.27). We will be primarily concerned with obtaining a condition for bounded solutions of Eqs.(2.27) and its representation. A condition for bounded relative orbit resulting from Eqs.(2.27), was derived by Inalhan[11]) et al. and is given in Eq.(2.28). This results from a solution to Eqs.(2.27) in terms of non-dimensional variables and with true anomaly as the independent variable. Different researchers have obtained the solution to Eqs.(2.27) but only Melton[12] provided a time explicit solution to these equations. We adopt Melton's state transition matrix solution for representing the bounded relative orbit solution.

$$
\begin{aligned}
&\ddot{x} - 2\dot{\theta}\dot{y} - \ddot{\theta}y - \dot{\theta}^2 x - 2\tfrac{\mu}{{r_c}^3}x = 0 \\
&\ddot{y} + 2\dot{\theta}\dot{x} + \ddot{\theta}x - \dot{\theta}^2 y + \tfrac{\mu}{{r_c}^3}\mathrm{y} = 0 \\
&\ddot{z} + \tfrac{\mu}{{r_c}^3}z = 0 \\
&\ddot{r}_c = r_c\dot{\theta}^2 - \tfrac{\mu}{r_c^2} \\
&\ddot{\theta} = -\tfrac{2\dot{r}_c\dot{\theta}}{r_c}
\end{aligned}
\tag{2.27}
$$

The bounded relative orbit condition when the chief is at the perigee at the initial time is:

$$
\frac{\dot{y}_0}{x_0} = -\frac{n(2+e)}{(1+e)^{\frac{1}{2}}(1-e)^{\frac{3}{2}}} \tag{2.28}
$$

For $e = 0$, the above condition reduces to $\dot{y}_0 + 2nx_0 = 0$, which is the condition for bounded relative orbit solutions to HCW equations. Therefore, the above criterion can be used to derive a correction to the $\dot{y}_0$ HCW initial condition which results in bounded orbits close to the HCW solutions. The correction could alternatively be derived for the $x_0$ initial condition as well. The correction $\delta(e)$ for $\dot{y}_0$, is computed as follows:

$$
\dot{y}_0 = -c_1 n \sin\alpha_0 + \delta(e) \tag{2.29}
$$

We can solve for $\delta(e)$ by substituting the above equation into Eqn.(2.28) and taking $x_0 = \frac{c_1}{2}\sin\alpha_0$, as follows:

$$
\delta(e) = nc_1 \sin\alpha_0 [1 - \frac{(2+e)}{2(1+e)^{0.5}(1-e)^{1.5}}] \tag{2.30}
$$

The above correction to the $\dot{y}$ HCW initial condition will be referred to as the linearized eccentricity correction. This correction is a function of eccentricity and becomes zero for $e = 0$. A closer look at Eqn.(2.30) shows that the effect of eccentricity

is maximum for the $\alpha_0 = 90^0$ deputy and zero for the $\alpha_0 = 0^0$ deputy. The correction has been found to result in perfectly bounded orbits from the integration of Eqs.(2.27). Shown in figures (2.13) and (2.14) are the evolution of PCO and GCO initial conditions on Eqs.(2.27), for 20 orbits, with and without the linearized eccentricity correction. The solid lines indicate the relative orbit obtained with the corrected initial conditions and the broken line represents the relative orbit obtained with the uncorrected initial conditions. In contrast to the circular nonlinearity correction, which is a first order correction, this is an exact correction required to obtain bounded relative orbits from Eqs.(2.27).

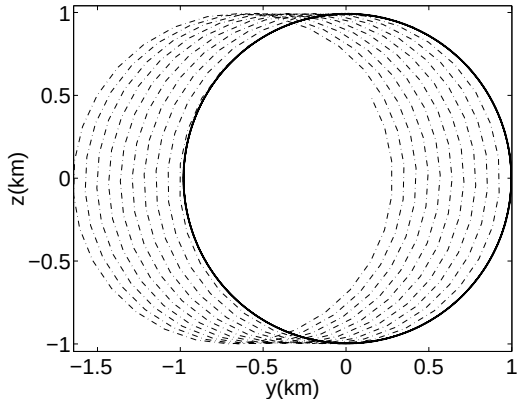


**Fig. 2.13:** Evolution of PCO initial conditions with and without eccentricity correction for an eccentricity = 0.005 and $\rho = 1$km, $\alpha_0 = 30^o$

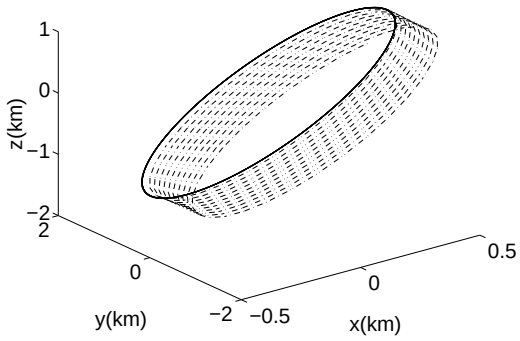


**Fig. 2.14:** Evolution of GCO initial conditions with and without eccentricity correction for an eccentricity = 0.005 and $\rho = 1$km, $\alpha_0 = 45^o$

It should be noted that this bounded relative orbit criterion could also be derived by using the geometric approach of Alfriend et al.[19] The result derived is applicable for all initial positions of the chief and is not restricted to that corresponding to the

perigee.

### *2.5.1 Generalized Eccentricity Correction*

In this section a generalized criterion will be developed which is valid for all positions of the chief. Alfriend et al.[19] derived a mapping between the relative motion co-ordinates and the linearized orbital elemental differences. Eqs.(2.27) also characterize the linearized relative motion dynamics. Hence, it is expected that setting the linearized semi-major axis difference to zero will result in bounded relative orbits from Eqs.(2.27). The relationship between the linearized semi-major axis difference and the relative motion coordinates is given by the following relation[19]

$$\delta a = A_{11}^{-1}x + A_{12}^{-1}\dot{x} + A_{13}^{-1}y + A_{14}^{-1}\dot{y} + A_{15}^{-1}z + A_{16}^{-1}\dot{z} \tag{2.31}$$

where $A_{ij}$ are the elements of the geometric transformation matrix between the incremental orbital element differences and the relative motion co-ordinates

$$A_{11}^{-1} = -\frac{V_t a\dot{\theta}}{E}(1+\frac{r_c}{p_c}),\ A_{12}^{-1} = -\frac{V_r a}{E},\ A_{13}^{-1} = \frac{V_r a\dot{\theta}}{E},\ A_{14}^{-1} = -\frac{V_t a}{E},\ A_{15}^{-1} = A_{16}^{-1} = 0 \tag{2.32}$$

where $V_t$ is the transverse velocity of the chief and $V_r$ is the radial velocity, $p$ is the semi-latus rectum of the chief, and $E$ is the energy of the chief.

$$V_t = r_c\dot{\theta} = \frac{p}{1+e\cos f}\sqrt{\frac{\mu}{p^3}}(1+e\cos f)^2 = \sqrt{\frac{\mu}{p}}(1+e\cos f) \tag{2.33}$$

where $f$ is the true anomaly of the chief

$$V_r = \dot{r}_c = e\sqrt{\frac{\mu}{p}}\sin f \tag{2.34}$$

$$\dot{\theta} = \sqrt{\frac{\mu}{p^3}}(1 + e\cos f)^2 \tag{2.35}$$

$$r_c = \frac{p}{1 + e\cos f} \tag{2.36}$$

Applying Eqn.(2.31) at time $t = 0$ we get the following constraint on initial conditions, for zero linearized semi-major axis difference,

$$-V_{t_0}\dot{\theta}_0(1 + \frac{r_{c_0}}{p})x_0 - V_{r_0}\dot{x}_0 + V_{r_0}\dot{\theta}_0 y_0 - V_{t_0}\dot{y}_0 = 0 \tag{2.37}$$

$$\begin{aligned} &\Rightarrow -\sqrt{\tfrac{\mu}{p}}(1 + e\cos f_0)\sqrt{\tfrac{\mu}{p^3}}(1 + e\cos f_0)^2(1 + \tfrac{1}{1+e\cos f_0})x_0 - e\sqrt{\tfrac{\mu}{p}}\sin f_0\dot{x}_0 \\ &+e\sqrt{\tfrac{\mu}{p}}\sin f_0\sqrt{\tfrac{\mu}{p^3}}(1 + e\cos f_0)^2 y_0 - \sqrt{\tfrac{\mu}{p}}(1 + e\cos f_0)\dot{y}_0 = 0 \end{aligned} \tag{2.38}$$

$$\begin{aligned} &\Rightarrow -\sqrt{\tfrac{\mu}{p^3}}(1 + e\cos f_0)^3(1 + \tfrac{1}{1+e\cos f_0})x_0 - e\sin f_0\dot{x}_0 + \\ &e\sin f_0\sqrt{\tfrac{\mu}{p^3}}(1 + e\cos f_0)^2 y_0 - (1 + e\cos f_0)\dot{y}_0 = 0 \end{aligned} \tag{2.39}$$

Equation(2.39) is the generalized condition for zero secular growth from Eqns.(2.27) It can be used for any initial position of the chief. It involves all the four relative motion initial conditions, $x_0, \dot{x}_0, y_0, \dot{y}_0$, and $f_0$, the initial true anomaly of the chief.

When the chief is at the perigee, $f_0 = 0$. Substituting this result into the above equation, we obtain the following:

$$-\sqrt{\frac{\mu}{p^3}}(1 + e)^3(\frac{2 + e}{1 + e})x_0 - (1 + e)\dot{y}_0 = 0 \tag{2.40}$$

$$\Rightarrow \frac{\dot{y}_0}{x_0} = -\sqrt{\frac{\mu}{p^3}}(1+e)^2(\frac{2+e}{1+e}) = -\frac{n}{(1-e^2)^{\frac{3}{2}}}\frac{(1+e)^2(2+e)}{(1+e)} = -n\frac{(2+e)}{(1+e)^{\frac{1}{2}}(1-e)^{\frac{3}{2}}} \tag{2.41}$$

It should be noted that Eqn.(2.41) is exactly same as Eqn.(2.28). The generalized condition has been tested on Eqs.(2.27), for different initial conditions of the deputy and different initial positions of the chief. HCW initial conditions are retained for $x_0, \dot{x}_0$ and the $y_0$. The $\dot{y}_0$ initial condition is then computed to satisfy Eqn.(2.39) for any given value of $f_0$. Figures (2.15) and (2.16) show the relative orbits obtained by making the generalized eccentricity correction. It should be noted that the eccentricity correction results in bounded relative orbits that are close to the HCW solutions. PCO initial conditions are used to generate the results in both the figures. It can be seen that though the projected relative orbits are bounded, they are not circular. It should also be noted that these solutions are obtained from the linearized equations of relative motion(Eqn.(2.27)) and not the complete nonlinear simulation(Eqn.(2.1)).

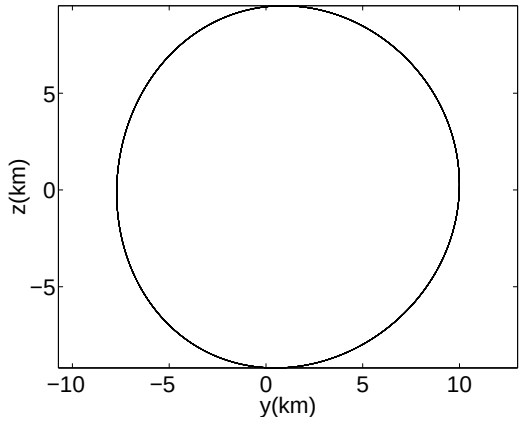


**Fig. 2.15:** Relative orbit obtained for $\alpha_0 = 30^o$, $e = 0.1$, $\rho = 10$km and $f_0 = 45^o$

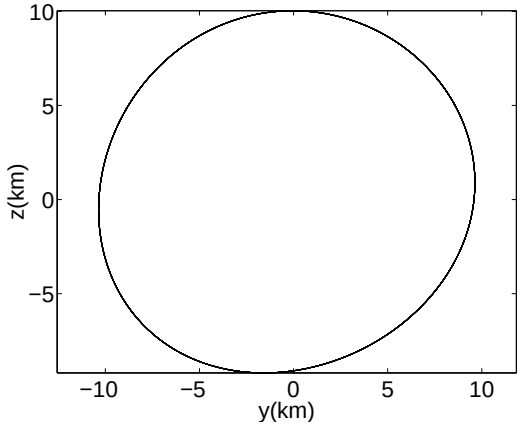


**Fig. 2.16:** Relative orbit obtained for $\alpha_0 = 60^o$, $e = 0.1$, $\rho = 10$km and $f_0 = 90^o$

### *2.5.2 Time Explicit Solution*

Melton[12] reduced the system of tenth-order equations represented by Eqs.(2.27), to a system of sixth order linear time varying equations, using the following series expansions:

$$\frac{r_c}{a} = 1 + \frac{e^2}{2} - e\cos nt - \frac{e^2}{2}\cos 2nt + ... \tag{2.42}$$

$$\dot{\theta} = \frac{\sqrt{(\mu a(1-e^2))}}{a^2}[1 + 2e\cos nt + \frac{5e^2}{2}\cos 2nt + \frac{5e^2}{2} + ...] \tag{2.43}$$

Therefore, the linearized dynamics with eccentricity, given by Eqs.(2.27), can be written as follows:

$$\dot{\mathbf{X}} = A(t)\mathbf{X} \tag{2.44}$$

$$\text{where } A(t) = A_h + eA_{1e} + e^2A_{2e} + .....$$

Melton also obtained a state transition matrix solution to Eqn.(2.27), as a series expansion in $e$ as shown below:

$$\Phi = \Phi_0 + e\Phi_1 + e^2\Phi_2 + ..... \tag{2.45}$$

The accuracy of the solution depends on the value of $e$ and the order of terms considered in the expansion. The solution as obtained by Melton, accounts for terms up to $e^2$. Therefore, for higher values of eccentricity, the solution obtained is not very accurate. Also, Melton's state transition matrix solution contains secular terms in the $x$ and $y$ directions. The accuracy of the solution improves by computing the solution until $e^3$ terms. It is expected that as we go to higher orders, the secular terms cancel

each other in the $x$ direction and the secular terms in the $y$ direction account for the secular growth that results due to the violation of Eqn.(2.28). The solution along the $z$ direction is very accurate, even with terms only up to $O(e^2)$. Therefore, in order to get a time-explicit representation for the bounded relative motion, obtained by making the linearized eccentricity correction on HCW initial conditions, we drop all the secular terms in $x$ and $y$ directions in Melton's state transition matrix. Melton's state transition matrix solution captures the bias terms and higher order harmonics very accurately. The solution, retaining just the constant and harmonic terms, is given below:

$$
\begin{aligned}
&x_{le}(t) = [(4-3cnt) + (-5cnt - 3c2nt + 13 - 5cnt)e + (40 - 40c2nt - 40cnt - \\
&27c3nt - 24c2nt + 152 - 61cnt)e^2/8 + (-33/4c3nt - 7c2nt - 55/4cnt - 4c4nt + \\
&33)e^3]x_0 + [snt/n + (-3snt + s2nt + snt)e/n + (-4snt + 8s2nt + 9s3nt - 24s2nt \\
&+9snt)e^2/(8n) + (16s4nt + 9snt + 4s2nt - 27s3nt)e^3/(12n)]\dot{x}_0 \\
&+[(2snt - 4s2nt + 7snt + 4s2nt - 9snt)e^2/4]y_0 + [2(1-cnt)/n + \\
&(8 - 4cnt - 4c2nt)e/(2n) + (8 - 5cnt - 4c2nt - 9c3nt)e^2/(4n) - \\
&(-24 - 64c2nt + 6cnt + 18c3nt + 64c4nt)e^3/(24n)]\dot{y}_0
\end{aligned}
\tag{2.46}
$$

$$
\begin{aligned}
&y_{le}(t) = [6snt + (4snt + 9s2nt + 20snt)e/2 + (42snt + 36s2nt + 18s3nt)e^2/4 + \\
&(9snt + 23/4s2nt + 9s3nt + 5s4nt)e^3]x_0 + [1 + (1-cnt)e + \\
&(3 - 2cnt - c2nt)e^2/2 + (-5/8cnt - 1/2c2nt - 3/8c3nt + 3/2)e^3]y_0 \\
&+[-2/n(1-cnt) + (-4cnt + 3c2nt + 1)e/(2n) + (4 - 2cnt - 8c2nt + 6c3nt)e^2/(4n) \\
&+(-5c2nt + 15cnt - 27c3nt + 20c4nt - 3)e^3/(12n)]\dot{x}_0 \\
&+[4snt/n + 3es2nt/n + (-12snt + 12s3nt)e^2/(4n) + (-88s2nt + 80s4nt)e^3/(24n)]\dot{y}_0
\end{aligned}
\tag{2.47}
$$

$$z_{le}(t) = [cnt + (c2nt/2 - 3/2 + cnt)e + (5cnt + 4c2nt + 3c3nt - 12)e^2/8]z_0 + [snt/n + (-2snt + s2nt)e/(2n) + (-4snt + 2s2nt + 3s3nt - 6s2nt + 3snt)e^2/(8n)]\dot{z}_0 \tag{2.48}$$

where $cjnt = \cos(njt)$, $sjnt = \sin(njt)$ and the subscript $le$ refers to linearized problem with eccentricity.

It should be noted that the above solution is valid only for the eccentricity corrected initial conditions. The maximum error incurred between the above approximate solution and the numerical integration of Eqs.(2.27) is found to be less than 0.3% of the disc size, for an eccentricity of $e = 0.1$. It should also be noted that the solution is valid only for the initial position of the chief being its perigee, i.e., the time of perigee passage is zero.

### *2.5.3 Bias Correction*

While the eccentricity corrected PCO initial conditions results in bounded orbits, they do not result in relative orbits that are exactly circular in the $y - z$ plane. It can be seen from Eqs.(4.26) and (2.48) that there are significant bias terms in the $y$ and the $z$ directions due to the eccentricity of the chief orbit. These terms offset the relative orbit w.r.t the chief. The bias term along the $y$ direction can be eliminated by making a correction to the $\dot{x}_0$ initial condition or the $y_0$ initial condition. The following corrected $\dot{x}_0$ initial condition is obtained to cancel the bias term in $y$ direction:

$$\dot{x}_0 = \frac{\rho n}{2}\sin\alpha_0 + \rho\ e\ n\cos\alpha_0 \frac{8e\ +\ 5}{8\ -\ 2e\ -\ 4e^2} \tag{2.49}$$

The above correction has been derived by isolating the bias terms in Eqn.(4.26). The

bias is maximum for the $\alpha_0 = 0^0$deputy and minimum for the $\alpha_0 = 90^0$ deputy. Figure 6 demonstrates the benefit of the bias correction. The dotted line is the relative orbit obtained by integrating Eqs.(2.27) with the eccentricity alone corrected initial conditions. It can be seen that the orbit is bounded but not symmetric about the chief. The solid line represents the relative orbit obtained with initial conditions corrected for eccentricity as well as bias. It can be seen that the bias corrected relative orbit is more symmetric about the origin.

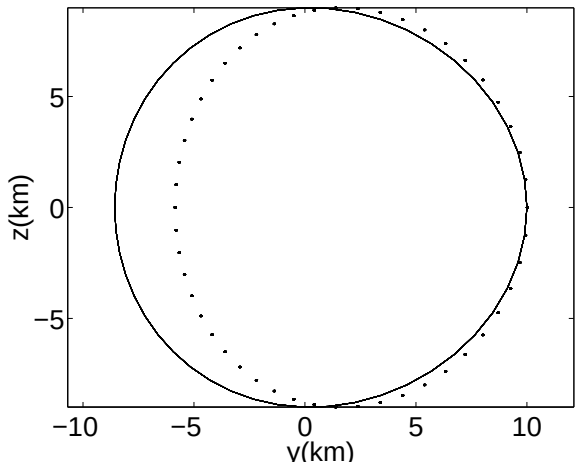


**Fig. 2.17:** Relative orbit obtained with and without the bias correction for the $\alpha_0 = 0^o$ deputy and $e = 0.1$

The bias correction and the linearized eccentricity correction are independent of each other. While the linearized eccentricity correction depends on $x_0$ and $\dot{y}_0$, the bias correction depends on $y_0$ and $\dot{x}_0$. It should be noted that the eccentricity correction and the bias correction to the relative motion initial conditions given in this section, are for the initial location of the chief being its perigee. Also, the bias correction is

specific to the PCO initial conditions.

## 2.6 Combining the Effects of Nonlinearity and Eccentricity

The previous section addressed the problem of eccentricity without nonlinearity. The section prior to that addressed the problem of nonlinearity in the absence of eccentricity. However, The main problem consists of both the effects acting together. Neither of the corrections derived, by itself, produces bounded solutions from the complete non-linear simulation for an eccentric reference orbit. In this section, we look at the solution to the combined problem and derive the corresponding conditions for bounded solutions. The approach is similar to the perturbation technique adopted earlier, for the non-linear problem without eccentricity.

We have seen in the previous section that the linearized dynamics for an eccentric reference orbit can be written as follows:

$$\dot{\mathbf{X}} = A(t)\mathbf{X} \tag{2.50}$$

$$\text{where } A(t) = A_h + eA_{1e} + e^2A_{2e} + \text{.....}$$

Adding the quadratic nonlinearities as shown in Eqs.(2.3), results in the following perturbed problem

$$\dot{\mathbf{X}} = A(t)\mathbf{X} + \varepsilon\mathbf{f}(\mathbf{X}) \tag{2.51}$$

where $\varepsilon$ is the perturbation parameter and $\mathbf{f}(\mathbf{X})$ represents the quadratic nonlinearities, terms on the RHS of Eqs.(2.3).

The solution to the perturbed problem is assumed to be of the form,

$$\mathbf{X} = \mathbf{X_{le}} + \varepsilon \mathbf{X_1} \tag{2.52}$$

where $\mathbf{X_{le}}$is the solution to linearized problem with eccentricity given by Eqs.(2.50).

Substituting the above expression in the perturbed form of the linearized equations with eccentricity, we get the following differential equations for the perturbation variables $\mathbf{X_1}$

$$\dot{\mathbf{X}}_\mathbf{1} = A(t)\mathbf{X_1} + \varepsilon \mathbf{f}(\mathbf{X_{le}}) \tag{2.53}$$

The solution to the linearized problem with eccentricity effects, for the eccentricity corrected initial conditions, can be written as

$$\mathbf{X_{le}} = \mathbf{X_{le_0}} + e\mathbf{X_{le_1}} + e^2\mathbf{X_{le_2}} + ..... \tag{2.54}$$

Terms up to $e^3$ in the $\mathbf{X_{le}}$ series expansion are given by Eqs.(2.46) - (2.48).

$\mathbf{X_{le}}$forms the zeroth-order solution to Eqs.(2.51). It should be noted the first term in the above series represents the HCW solution. The state transition matrix to the linearized problem with eccentricity, can also be written as

$$\Phi = \Phi_0 + e\Phi_1 + e^2\Phi_2 + ..... \tag{2.55}$$

Again, the first term in the above series is the same($\Phi_0 = \Phi_h$) as the state transition matrix to HCW equations, given by Eqn.(4.24).

The forcing function in Eqn.(2.53) can be written as follows,

$$\mathbf{f}(\mathbf{X_{le}}) = B\mathbf{u}$$

$$\mathbf{u} = \mathbf{u_0} + e\mathbf{u_1} + e^2\mathbf{u_2} + .....$$

$\mathbf{u_0}$ is the same as $\mathbf{u_h}$, given by Eqn.(2.15). Therefore, the above equation can be written as :

$$\mathbf{u} = \mathbf{u}_h + e\mathbf{u_1} + e^2\mathbf{u_2} + ..... \tag{2.56}$$

Substituting Eqn.(4.28) into Eqn.(2.53) we obtain

$$\dot{\mathbf{X}}_\mathbf{1} = A(t)\mathbf{X_1} + \varepsilon B\mathbf{u} \tag{2.57}$$

The solution to this problem can be written as

$$\mathbf{X_1}(t) = \Phi(t)\mathbf{X_1}(0) + \textstyle\int_0^t \Phi(t-\tau)B\mathbf{u}(\tau)d\tau$$

and the overall solution is of the form

$$\mathbf{X}(t) = \mathbf{X}_{le}(t) + \varepsilon\Phi(t)\mathbf{X_1}(0) + \varepsilon\int_0^t \Phi(t-\tau)B\mathbf{u}(\tau)d\tau$$

$$= \mathbf{X}_{le}(t) + \varepsilon\Phi(t)\mathbf{X_1}(0) + \varepsilon\Phi(t)\int_0^t [\Phi_h(-\tau) + e\Phi_{1e}(-\tau) + ...]B[\mathbf{u}_h(\tau) + e\mathbf{u_1}(\tau) + ....]d\tau \tag{2.58}$$

$\mathbf{X_{le}}(t)$ is a bounded solution and the terms appearing to the right of it in the above expression, are a result of the nonlinear perturbation. There are two perturbations in the above solution: (i) $\varepsilon$, the nonlinearity perturbation and (ii) $e$, the eccentricity perturbation. The terms containing the product of these parameters can be neglected for values of eccentricity less than 0.1. The solution retaining the significant terms

can be written as follows:

$$\mathbf{X}(t) = \mathbf{X_{le}}(t) + \varepsilon\Phi(t)\mathbf{X_1}(0) + \varepsilon\Phi(t)\int_0^t \Phi(-\tau)B\mathbf{u_h}(\tau)d\tau \tag{2.59}$$

It should be noted that the only perturbation terms remaining in the above expression, are the nonlinearity perturbations originating from the circular reference orbit problem. Therefore, a first order solution to the nonlinear problem with eccentricity, considering just the circular orbit nonlinearity effects is :

$$X(t) = X_{le}(t) + \varepsilon X_p(t) \tag{2.60}$$

where $X_p(t)$ is the same as given the circular orbit perturbation solution given by Eqs.(2.18)-(2.20). Bounded solutions to $X(t)$ require choosing another correction to the eccentricity corrected initial conditions in order to eliminate secular growth from the perturbation variables in Eqn.(2.60). This correction would be the same as the nonlinearity correction for the circular reference orbit, since all the terms containing the product of eccentricity and nonlinearity parameter have been neglected. Therefore, two corrections to the Hill's initial conditions to obtain bounded relative orbit solutions for the nonlinear problem with non-zero eccentricity. The first correction is the linearized eccentricity correction and the second term is the circular nonlinearity correction. Both these corrections are made to the $\dot{y}(0)$ initial condition. Combining the two corrections, we obtain the following initial condition for $\dot{y}(0)$ :

$$\dot{y}(0) = -c_1 n \sin\alpha_0 + \delta(e) + \gamma \tag{2.61}$$

where $\gamma$is the same as the circular orbit nonlinearity correction, given by Eqn.(2.23).

## 2.7 Results

The following simulations demonstrate the effectiveness of the nonlinearity correction for the nonlinear eccentricity problem. It should be noted that the following simulations are conducted on the complete nonlinear model given by Eqs.(2.1). The initial conditions are the same as PCO initial conditions, on all the variables except for $\dot{y}(0)$ and $\dot{x}(0)$. The initial condition $\dot{x}(0)$ has been corrected, as per Eqn.(2.49), to eliminate the bias in the $y$direction. The plots in Figures (2.18) and (2.19), show the relative orbits obtained with and without the circular nonlinearity correction on $\dot{y}(0)$. The broken lines in both the plots, are used to represent the relative orbits obtained with just the linearized eccentricity correction and the solid line represents the relative orbit obtained with the combined linearized eccentricity correction and circular nonlinearity corrections. The semi-major axis of the chief in this example, has been chosen to be 8000km and the disc size is 10km. The simulation is conducted for 20 orbits.

The various plots in Figures (2.20) - (2.23) show the secular drift in the $y$ direction at the end of 20 orbits, w.r.t the disc size, for different satellites and different eccentricities, with and without the circular nonlinearity correction. The broken lines correspond to the eccentricity alone corrected initial conditions and the solid lines are for the initial conditions obtained by using the both the corrections. It can be seen from the plots in Figures (2.18) - (2.23), that there still exists some secular growth in the $y$ direction. This is due to the nonlinearity effects from the higher order eccentricity terms. For higher values of eccentricity, one has to take the higher powers of eccentricity into account, in Eqn.(4.30) into consideration for the correction term.

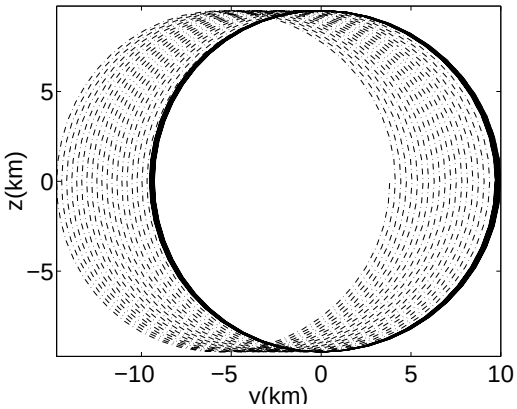


**Fig. 2.18:** Relative orbit with and without the nonlinearity correction for $\alpha_0 = 0^o$ and $e = 0.05$

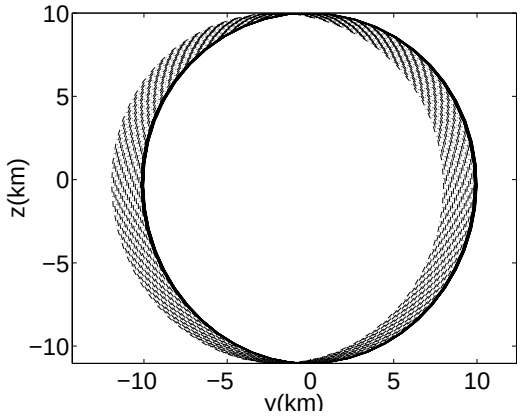


**Fig. 2.19:** Relative orbit with and without the nonlinearity correction for $\alpha_0 = 90^o$ and $e = 0.05$

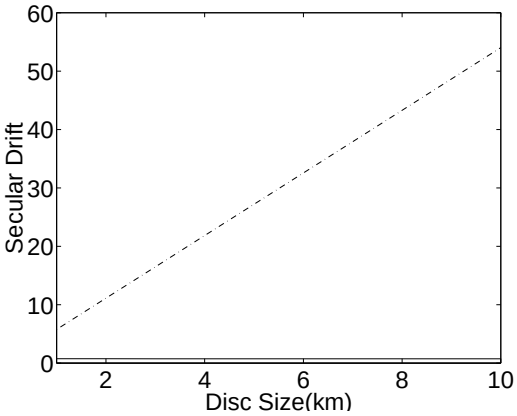


**Fig. 2.20:** Secular drift along the $y$ direction as a percentage of the disc size, with and without the nonlinearity correction for $\alpha_0 = 0^o$ and $e = 0.005$

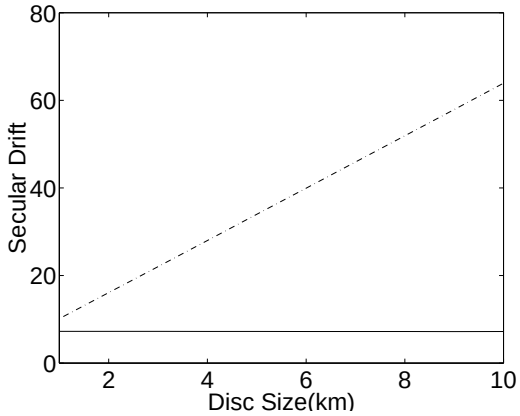


**Fig. 2.21:** Secular drift along the $y$ direction as a percentage of the disc size, with and without the nonlinearity correction for $\alpha_0 = 0^o$ and $e = 0.05$

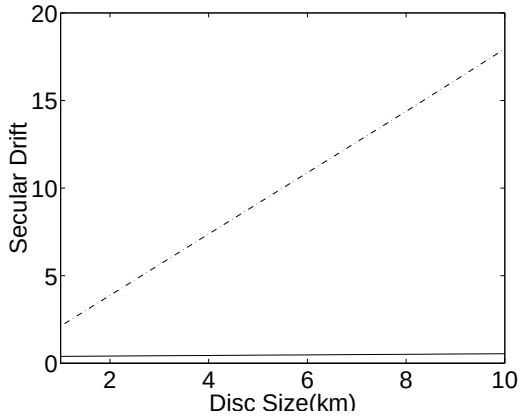


**Fig. 2.22:** Secular drift along the $y$ direction as a percentage of the disc size, with and without the nonlinearity correction for $\alpha_0 = 90^o$ and $e = 0.005$

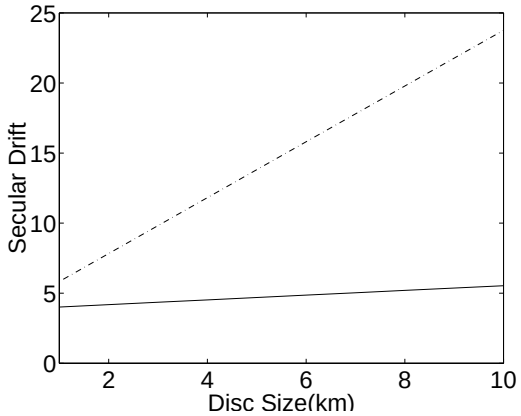


**Fig. 2.23:** Secular drift along the $y$ direction as a percentage of the disc size, with and without the nonlinearity correction for $\alpha_0 = 90^o$ and $e = 0.05$

# CHAPTER III

# LINEAR AND NONLINEAR CONTROL LAWS FOR FORMATION FLYING

## 3.1 Abstract

In this chapter, we will analyze different control schemes for formation flying satellites. The objective is to devise control strategies that can stabilize large formations optimally. Three types of controllers are studied in this chapter:(i) Lyapunov stabilized controller (ii) LQR controllers and (iii) Period matching controllers. The Lyapunov controller offers global stability and zero steady-state tracking errors but the associated control cost is very high. The LQR controllers guarantee only local stability, but offer significant cost benefits. The period- matching controllers exploit the existence of control-free natural solutions and force the dynamics to the nearest period matched trajectory. The period matching control law is globally stable and results in zero steady state controls.

## 3.2 Introduction

In the previous chapter we have seen that the equations of relative motion dynamics between a chief satellite in a circular orbit and a deputy, can be written as follows:

$$\begin{aligned} \ddot{x} - 2n\dot{y} - n^2 x &= \frac{\mu}{a^2} - \frac{\mu(a+x)}{[(a+x)^2+y^2+z^2]^{\frac{3}{2}}} + u_x \\ \ddot{y} + 2n\dot{x} - n^2 y &= -\frac{\mu y}{[(a+x)^2+y^2+z^2]^{\frac{3}{2}}} + u_y \\ \ddot{z} &= -\frac{\mu z}{[(a+x)^2+y^2+z^2]^{\frac{3}{2}}} + u_z \end{aligned} \tag{3.1}$$

where $a$ is the semi-major axis of the chief spacecraft, $n = \sqrt{\frac{\mu}{a^3}}$ is the mean motion of the chief and $u_x$, $u_y$, and $u_z$ are the external controls.

We have also seen that the linearized version of the above equations can be written as:

$$\begin{aligned} \ddot{x} - 2n\dot{y} - 3n^2 x &= u_x \\ \ddot{y} + 2n\dot{x} &= u_y \\ \ddot{z} + n^2 z &= u_z \end{aligned} \tag{3.2}$$

In the previous chapter, nonlinearity corrections to HCW initial conditions were derived to accommodate the quadratic nonlinear effects ignored by the HCW equations. The relative motion dynamics is sensitive to initial condition errors and hence a controller is required to stabilize the relative motion dynamics. In the following, different controllers are analyzed to stabilize the projected circular orbit.

### 3.3 Lyapunov Controller

The exact nonlinear equations can be rewritten as follows:

$$\ddot{\mathbf{X}} = \mathbf{F}\begin{pmatrix} \mathbf{X} \\ \dot{\mathbf{X}} \end{pmatrix} + \mathbf{G}(\mathbf{X}) + \mathbf{u} \tag{3.3}$$

where $\mathbf{X} = [x \quad y \quad z]^T$, $\dot{\mathbf{X}} = [\dot{x} \quad \dot{y} \quad \dot{z}]^T$ and $\mathbf{u} = [u_x \quad u_y \quad u_z]^T$. $\mathbf{F}$ and $\mathbf{G}$ are given below :

$$\mathbf{F} = \begin{bmatrix} 3n^2 & 0 & 0 & 0 & 2n & 0 \\ 0 & 0 & 0 & -2n & 0 & 0 \\ 0 & 0 & -n^2 & 0 & 0 & 0 \end{bmatrix} \quad \mathbf{G}(\mathbf{X}) = \begin{bmatrix} \frac{\mu}{a^2} - \frac{\mu(a+x)}{[(a+x)^2+y^2+z^2]^{\frac{3}{2}}} - 2n^2 x \\ \frac{\mu y}{a^3} - \frac{\mu y}{[(a+x)^2+y^2+z^2]^{\frac{3}{2}}} \\ \frac{\mu z}{a^3} - \frac{\mu z}{[(a+x)^2+y^2+z^2]^{\frac{3}{2}}} \end{bmatrix} \tag{3.4}$$

The linearized version of the above equations that correspond to Eqn.(3.2) can similarly be rewritten as:

$$\ddot{\mathbf{X}} = \mathbf{F} \begin{pmatrix} \mathbf{X} \\ \dot{\mathbf{X}} \end{pmatrix} \tag{3.5}$$

The reference trajectory for the tracking problem is a natural solution to the above equation. Hence, the model plant dynamics is taken as follows:

$$\ddot{\mathbf{X}}_\mathbf{r} = \mathbf{F} \begin{pmatrix} \mathbf{X}_\mathbf{r} \\ \dot{\mathbf{X}}_\mathbf{r} \end{pmatrix} \tag{3.6}$$

The error dynamics can be written as follows:

$$\ddot{\mathbf{e}} = \ddot{\mathbf{X}} - \ddot{\mathbf{X}}_\mathbf{r} = \mathbf{F} \begin{pmatrix} \mathbf{X} \\ \dot{\mathbf{X}} \end{pmatrix} + \mathbf{G}(\mathbf{X}) - \mathbf{F} \begin{pmatrix} \mathbf{X}_\mathbf{r} \\ \dot{\mathbf{X}}_\mathbf{r} \end{pmatrix} + \mathbf{u} \tag{3.7}$$

$$\ddot{\mathbf{e}} = \mathbf{F} \begin{pmatrix} \mathbf{e} \\ \dot{\mathbf{e}} \end{pmatrix} + \mathbf{G}(\mathbf{X}) + \mathbf{u} \tag{3.8}$$

where $\mathbf{e} = \mathbf{X} - \mathbf{X}_\mathbf{r}$. The above equations are obtained by subtracting Eqn.(3.6) from Eqn.(3.3).

A Lyapunov function is chosen as follows:

$$V = \frac{n^2}{2}\mathbf{e}^T\mathbf{e} + \frac{1}{2}\dot{\mathbf{e}}^T\dot{\mathbf{e}} \tag{3.9}$$

$$\Rightarrow \dot{V} = n^2\dot{\mathbf{e}}^T\mathbf{e} + \dot{\mathbf{e}}^T\ddot{\mathbf{e}} \tag{3.10}$$

$$\Rightarrow \dot{V} = \dot{\mathbf{e}}^T(n^2\mathbf{e} + \mathbf{F}\begin{pmatrix} \mathbf{e} \\ \\ \dot{\mathbf{e}} \end{pmatrix} + \mathbf{G}(\mathbf{X}) + \mathbf{u}) \tag{3.11}$$

It can be seen from the above equation that the following choice of the control law will make the origin of error dynamics globally stable:

$$\mathbf{u} = -\mathbf{F}\begin{pmatrix} \mathbf{e} \\ \\ \dot{\mathbf{e}} \end{pmatrix} - \mathbf{G}(\mathbf{X}) - n^2\mathbf{e} - n\dot{\mathbf{e}} \tag{3.12}$$

Since the error dynamics is stable, $\mathbf{e}$, and $\dot{\mathbf{e}}$ are bounded and hence the control $\mathbf{u}$, is also bounded. The error dynamics for the above choice of the control law takes the following form:

$$\ddot{\mathbf{e}} = -n^2\mathbf{e} - n\dot{\mathbf{e}} \tag{3.13}$$

Equation (3.13) represents an asymptotically stable dynamical system. Hence, the tracking errors are guaranteed to go to zero as $t \to \infty$. Shown in figures (3.1) and (3.2) are the projected circular orbits obtained by the Lyapunov controller. PCO initial conditions are propagated for 20 orbits on the true nonlinear equations for a disc size of 10km. The trajectories shown in figures (3.1) and (3.2) are exact circular projected relative orbits.

Since the steady state errors go to zero, $\mathbf{X}$ goes to $\mathbf{X_r}$, hence, the steady state controls

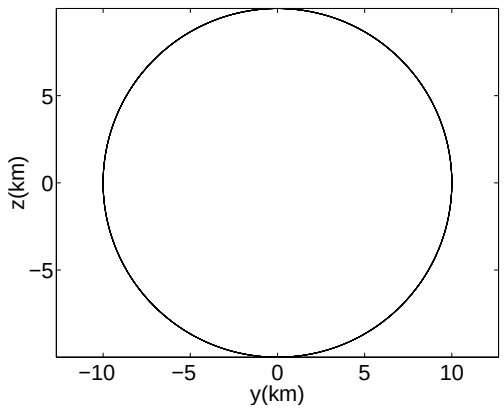


**Fig. 3.1:** Projected circular orbit obtained by the Lyapunov controller for $\alpha_0 = 0^o$ deputy

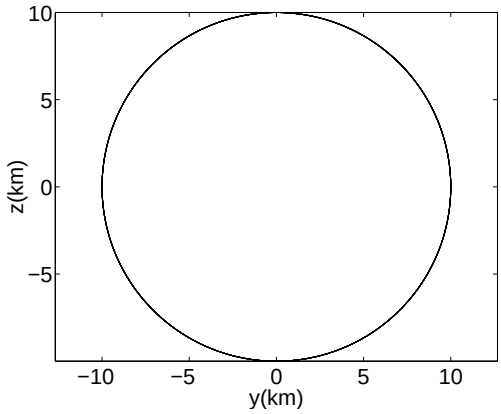


**Fig. 3.2:** Projected circular orbit obtained by the Lyapunov controller for $\alpha_0 = 90^o$ deputy

can be computed as :

$$\mathbf{u} = -\mathbf{G}(\mathbf{X_r}) \tag{3.14}$$

### 3.4 LQR Controllers

In the previous section we discussed Lyapunov controllers. Though the Lyapunov controllers make the error dynamics globally stable, they have a very high control cost associated with them because the nonlinearities are explicitly cancelled. In this section we will be discussing LQR controllers for the same problem. The motivation for using a LQR controller is to exercise some optimization options in the controller design.

The equations of motion are again rewritten for this approach, this time in state space form, as follows:

$$\dot{\mathbf{X}} = \mathbf{A}\mathbf{X} + \mathbf{C}(\mathbf{X}) + \mathbf{B}\mathbf{u} \tag{3.15}$$

where,

$$\mathbf{X} = [x \quad y \quad z \quad \dot{x} \quad \dot{y} \quad \dot{z}]^T \tag{3.16}$$

$$\mathbf{A} = \begin{pmatrix} 0 & 0 & 0 & 1 & 0 & 0 \\ 0 & 0 & 0 & 0 & 1 & 0 \\ 0 & 0 & 0 & 0 & 0 & 1 \\ 3n^2 & 0 & 0 & 0 & 2n & 0 \\ 0 & 0 & 0 & -2n & 0 & 0 \\ 0 & 0 & -n^2 & 0 & 0 & 0 \end{pmatrix} \quad \mathbf{C}(\mathbf{X}) = \begin{pmatrix} 0 \\ 0 \\ 0 \\ \frac{\mu}{a^2} - \frac{\mu(a+x)}{[(a+x)^2+y^2+z^2]^{\frac{3}{2}}} - \frac{2\mu x}{a^3} \\ \frac{\mu y}{a^3} - \frac{\mu y}{[(a+x)^2+y^2+z^2]^{\frac{3}{2}}} \\ \frac{\mu z}{a^3} - \frac{\mu z}{[(a+x)^2+y^2+z^2]^{\frac{3}{2}}} \end{pmatrix} \tag{3.17}$$

$$\mathbf{B} = \begin{pmatrix} 0 & 0 & 0 \\ 0 & 0 & 0 \\ 0 & 0 & 0 \\ 1 & 0 & 0 \\ 0 & 1 & 0 \\ 0 & 0 & 1 \end{pmatrix} \quad \mathbf{u} = \begin{pmatrix} u_x \\ u_y \\ u_z \end{pmatrix} \tag{3.18}$$

An LQR controller is designed by ignoring the nonlinear component $\mathbf{C}(\mathbf{X})$ in the above equations. The gain thus designed is used for the tracking problem as well. Therefore, a gain $\mathbf{K}$ is designed with a positive definite choice of $\mathbf{Q}$ and $\mathbf{R}$, along with $\mathbf{A}$ and $\mathbf{B}$. These matrices $\mathbf{Q}$ and $\mathbf{R}$ are picked as follows:

$$\mathbf{Q} = \begin{pmatrix} 0.1 & 0 & 0 & 0 & 0 & 0 \\ 0 & 1 & 0 & 0 & 0 & 0 \\ 0 & 0 & 0.1 & 0 & 0 & 0 \\ 0 & 0 & 0 & \frac{1}{n^2} & 0 & 0 \\ 0 & 0 & 0 & 0 & \frac{1}{n^2} & 0 \\ 0 & 0 & 0 & 0 & 0 & \frac{1}{n^2} \end{pmatrix} \quad \mathbf{R} = \begin{pmatrix} \frac{w}{n^4} & 0 & 0 \\ 0 & \frac{1}{n^4} & 0 \\ 0 & 0 & \frac{1}{n^4} \end{pmatrix} \tag{3.19}$$

where $w$ is a weight on the radial thrusting. The control law implemented is of the form :

$$\mathbf{u} = -\mathbf{K}(\mathbf{X} - \mathbf{X_r}) = -\mathbf{K}\mathbf{e} \tag{3.20}$$

Substituting the above expression for $\mathbf{u}$ in Eqn.(3.15) we obtain the following closed-loop system:

$$\dot{\mathbf{X}} = (\mathbf{A} - \mathbf{BK})\mathbf{X} + \mathbf{C}(\mathbf{X}) + \mathbf{BKX_r} \tag{3.21}$$

The stability of the above system is analyzed in two steps. First, we study the stability of the origin of the nonlinear system given by

$$\dot{\mathbf{X}} = (\mathbf{A} - \mathbf{BK})\mathbf{X} + \mathbf{C}(\mathbf{X}) \tag{3.22}$$

and then we study the effect of the forcing term $\mathbf{BKX_r}$.

$(\mathbf{A} - \mathbf{BK})$ is Hurwitz, i.e the linearized system is asymptotically stable. But the nonlinear system given by Eqn.(3.22) is only guaranteed local stability. Hence, we study the region of attraction of the nonlinear system and relate it to the LQR gain $\mathbf{K}$. The region of attraction is the set of initial conditions of Eqn.(3.21) that are asymptotically stable w.r.t the origin. $\mathbf{BKX_r}$ is the forcing term that results from

tracking the reference trajectory. Since, the forcing term is bounded, the output of Eqn.(3.21) will also be bounded for initial conditions and $\mathbf{X_r}$ that are within the region of attraction. The stability criterion and the region of attraction are further analyzed below.

The solution to Eqn.(3.21) can be written as follows :

$$\mathbf{X}(t) = \mathbf{e}^{(\mathbf{A}-\mathbf{BK})t}\mathbf{X_0} + \int_0^t \mathbf{e}^{(\mathbf{A}-\mathbf{BK})(t-\tau)}(\mathbf{BKX_r} + \mathbf{C}(\mathbf{X}))d\tau \tag{3.23}$$

Taking the norm on both sides of the equation we obtain:

$$\|\mathbf{X}(t)\| \leq Me^{-\lambda_{max}t}\|\mathbf{X_0}\| + \int_0^t Me^{-\lambda_{max}(t-\tau)}(L_1\|\mathbf{X_r}\| + L_2\|\mathbf{X}\|) \tag{3.24}$$

where, $M$ is the condition number of the eigen value matrix of $\mathbf{A} - \mathbf{BK}$, $\lambda_{max}$ is the absolute value of the maximum of the real parts of the eigen-values of $\mathbf{A} - \mathbf{BK}$, $L_1$ is a constant such that $\|\mathbf{BKX_r}\| \leq L_1\|\mathbf{X_r}\|$ and $L_2$ is the Lipschitz constant of the nonlinear vector field associated with $\mathbf{C}(\mathbf{X})$.

Adding $\frac{L_1}{L_2}\|\mathbf{X_r}\|$ on both sides of the Eqn.(3.24) we obtain:

$$\frac{L_1}{L_2}\|\mathbf{X_r}\| + \|\mathbf{X}\| \leq \frac{L_1}{L_2}\|\mathbf{X_r}\| + Me^{-\lambda_{max}t}\|\mathbf{X_0}\| + \int_0^t Me^{-\lambda_{max}(t-\tau)}L_2(\frac{L_1}{L_2}\|\mathbf{X_r}\| + \|\mathbf{X}\|)d\tau \tag{3.25}$$

Defining $y(t) = \frac{L_1}{L_2}(\|\mathbf{X_r}(t)\| + \|\mathbf{X}(t)\|)$, the above equation can be rewritten as:

$$y(t) \leq C_1 + \int_0^t L_2Me^{-\lambda_{max}t}y(\tau)d\tau \tag{3.26}$$

where $C_1$ is the maximum value of $\frac{L_1}{L_2}\|\mathbf{X_r}(t)\| + Me^{-\lambda_{max}t}\|\mathbf{X_0}\|$. $C_1$ is a finite quantity because $\|\mathbf{X_r}\|$ is bounded and $\lambda_{max} > 0$. It can be shown by using Bellman-Gronwall

lemma[36] that $y(t)$ and hence $x(t)$ is bounded, if the following inequality is satisfied :

$$L_2 M \leq \lambda_{max} \tag{3.27}$$

Both $M$ and $\lambda_{max}$ can be varied by varying the gain $\mathbf{K}$, which in turn is varied by varying the weight $w$ in the $\mathbf{R}$ matrix, as given by Eqn.(3.19). Increasing the weight $w$ penalizes the control and results in lesser fuel consumption, which is characterized by $\int_0^T \|\mathbf{u}\|^2 dt$. Increasing the weight too much results in saturation of the cost and can even destabilize the nonlinear system. The value of $M$ and $\lambda_{max}$ are found to be relatively constant over the range of values of $w$ in the range $10^3 - 10^5$. $M$ is approximately equal to $1.14e4$ and $\lambda_{max}$ is approximately $0.55e-3$ in the range of interest. Therefore, the largest Lipschitz constant that satisfies Eqn.(3.27) for the above values of $M$ and $\lambda_{max}$, is $0.48e-7$

$L_2$ is the local Lipschitz constant computed in a region surrounding the origin. The region $\mathbf{S}$ is chosen as follows:

$$-\frac{\rho}{2} \leq x \leq \frac{\rho}{2} \tag{3.28}$$

$$-\rho \leq y \leq \rho \tag{3.29}$$

$$\rho \leq z \leq \rho \tag{3.30}$$

It should be noted that the nonlinearity is a function of position states only. The above region is of interest because the projected circular orbit reference trajectory for a disc size $\rho$, lies within this region. Different estimates of the Lipschitz constant can be obtained by adopting different computation procedures. One estimate of the Lipschitz constant is the maximum value of the norm of the gradient of the vector

field, in the region of interest. It is found that this leads to a very conservative estimate of the Lipschitz constant for this problem. The other approach is to scan the region of interest on a predefined grid of points and compute the ratio $\frac{\|\mathbf{C}(\mathbf{X})\|}{\|\mathbf{X}\|}$ at these points. The maximum value of these ratios can be taken as the Lipschitz constant. By choosing a sufficiently small grid, the estimate thus obtained can be expected to approach the true value of the Lipschitz constant. The above procedure has been used to compute the Lipschitz constant in the region $\mathbf{S}$. Clearly, the Lipschitz constant thus computed depends on the size of region $\mathbf{S}$ around the origin, which is characterized by $\rho$. Figure(3.3) gives the value of the Lipschitz constant thus computed for different values of the disc size. The dotted line indicates the largest Lipschitz constant that can be be accommodated by the LQR controller, for the range of $w$ values from $10^3 - 10^5$. It can be seen from figure(3.3) that a 150km disc size has a Lipschitz constant around $0.48e-7$, which is the limit for satisfying stability criterion given by Eqn.(3.27). Therefore, the LQR controller is guaranteed to stabilize formations up to a disc size of 150km.

Shown in figures (3.4) and (3.5), are the projected circular orbits obtained by the LQR controller. All simulation parameters are chosen to be the same as their corresponding values in the previous simulations. The weight $w$ on radial thrusting has been chosen to be $10^3$.

The relative orbits obtained by the LQR controller in figures (3.4) and (3.5), compare very well with the relative orbits obtained by the Lyapunov controller. We have also seen that the LQR controller is capable of stabilizing formations with disc sizes as large as 150km. The LQR controller guarantees bounded relative orbits, but the steady state tracking errors are not guaranteed to go to zero. For large values of the

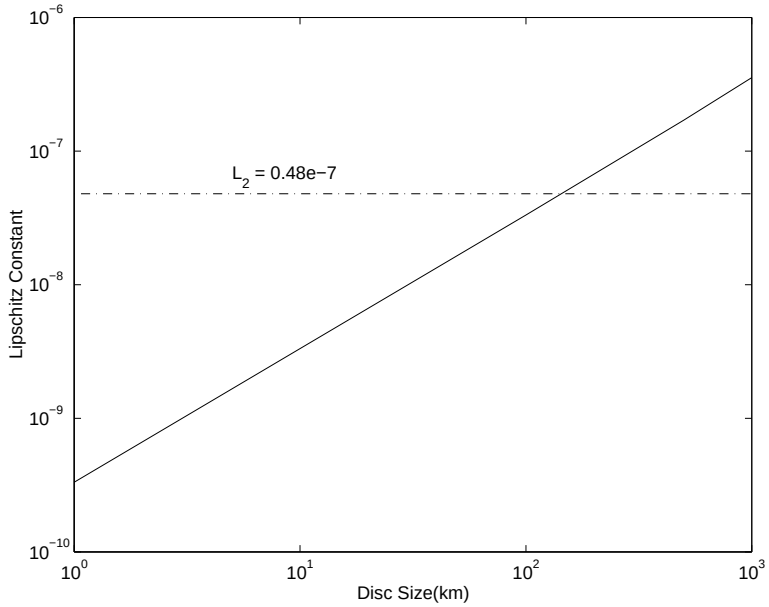


**Fig. 3.3:** Lipschitz constant as a function of disc size

disc size, these errors result in an offset along the $y$ direction, as seen in figures (3.6) and (3.7). These figures were generated by propagating PCO initial conditions for 20 orbits, with a $\rho = 150$km and $w = 10^3$.

### 3.5 Period-Matching Controller

It is well known that relative motion between two Earth orbiting spacecraft will always be bounded if the period of the two spacecraft is the same. Period-matching is equivalent to matching the energy of the two spacecraft. Energy-matching results in bounded relative orbits that are natural and hence consume zero fuel in steady state. The relative motion initial conditions determine the energy of the deputy, given the initial conditions of the chief. There exist energy matched manifolds in the state- space of relative motion dynamics, that result in bounded relative orbits. However the PCO initial conditions and the HCW initial conditions in general do not lie on these manifolds. This constitutes the reason for the breakdown of the HCW

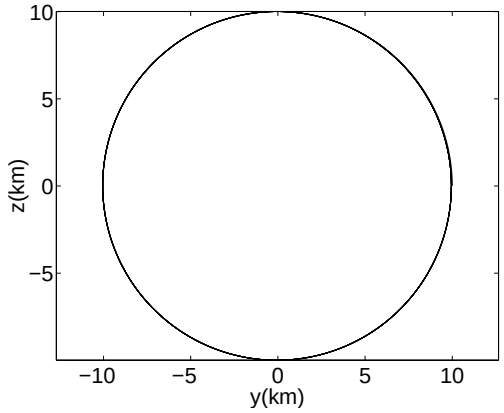


**Fig. 3.4:** Projected circular orbit obtained by the LQR controller for $\alpha_0 = 0^o$ deputy

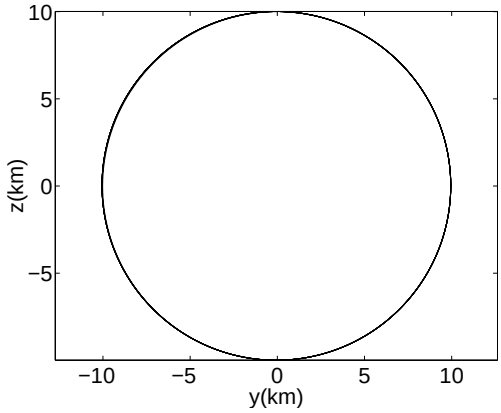


**Fig. 3.5:** Projected circular orbit obtained by the LQR controller for $\alpha_0 = 90^o$ deputy

solutions. The period matched initial conditions and the manifolds cannot be analytically solved for. However, the criterion for period matching can be written as a constraint in terms of the relative motion co-ordinates. By stabilizing this constraint, we can draw the trajectory originating from PCO initial conditions to the nearest period matched trajectory. We now develop the constraint and the stabilizing control law.

The energy expressions can be written as follows :

$$E_d = \frac{{v_d}^2}{2} - \frac{\mu}{R_d} \tag{3.31}$$

$$E_c = -\frac{1}{2a} \tag{3.32}$$

where $E_d$ and $E_c$ define the energy of the deputy and chief spacecraft respectively, $v_d$ defines the scalar absolute velocity of the deputy spacecraft, $R_d$ defines its radius,

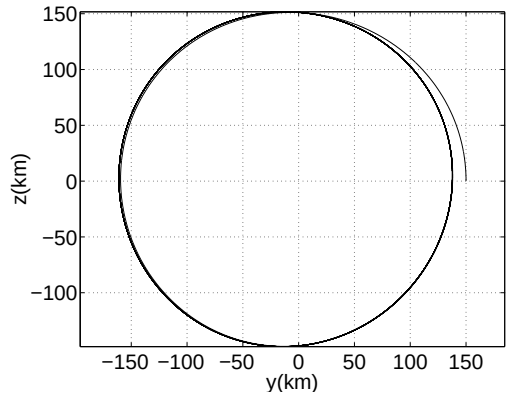


**Fig. 3.6:** Projected circular orbit obtained by the LQR controller for $\alpha_0 = 0^o$ and $\rho = 150$km

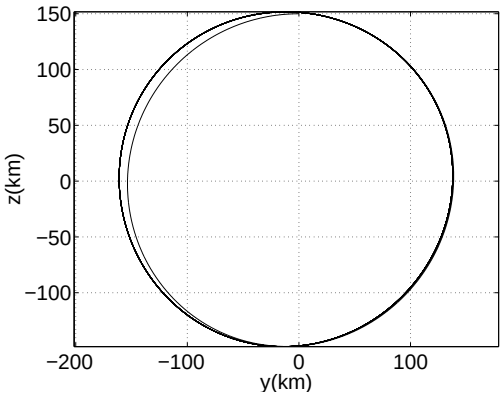


**Fig. 3.7:** Projected circular orbit obtained by the LQR controller for $\alpha_0 = 90^o$ and $\rho = 150$km

and $a$ defines the semi-major axis of the chief spacecraft. Expressions for $v_d$ and $R_d$ can be written in relative motion co-ordinates as follows:

$$\mathbf{V_d} = \mathbf{V_c} + \omega \times \mathbf{r} + \dot{\mathbf{r}} \tag{3.33}$$

$$\omega = n\hat{\mathbf{k}} \tag{3.34}$$

$$\Rightarrow \mathbf{V_d} = (\dot{x} - ny)\hat{\mathbf{i}} + (\dot{y} + nx + v_c)\hat{\mathbf{j}} + \dot{z}\hat{\mathbf{k}} \tag{3.35}$$

$$\Rightarrow {v_d}^2 = (\dot{x} - ny)^2 + (\dot{y} + nx + v_c)^2 + \dot{z}^2 \tag{3.36}$$

$$\frac{1}{R_d} = \frac{1}{\sqrt{(a+x)^2 + y^2 + z^2}} \tag{3.37}$$

The energy expression for the deputy can now be written in terms of the relative

motion co-ordinates as follows:

$$E_d = \frac{(\dot{x} - ny)^2 + (\dot{y} + nx + v_c)^2 + \dot{z}^2}{2} - \frac{\mu}{\sqrt{(a+x)^2 + y^2 + z^2}} \tag{3.38}$$

The differential energy $E_d - E_c$ is denoted by $\delta E$ . The energy matching requirement can be attained by realizing the following constraint on the relative motion dynamics:

$$\delta\dot{E} + k\delta E = 0 \tag{3.39}$$

Therefore, given the semi-major axis of the chief, the control objective can be posed as stabilizing the constraint defined by Eqn.(3.39), w.r.t Eqn.(3.3). Since the chief is in a two-body orbit, its energy is constant. Hence, the derivative of the difference in the energies of the two spacecraft can be written as:

$$\delta\dot{E} = \dot{E}_d \tag{3.40}$$

In the absence of external disturbances, $\dot{E}_d$ also remains constant. External controls are necessary to establish $\delta E = 0$, if it is initially not so. The term $k\delta E$ in Eqn.(3.39) establishes $\delta E = 0$ starting from $\delta E \neq 0$. There are three controls $u_x$, $u_y$ and $u_z$ and only one constraint. Therefore, two of the controls can be arbitrarily chosen to be identically equal to zero. We choose $u_x = 0$ and $u_z = 0$. In the presence of the control input $u_y$, $\dot{E}_d$ can be written as follows:

$$\dot{E}_d = (\dot{y} + nx + v_c)u_y \tag{3.41}$$

$$\Rightarrow \delta\dot{E} = (\dot{y} + nx + v_c)u_y \tag{3.42}$$

Substituting the above equation in Eqn.(3.39), we obtain:

$$\dot{y}u_y + nxu_y + v_c u_y = -k\delta E \tag{3.43}$$

$u_y$ can be computed from the above equation as follows:

$$u_y = k\frac{[\frac{{v_c}^2 - {v_d}^2}{2} + \mu(\frac{1}{R_d} - \frac{1}{a})]}{\dot{y} + nx + v_c} \tag{3.44}$$

The above controller draws the deputy spacecraft to the closest period-matched orbit. The period matched solutions are natural to the relative motion dynamics and hence need zero controls, once the period matching requirement is established. It should also be noted that the above controller can be implemented by state feedback. The period matched relative orbits are guaranteed to be bounded, they are not guaranteed to be circular. But it is seen from Figures (3.8) and (3.9) that it is possible to generate nearly circular relative orbits by starting close to the PCO initial conditions. Numerical studies indicate that the period matching controller can result in near-circular projected relative orbits for initial conditions that differ by 5% from the PCO initial conditions, even for disc sizes as large as 100km. The plots were generated by integrating PCO initial conditions for 20 orbits, with the period matching controller.

The period matching controller works on the premise that there exist period matched initial conditions close to the PCO initial conditions which lead to bounded circular relative orbits. As seen in the previous chapter, PCO initial conditions need a small correction in order to generate bounded relative orbits that are near circular. The period matching control law achieves exactly the same result. It transfers the PCO initial conditions to the nearest period matched initial conditions.

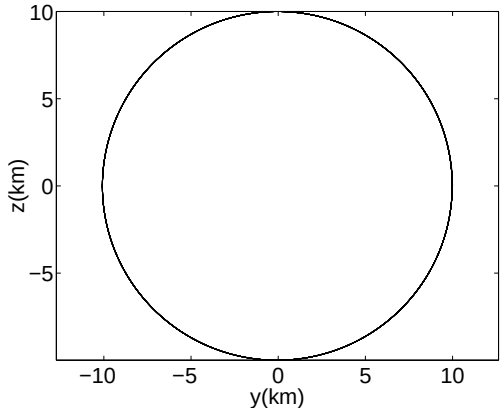


**Fig. 3.8:** Projected circular orbit obtained by the period matching controller for $\alpha_0 = 0^0$, and $k = 0.001$

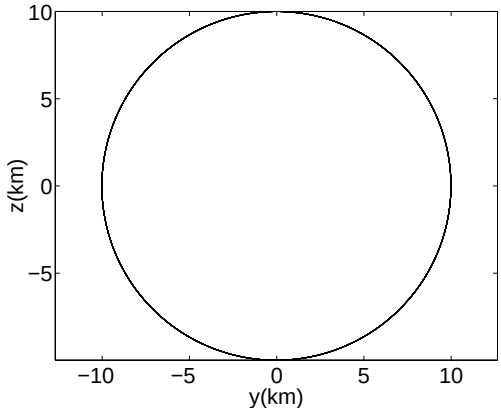


**Fig. 3.9:** Projected circular orbit obtained by the period matching controller for $\alpha_0 = 90^0$, $k = 0.001$

### 3.6 Period Matching Controller for Elliptic Chief Orbits

The period matching controller can also be extended to the elliptic chief orbit problem. Even in the presence of the eccentricity of the chief orbit, period matching results in bounded relative orbits. The energy expressions for the deputy and chief are the same as Eqn.(3.31) and Eqn.(3.32).

The control objective remains the same, i.e., to stabilize Eqn.(3.39) but w.r.t a different set of equations. The set of differential equations given by Eqn.(3.3) do not model the eccentricity of the chief's orbit. Therefore, we use the following set of equations for the elliptic chief orbit problem:

$$\begin{aligned}
\ddot{x} - 2\dot{\theta}\dot{y} - \ddot{\theta}y - \dot{\theta}^2 x &= -\frac{\mu(r_c + x)}{\left[(r_c + x)^2 + y^2 + z^2\right]^{\frac{3}{2}}} + \frac{\mu}{r_c^2} + u_x \\
\ddot{y} + 2\dot{\theta}\dot{x} + \ddot{\theta}x - \dot{\theta}^2 y &= -\frac{\mu y}{\left[(r_c + x)^2 + y^2 + z^2\right]^{\frac{3}{2}}} + u_y \\
\ddot{z} &= -\frac{\mu z}{\left[(r_c + x)^2 + y^2 + z^2\right]^{\frac{3}{2}}} + u_z \\
\ddot{r}_c &= r_c\dot{\theta}^2 - \frac{\mu}{r_c^2} \\
\ddot{\theta} &= -\frac{2\dot{r}_c\dot{\theta}}{r_c}
\end{aligned} \tag{3.45}$$

where $r_c$ is the radius of the chief's orbit and $\theta$ is its latitude angle.

The expression for the velocity of the deputy gets modified as follows :

$$\mathbf{V_d} = \mathbf{V_c} + \omega \times \mathbf{r} + \dot{\mathbf{r}} \tag{3.46}$$

For a circular orbit, $\mathbf{V_c}$ and $\omega$ are constant. Also, $\mathbf{V_c}$ is purely tangential. For the eccentric chief orbit, neither $\mathbf{V_c}$ nor $\omega$, is constant. Furthermore $\mathbf{V_c}$ has both tangential and radial components, respectively, $V_r$ and $V_t$. We can write $\mathbf{V_d}$ as :

$$\Rightarrow \mathbf{V_d} = (V_r + \dot{x} - \omega y)\hat{\mathbf{i}} + (V_t + \dot{y} + \omega x)\hat{\mathbf{j}} + \dot{z}\hat{\mathbf{k}} \tag{3.47}$$

$$\Rightarrow {v_d}^2 = (V_r + \dot{x} - \omega y)^2 + (V_t + \dot{y} + \omega x)^2 + (\dot{z})^2 \tag{3.48}$$

Following the procedure used in the previous section, we obtain the control $u_y$ to stabilize Eqn.(3.39) w.r.t Eqn.(3.45).

$$u_y = k\frac{\left[\frac{{v_c}^2 - {v_d}^2}{2} + \mu(\frac{1}{R_d} - \frac{1}{R_c})\right]}{\dot{y} + \omega x + V_t} \tag{3.49}$$

The period-matching controller can only result in relative orbits that are natural so-

lutions to the family of zero differential energy solutions. It is still not known whether exactly circular relative orbit solutions belong to this class of solutions even for a circular chief orbit. The relative orbits shwon in Figures (3.8) and (3.9), indicate, that it is possible to generate period matched relative orbits that are almost circular. For higher values of eccentricity, the resulting orbits will be bounded but not necessarily circular. Shown in Figures (3.10) and (3.11), are the relative orbits obtained without and with the period-matching controller, respectively for an eccentric chief orbit. PCO initial conditions are propagated for five orbits, with an eccentricity of $e = 0.2$ and $a = 16000km$ chosen for the reference orbit. In the presence of eccentricity, the relative orbit breaks down as seen in Fig.(3.10). In contrast, the relative obtained by the period matching controller in Fig.(3.11) is bounded, though not circular. Furthermore, the steady state control, required to establish this orbit, is identically zero.

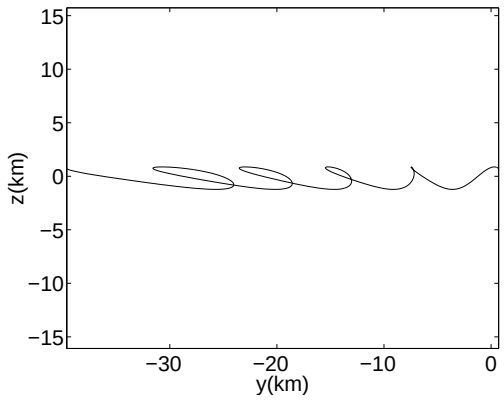


**Fig. 3.10:** Relative orbit obtained with PCO initial conditions for $\alpha_0 = 45^o, \rho = 1km, e = 0.2$ without any controller

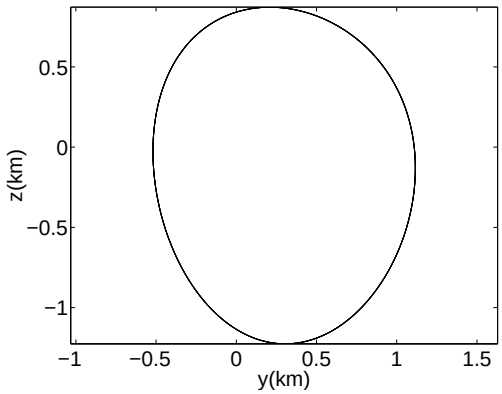


**Fig. 3.11:** Relative orbit obtained with PCO initial conditions for $\alpha_0 = 45^o, \rho = 1km, e = 0.2$ with the period matching controller for $k = 0.1$

### 3.7 Results and Conclusions

Figures (3.1 - 3.2), (3.4 - 3.5), and (3.8 - 3.9) are the relative orbits obtained by the Lyapunov, LQR and the period matching controllers, respectively, for a circular orbit. The relative orbits obtained by all the three controllers, are almost identical but the cost incurred by each controller is different. Tables 3.1 and 3.2 compare the fuel consumed by the different controllers for a disc size of $\rho = 10km$ and $\rho = 100km$, respectively. A circular orbit of semi-major axis 7100km, is chosen to generate these results. The following integral is used as a measure of the fuel consumption:

$$\int_0^t ||\mathbf{u}||^2 dt \tag{3.50}$$

$$||\mathbf{u}||^2 = {u_x}^2 + {u_y}^2 + {u_z}^2 \tag{3.51}$$

'LYAP' stands for the Lyapunov controller, 'LQR' stands for LQR controllers and 'PMC' stands for the period matching controller. The units for the fuel consumption measure in tables 3.1 and 3.2 are $m^2/s^3/yr$.

Table 3.1 Fuel consumption by different controllers for $\rho = 10km$

| | LYAP | LQR($w = 10^3$) | LQR($w = 10^4$) | LQR($w = 10^5$) | PMC($k = 0.001$) |
|---|---|---|---|---|---|
| $\alpha_0 = 0^o$ | 0.0191 | 0.00337 | 0.003387 | 0.003388 | 0.000037 |
| $\alpha_0 = 90^o$ | 0.0191 | 0.003216 | 0.0032288 | 0.00323 | 0.00004 |

It can be seen from the tables that the Lyapunov controller consumes the maximum fuel and the period matching controller consumes minimum fuel. The Lyapunov controller has a non-zero steady state control, given by $\mathbf{u} = -\mathbf{G}(\mathbf{X_r})$, which results in high control cost. The Lyapunov controller on the other hand is globally asymptoti-

Table 3.2 Fuel consumption by different controllers for $\rho = 100km$

| | LYAP | LQR($w = 10^3$) | LQR($w = 10^4$) | LQR($w = 10^5$) | PMC($k = 0.001$) |
|---|---|---|---|---|---|
| $\alpha_0 = 0^o$ | 190.93 | 34.196 | 34.331 | 34.345 | 0.372 |
| $\alpha_0 = 90^o$ | 190.93 | 32.61 | 32.74 | 32.75 | 0.039 |

cally stable controller and guarantees an exact projected circular orbit. The control law for the LQR controller is $\mathbf{u} = -\mathbf{Ke}$. Since, the errors are only guaranteed to be bounded, there exist non-zero steady state controls with the LQR controller as well. These errors are very small and hence result in much smaller controls than the Lyapunov controller. The LQR controller is guaranteed to be stable for formations as large as 150km. For large formations, the relative orbit obtained by the LQR controller is offset from the origin. The period matching controller tries to establish relative orbits that are natural to the relative motion dynamics. Therefore, the steady state controls obtained using the period- matching controller, are identically zero. Hence, the fuel consumed is also minimum for the period-matching controller. However, it is necessary for the period matching controller to start with initial conditions that only differ, at a maximum, by as much as 5% from the PCO initial conditions, even for disc sizes up to 100km, to obtain near circular projected relative orbits.

# CHAPTER IV

# $J_2$, MODELLING AND CONTROL

## 4.1 Abstract

This chapter deals with the dynamics and control of the formation flying problem in the presence of $J_2$. A rate-matching condition is developed which prevents secular growth in the along-track direction. The effect of $J_2$ is modelled on the out-of-plane motion using mean elements and a geometric approach. A new control concept is introduced which not only minimizes the overall fuel consumption of the formation, but also results in homogeneous fuel consumption by different satellites in the formation. The concept is implemented using a disturbance accommodating controller.

## 4.2 Introduction

In the presence of $J_2$, the standard orbital elements are not constant as they are with a spherical earth. The $J_2$ perturbation results in periodic oscillations as well as secular growth in the orbital elements. A new set of orbital elements, called mean elements can be defined using Brouwer's theory. The mean elements are obtained by averaging the effects of the short and long periodic oscillations that arise due to $J_2$. Only the secular effects of the $J_2$ perturbation are retained. The resulting mean semi-major axis, mean eccentricity and mean inclination of each satellite are constant. The mean ascending node, mean argument of perigee and the mean mean anomaly vary linearly with time. Their rates are constant and are functions of the mean semi-major axis, mean eccentricity and mean inclination only.

$$\dot{\Omega} = -1.5 J_2 (\frac{R_e}{p})^2 n \cos i \tag{4.1}$$

$$\dot{\omega} = 0.75 J_2 (\frac{R_e}{p})^2 n (5\cos^2 i - 1) \tag{4.2}$$

$$\dot{M} = n + 0.75 J_2 (\frac{R_e}{p})^2 n (3\cos^2 i - 1) \tag{4.3}$$

The mean semi-major axis, mean eccentricity and mean inclination are constant for both the chief and the deputy. Therefore, their differences are also constant.

$$\delta a_m = \delta a_{m_0} \tag{4.4}$$

$$\delta e_m = \delta e_{m_0} \tag{4.5}$$

$$\delta i_m = \delta i_{m_0} \tag{4.6}$$

The differences of mean nodal angle, argument of perigee and mean anomaly, depend on the mean values of the other three elements.

$$\delta\Omega_m = \delta\Omega_{m_0} + (\dot{\Omega}_d - \dot{\Omega}_c)t = \delta\Omega_{m_0} + \Delta\dot{\Omega}t \tag{4.7}$$

$$\delta\omega_m = \delta\omega_{m_0} + (\dot{\omega}_d - \dot{\omega}_c)t = \delta\omega_{m_0} + \Delta\dot{\omega}t \tag{4.8}$$

$$\delta M_m = \delta M_{m_0} + (\dot{M}_d - \dot{M}_c)t = \delta M_{m_0} + \Delta\dot{M}t \tag{4.9}$$

The following relations have been derived in Ref.19 for the along-track separation and the out -of-plane separation, using the geometry of orbits.

$$\frac{y}{r_c} \approx \delta\theta + \delta\Omega\cos i_c = \delta\omega + \delta f + \delta\Omega\cos i_c \tag{4.10}$$

$$\frac{z}{r_c} \approx \delta i \sin\theta_c - \sin i_c \delta\Omega\cos\theta_c \tag{4.11}$$

where $y$ is the along-track separation in the LVLH co-ordinate system, $r_c$ is the radius of the chief satellite from the center of the Earth, and $\theta = \omega + f$, where $\omega$ is the argument of perigee, $f$ is the true anomaly, $\Omega$ is the angle of ascending node and $i_c$ is the inclination of the chief. The relation between true and mean anomaly can be approximated for low values of eccentricity of the chief as follows :

$$f \approx M + 2e \sin M \tag{4.12}$$

The following expression for $\delta f$ can be derived from Eqn.(4.12):

$$\delta f \approx \delta M + 2\delta e \sin M + 2e \cos M \delta M \tag{4.13}$$

Substituting Eqn.(5.5) in Eqn.(5.2) we obtain the following:

$$\frac{y}{r_c} \approx (\delta\omega + \delta M + \delta\Omega \cos i_c) + 2\delta e \sin M_c + 2e_c \cos M_c \delta M \tag{4.14}$$

Equations (4.14) and (4.11) represent the linearized relationship between the relative motion co-ordinates and the osculating orbital elements differences. As mentioned earlier, $J_2$ induces short and long period oscillations along with secular drifts in the relative motion dynamics. However, it is the secular drift that is of primary concern to formation flying. Hence, it is convenient to deal with mean relative motion variables instead of the actual LVLH co-ordinates. These variables are obtained by transforming the mean elements of the chief and deputy directly to inertial co-ordinates and extracting the LVLH co-ordinates from them. Equations (4.14) and (4.11) for the mean relative motion co-ordinates are approximated by using mean elements on the right hand side of these two equations. Therefore the geometric relations for $y_m$ and $z_m$ can be written as follows:

$$\frac{y_m}{r_c} = \delta\omega_m + \delta M_m + \delta\Omega_m \cos i_c + 2\delta e_m \sin M_c + 2e_c \cos M_c \delta M_m \tag{4.15}$$

$$\frac{z_m}{r_c} \approx \delta i_m \sin\theta_c - \sin i_c \delta\Omega_m \cos\theta_c \tag{4.16}$$

Substituting equations (4.7)-(4.9) in the above equations, we obtain the following relations:

$$\frac{y_m}{r_c} = (\delta\omega_{m_0} + \delta M_{m_0} + \delta\Omega_{m_0} \cos i_c) + (\Delta\dot{\omega}_m + \delta\dot{M}_m + \delta\dot{\Omega}_m \cos i_c)t + ht \tag{4.17}$$

where $ht$ stands for harmonic terms.

$$\frac{z_m}{r_c} \approx \delta i_{m_0} \sin\theta_c - \sin i_c \delta\Omega_{m_0} \cos\theta_c - \sin i_c \Delta\dot{\Omega}_m t \cos\theta_c \tag{4.18}$$

It can be seen from Eqn.(4.17), that there exists secular growth in the $y$ direction, unless the following condition is satisfied:

$$\Delta\dot{\omega}_m + \delta\dot{M}_m + \delta\dot{\Omega}_m \cos i_c = 0 \tag{4.19}$$

The above equation places a constraint between the mean semi-major axes, mean eccentricities and mean inclinations of the chief and the deputy. A non-zero $\delta a_m$ of the order $J_2$ is required for satisfying the above equation.

It can be seen from Eqn.(4.18) that there exists a secular growth in the $z$ direction also, for non-zero $\Delta\dot{\Omega_m}$.

### 4.3 Determination of Initial Conditions

In the previous section, a condition for zero secular growth in the $y$ direction was developed. In this section we address the problem of finding the six initial mean elements of the deputy, given the mean elements of the chief. The desired mean elements of the deputy should not only result in the HCW initial conditions, but should also satisfy Eqn.(4.19). This poses seven constraints on choosing the six mean elements of the deputy. These are six HCW initial conditions and the zero secular drift condition along the $y$ direction, given by Eqn.(4.19). Hence, it is necessary to drop one of the constraints. HCW initial conditions do not satisfy Eqn.(4.19). Therefore, we drop one of the HCW initial conditions to satisfy Eqn.(4.19). It was seen in Chapter I, that the HCW initial condition on $\dot{y}$ needs to be corrected, to eliminate secular growth in the $y$ direction. Therefore, we drop the HCW initial condition on $\dot{y}$, to satisfy Eqn.(4.19). It should be noted that the five HCW initial conditions on $x, y, z, \dot{x}, \dot{z}$ are imposed using mean variables. The following set of mean elements are chosen for the chief, for all the simulations in this chapter : $[a\ e\ i\ \Omega\ \omega\ M] = [7100\ 0.005\ 70^o\ 0^o\ 0^o\ 0^o]$. A disc size of 0.5km was chosen for the relative orbit. The initial conditions of the deputies are obtained by a iterative numerical process, while attempting to satisfy the constraints. Shown in figures (4.1) and (4.2), are the relative orbits resulting from such initial conditions, for the $\alpha_0 = 0^o, 90^o$, deputies respectively.

We have seen in the previous section that there exists a secular growth in the out-of-plane direction also, for non-zero $\delta\dot{\Omega_m}$. The differential mean nodal precession rate $\delta\dot{\Omega_m}$, depends on the difference of mean semi-major axis, mean eccentricity and mean inclination. The differential nodal precession rate can be computed as follows:

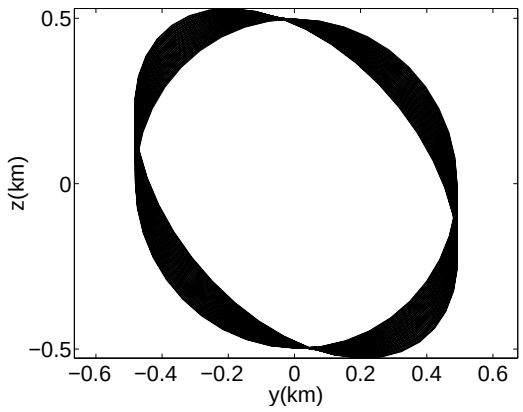


**Fig. 4.1:** Relative orbit obtained for the $\alpha_0 = 0^o$ deputy

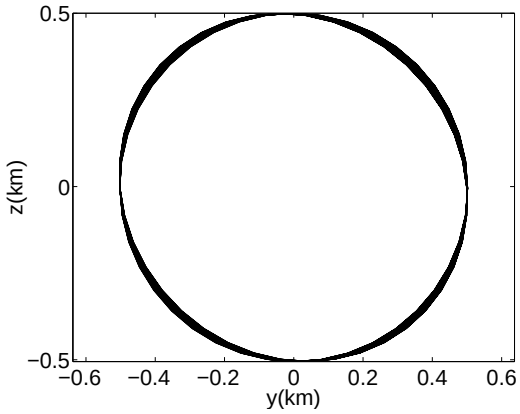


**Fig. 4.2:** Relative orbit obtained for the $\alpha_0 = 90^o$ deputy

$$\delta\dot{\Omega}_m = \frac{\partial\dot{\Omega}_m}{\partial a}\delta a_m + \frac{\partial\dot{\Omega}_m}{\partial e}\delta e_m + \frac{\partial\dot{\Omega}_m}{\partial i}\delta i_m \tag{4.20}$$

$\delta a_m$ is of the order of $J_2$ hence its contribution to $\delta\dot{\Omega}_m$ would be of the order ${J_2}^2$ and can be neglected. For values of eccentricity of the order of $1e-3$, $\frac{\partial\dot{\Omega}_m}{\partial e}$ is much smaller than $\frac{\partial\dot{\Omega}_m}{\partial i}$. Therefore computing $\delta\dot{\Omega}_m$ due to mean inclination difference alone, we obtain the following expression :

$$\delta\dot{\Omega}_m = 1.5J_2\left(\frac{R_e}{a_c}\right)^2 n_c \sin i_c \ \delta i_m \tag{4.21}$$

$\delta i_m$ is a constant and is dependent on the choice of mean initial conditions. A suitable choice of $\delta i_m$ can be made from Eqn.(4.18). The following choice are made for the values of $\delta i_{m_0}$ and $\delta\Omega_{m_0}$:

$$\delta i_{m_0} = \frac{\rho\cos\alpha_0}{a_c} \tag{4.22}$$

$$\delta\Omega_{m_0} = \frac{\rho\sin\alpha_0}{\sin i_c a_c} \tag{4.23}$$

Substituting the above relations into Eqn.(4.18), we obtain the following:

$$\frac{z_m}{r_c} = \frac{\rho}{a_c}\sin(\theta_c + \alpha_0) + \sin i_c \cos\theta_c \Delta\dot{\Omega}_m t \tag{4.24}$$

For near circular orbits the above equation is a perturbed version of the desired HCW out-of-plane solution. The above solution gradually drifts away from the HCW solution due to the effect of $\Delta\dot{\Omega}_m$. Combining equations (4.21), (4.22), and (4.24), we can obtain the secular drift in the out-of-plane direction as a function of $\alpha_0$.

$$\frac{z_m}{r_c} = \frac{\rho}{a_c}\sin(\theta_c + \alpha_0) + 1.5 J_2 n_c \sin^2 i_c \cos\theta_c (\frac{R_e}{a_c})^2 \frac{\rho\cos\alpha_0}{a_c} t \tag{4.25}$$

It can be seen from the above equation that the secular growth is maximum for the $\alpha_0 = 0^o$ deputy and minimum for the $\alpha_0 = 90^o$ deputy. This is also verified by figures (4.1) and (4.2).

### 4.4 The Fuel Balancing Control Concept

In the previous section it was seen that the effect of $J_2$ on the out-of-plane motion depends on the initial phase angle, $\alpha_0$ of the deputy. In the second chapter the effects of nonlinearity and eccentricity were also seen to be a function of $\alpha_0$. Therefore, it is only expected that the controls required to maintain the projected circular orbit, will be different for each deputy. The control effort and hence the fuel consumed will be a function of the particular $\alpha_0$ value of the deputy. To enforce homogenous fuel consumption among the different satellites, a dynamic phase shift is enforced. It was also shown by Vadali et al.[37] that rotating the formation reduces the overall fuel consumption and reaches a minimum for a particular value of $\dot{\alpha}$.

Therfore, we replace $\alpha_0$ by $\alpha = \alpha_0 + \dot{\alpha}t$ in the HCW solutions to obtain a set of

modified reference trajectories. It is emphasized that the modified reference trajectory still results in circle in the $y-z$plane. The modified reference trajectory is given as :

$$\begin{aligned} x_r &= \tfrac{\rho}{2}\sin(\theta_c+\alpha_0+\dot{\alpha}t) \\ y_r &= \rho\cos(\theta_c+\alpha_0+\dot{\alpha}t) \\ z_r &= \rho\sin(\theta_c+\alpha_0+\dot{\alpha}t) \\ \dot{x}_r &= (\bar{n}_c+\dot{\alpha})\tfrac{\rho}{2}\cos(\theta_c+\alpha_0+\dot{\alpha}t) \\ \dot{y}_r &= -(\bar{n}_c+\dot{\alpha})\rho\sin(\theta_c+\alpha_0+\dot{\alpha}t) \\ \dot{z}_r &= (\bar{n}_c+\dot{\alpha})\rho\cos(\theta_c+\alpha_0+\dot{\alpha}t) \end{aligned} \tag{4.26}$$

where $\theta_c = \bar{n}_c t$ and the modified mean motion definition is $\bar{n}_c = \dot{\omega}_m + \dot{M}_m$.

## 4.5 Control System Design

In this section, we present the methodology of control system design to achieve the desired tracking performance in the presence of disturbances and minimize the cost for control. The dynamical system under consideration is nonlinear but the control system design is based on the HCW equations. In designing control systems for spacecraft missions, closed-loop stability as well as the fuel optimality of the controller are equally important. Therefore, the controller cannot be very aggressive and should not respond to the disturbances that create short period oscillations. At the same time, the controller should be capable of preventing any secular growth or long period oscillations, which could distort the relative orbit beyond the tolerance bounds. To attain the desired objectives, the principles of persistent disturbance accommodation and rejection are utilized[23]. Higher frequencies than the orbit rate of the Chief are present in the solution. Since the mean eccentricity of the Chief is nonzero, the relative orbit may not be centered with respect to the Chief. The controller should not suppress these higher frequencies or treat the offsets along the $x$ and $z$ axes as errors,

if fuel savings are to be achieved. However, the controller must reject the disturbance along the $z$-axis with a frequency equal to the orbit rate. The desired objectives are achieved using the LQR design approach.

First, we state that the modified reference solutions given by Eqs. (4.26), satisfy the HCW equations, if $n_c$ is replaced by $\bar{n}_c + \dot{\alpha}$. However, as stated before, $\dot{\alpha}$ is small compared to $\bar{n}_c$ and is neglected in the control design process. The control design model is written in the form given below:

$$\Delta\dot{\mathbf{x}} = A\Delta\mathbf{x} + B\mathbf{u} + \Gamma \tag{4.27}$$

where

$$\Delta\mathbf{x} = [x - x_r; \dot{x} - \dot{x}_r; y - y_r; \dot{y} - \dot{y}_r; z - z_r; \dot{z} - \dot{z}_r]^T$$

and $\Gamma$ is the vector of disturbances whose magnitudes are unknown to the controller. The quantities with subscripts "r" are the modified reference trajectory states. The $A$ and $B$ matrices are obtained from the HCW equations, with $n_c$ replaced by $\bar{n}_c$.

Additional tuned filters of the form shown below are augmented to the model given in Eq. (4.27), to eliminate selected frequencies and bias components from the controls:

$$\begin{aligned} \dot{z}_{0x} &= u_x \\ \ddot{z}_{2x} + (2\bar{n}_c)^2 z_{2x} &= u_x \\ \ddot{z}_{3x} + (3\bar{n}_c)^2 z_{2x} &= u_x \end{aligned} \tag{4.28}$$

$$\begin{aligned} \ddot{z}_{2y} + (2\bar{n}_c)^2 z_{2y} &= u_y \\ \ddot{z}_{3y} + (3\bar{n}_c)^2 z_{3y} &= u_y \end{aligned} \tag{4.29}$$

$$\begin{aligned} \dot{z}_{0z} &= u_z \\ \ddot{z}_{2z} + (2\bar{n}_c)^2 z_{2z} &= u_z \\ \ddot{z}_{3z} + (3\bar{n}_c)^2 z_{3z} &= u_z \end{aligned} \tag{4.30}$$

A bias filter is not added along the y-axis, since this channel cannot accommodate a constant disturbance, as per the HCW equations.

The control weight matrix is chosen to be diagonal with the following entries: [1000, 1, 1]/$\bar{n}_c^4$. This choice penalizes the radial component of thrust severely. It is well known that radial thrusting for orbit corrections is quite inefficient. The state weight matrix is also diagonal. The radial and out-of-plane position error weights are both 0.1, whereas the along-track position error weight is 1. The rate error weights are selected as $\bar{n}_c^{-2}$ for each axis. All the filter state weights are set to 1.

The gain matrices for the in-plane and out-of-plane modes are designed separately and then assembled into a block diagonal matrix. The feedback controls are generated from the tracking errors and the filter states, by using the assembled gain matrix. The control acceleration components are first obtained in the LVLH coordinate system. The inertial components of the acceleration required to perform the nonlinear simulations are determined by coordinate transformations. Four satellites, uniformly spaced along the circle are selected to test the control concept. Initial conditions for different deputies are obtained using a iterative numerical procedure for different values of $\alpha_0$.

## 4.6 Results

A four-deputy formation has been simulated to verify the ideas of a filter based controller and the effect of rotating the formation. Shown in Figures (4.3) and (4.4) are the fuel consumption plots for different deputies, without and with formation rotation, respectively. It can be seen from Fig.(4.3) that the $\alpha_0 = \frac{\pi}{2}, \frac{3\pi}{2}$ deputies, consume almost zero fuel and the $\alpha_0 = \frac{\pi}{2}, \frac{3\pi}{2}$ deputies, consume maximum fuel. On the other hand, the fuel plots in Fig.(4.4) show that the fuel consumption curves for different deputies are nearly the same and show a symmetry with respect to the phase angle. This results in homogeneous fuel consumption for the formation.

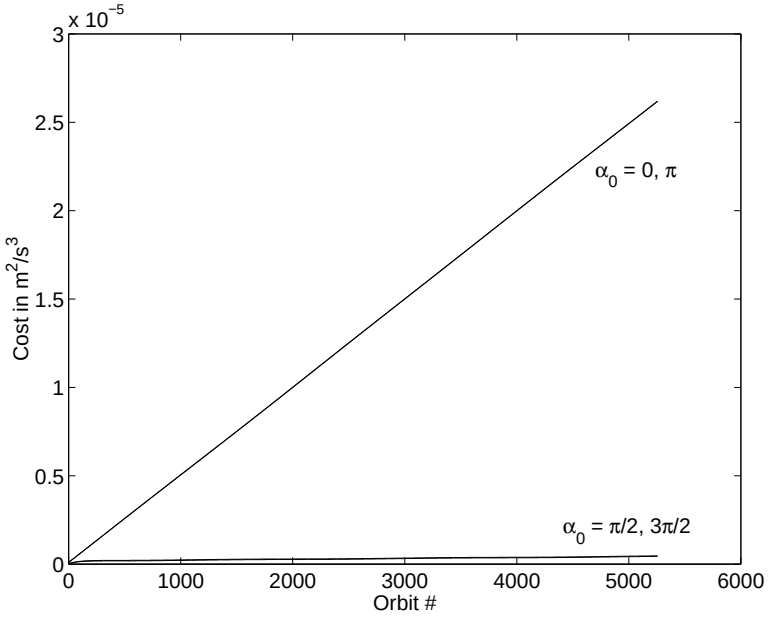


**Fig. 4.3:** Fuel consumption among different deputies for $\dot{\alpha} = 0$

Figures (4.5) and (4.6) illustrate the benefit of rotating the formation on the overall cost of maintaining the formation. It can be clearly seen from both the Figures that the overall cost attains a minimum at a non-zero value of $\dot{\alpha}$. Figure (4.5) shows the

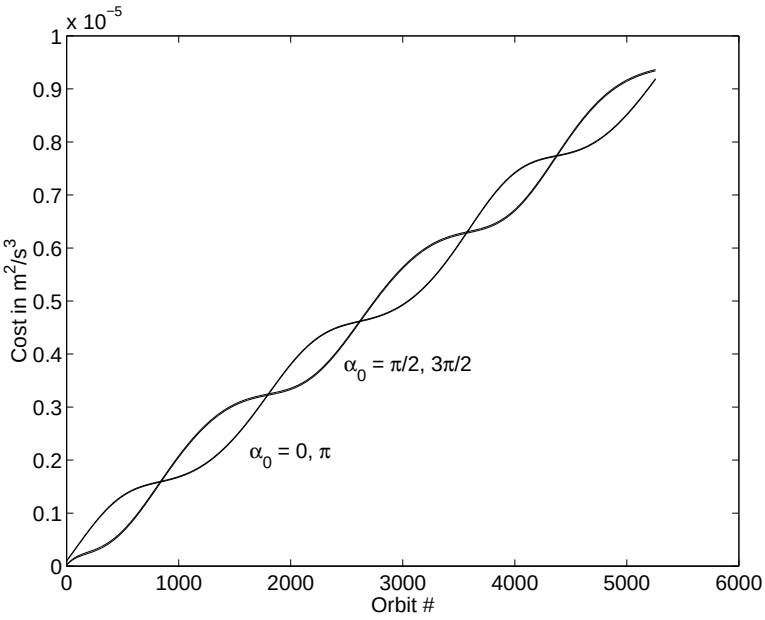


**Fig. 4.4:** Fuel consumption among different deputies for $\dot{\alpha} = -3e - 7\text{rad/s}$

cost curve as a function of $\dot{\alpha}$ without using a filter in the controller and Fig.(4.6) is for a controller with a filter. It can be seen that the filter reduces the cost by almost two orders. Furthermore, the relative orbit with the filter based controller is almost circular as shown in Fig.(4.7).

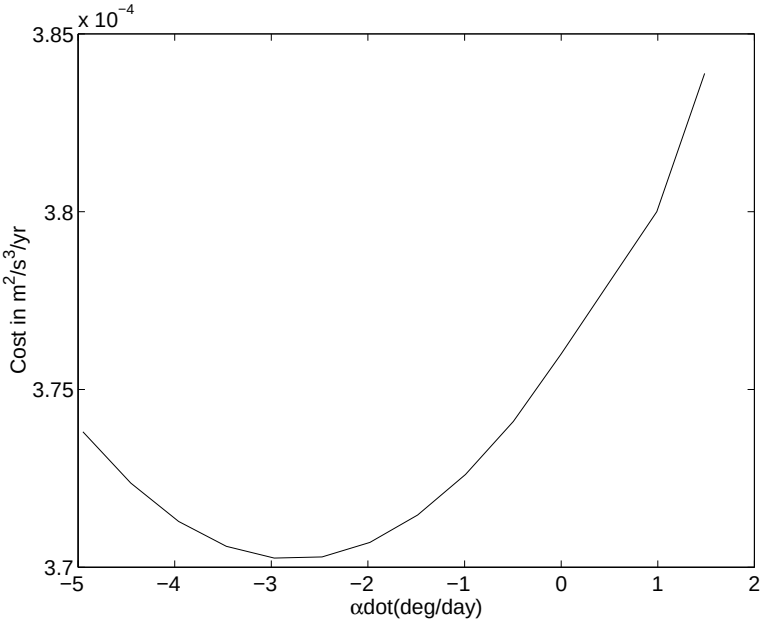


**Fig. 4.5:** Fuel consumption vs $\dot{\alpha}$ without a filter

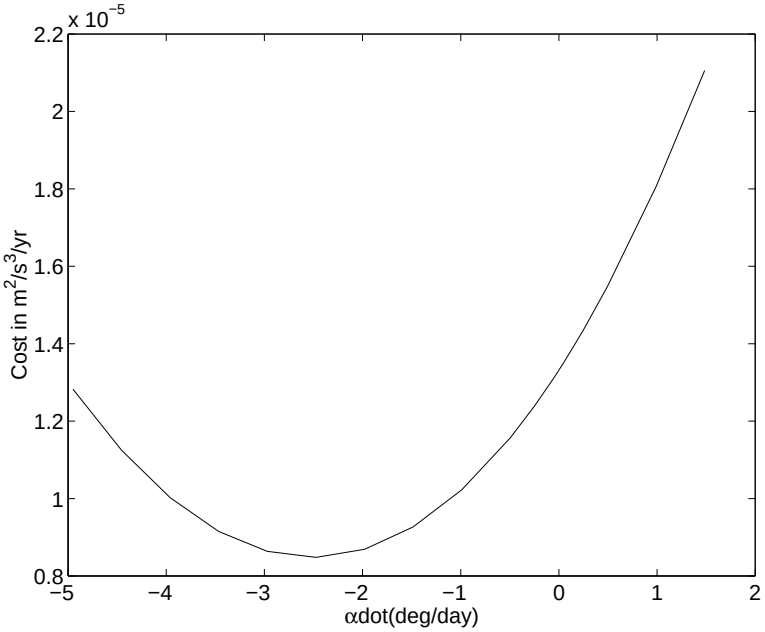


**Fig. 4.6:** Fuel consumption vs $\dot{\alpha}$ with a filter

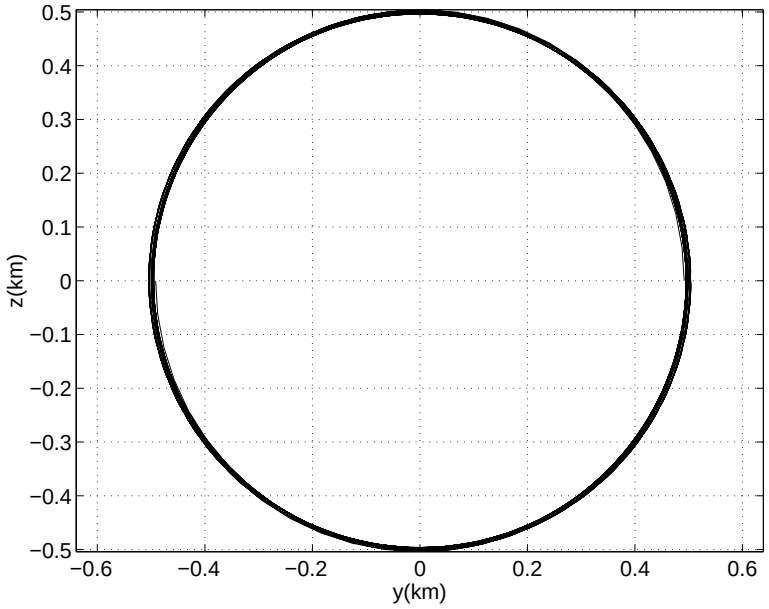


**Fig. 4.7:** Relative orbits obtained with the filter based controller

# CHAPTER V

# FORMATION RECONFIGURATION

## 5.1 Abstract

In this chapter we analyze the formation reconfiguration problem. The desired formations are characterized by the orbital elemental differences. Gauss's variational equations are used to compute impulses that establish the desired orbital elemental differences. An analytical, sub-optimal solution is proposed that can be easily implemented. The solution is also extended to the $J_2$ problem. The cost incurred with the analytical solution is found to be close to that incurred by the optimal solution obtained by a numerical optimization procedure.

## 5.2 Introduction

To achieve the desired objectives of a formation flying mission, it is often necessary for the formation to reconfigure itself. Shown in Fig.(5.1), is a schematic diagram of the reconfiguration problem that will be addressed in this chapter. We focus our attention on the formation that is circular when projected onto the local horizontal frame. The reconfiguration objective is to resize the radius of the circular relative orbit. Fig.(5.1) shows the initial(inner) and final(outer) relative orbit configurations. A four-deputy formation is shown in the initial configuration. The four deputies need to be transferred to four uniformly separated slots on the final relative orbit. Shown for the final configuration are two different sets of slots, ones with an empty circle and ones with dots at the centers at the circles. Though, the figure only shows two such sets, it is obvious that there are infinite possibilities and it is desired to pick the one with optimal features. The choice of the set is to be followed by assigning to each

deputy on the initial configuration, a unique slot in the chosen set. Also, an optimal control strategy is required to transfer the deputy from a given location on the initial configuration, to any given location on the final configuration.

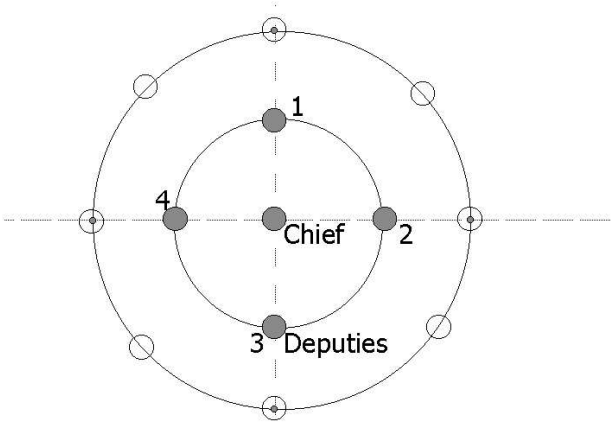


**Fig. 5.1:** Schematic diagram of the reconfiguration problem

Depending on the choice of pairing for each deputy on the initial configuration with a unique slot in the final configuration, different deputies will consume different amounts of fuel to transfer from their initial locations to the final locations. In this chapter, a sub-optimal impulsive control scheme will be derived to transfer a deputy from a given location on the initial configuration to any given location on the final configuration. An optimal solution to the pairing of each deputy satellite with a location on the final configuration can be derived using this control scheme. It is seen that this pairing scheme not only minimizes the overall fuel consumption for the formation, but also results in homogenous fuel consumption by each deputy.

## 5.3 Characterization of Formations

In this section we characterize formations in terms of elemental differences of the deputy w.r.t to the chief satellite, in the absence of $J_2$. Near-circular chief orbits will be assumed throughout this chapter. For bounded relative motion, it is essential that the semi-major axes of both the satellites be the same, hence the desired semi-major axis difference is zero.

$$\delta a = 0 \tag{5.1}$$

Since, five of the orbital elements are constant for each satellite, the corresponding five orbital element differences will also be constant for the relative motion. Equation(5.1) also enforces $\delta M$ = constant. Therefore, all the six orbital element differences are constant.

The following relations have been derived in[19] for the along track separation and the out-of-plane separation, using the geometry of orbits.

$$\frac{y}{r_c} \approx \delta\theta + \delta\Omega \cos i_c = \delta\omega + \delta f + \delta\Omega \cos i_c \tag{5.2}$$

where $y$ is the along track separation in the LVLH co-ordinate system, $r_c$ is the inertial radius of the chief satellite and $\theta = \omega + f$, $\omega$ is the argument of perigee, $f$ is the true anomaly, $\Omega$ is the angle of ascending node and $i_c$ is the inclination of the chief.

$$\frac{z}{r_c} \approx \delta i \sin\theta_c - \sin i_c \delta\Omega \cos\theta_c \tag{5.3}$$

Equations (5.2) and (5.3) represent the linearized relationship between the relative motion co-ordinates and the orbital elements differences, but they are found very

accurate for formations of the size of 1km. The relation between true and mean anomaly can be approximated as follows for low values of eccentricity of the chief

$$f \approx M + 2e \sin M \tag{5.4}$$

The above equation also has a high accuracy for eccentricities less than 0.005 and hence, is very useful in dealing with near circular orbits. The following expression for $\delta f$ can be derived from Eqn.(5.4):

$$\delta f \approx \delta M + 2\delta e \sin M + 2e \cos M \delta M \tag{5.5}$$

Substituting Eqn.(5.5) in Eqn.(5.2) we get the following:

$$\frac{y}{r_c} \approx (\delta\omega + \delta M + \delta\Omega \cos i_c) + 2\delta e \sin M_c + 2e_c \cos M_c \delta M \tag{5.6}$$

The above expression contains constant bias terms and periodic terms.

We seek to establish Hill's periodic solutions of the following form

$$\frac{y}{r_c} = \frac{\rho}{a_c} \cos(\theta_c + \alpha_0) = \frac{\rho}{a_c} \cos(\omega_c + f_c + \alpha_0) \tag{5.7}$$

$$\frac{z}{r_c} = \frac{\rho}{a_c} \sin(\theta_c + \alpha_0) = \frac{\rho}{a_c} \sin\theta_c \cos\alpha_0 + \frac{\rho}{a_c} \cos\theta_c \sin\alpha_0 \tag{5.8}$$

where $\rho$ is referred to as the disc size, and it represents the radius of the projected circular orbit, $\alpha_0$ is the phase angle, which characterizes different deputies in a formation.

Substituting Eqn.(5.4) into Eqn.(5.7) we obtain the following result:

$$\frac{y}{r_c} = \frac{\rho}{a_c}\cos(\omega_c + \alpha_0)\cos M_c - \frac{\rho}{a_c}[\sin(\omega_c + \alpha_0) + 2e_c \sin(M_c + \omega_c + \alpha_0)]\sin M_c \quad (5.9)$$

Equation(5.6) represents an approximate relation for the evolution of the along-track displacement, $y$. Equation(5.9) represents the desired periodic relative motion for the along track motion. Comparing the coefficients of $\cos M_c$ and $\sin M_c$ in Eqn.(5.9) and Eqn.(5.6), we obtain the following relations:

$$\delta e = -\frac{\rho}{2a_c}[\sin(\omega_c + \alpha_0) - 2e_c \sin(M_c + \omega_c + \alpha_0)] \quad (5.10)$$

$$\delta M = \frac{\rho}{2a_c e_c}\cos(\omega_c + \alpha_0) \quad (5.11)$$

$$\delta\omega + \delta M + \delta\Omega \cos i_c = 0 \quad (5.12)$$

Similarly, comparing Eqn.(5.8) with Eqn.(5.3), we can solve for $\delta i$ and $\delta\Omega$ as follows:

$$\delta i = \frac{\rho}{a_c}\cos\alpha_0 \quad (5.13)$$

$$\delta\Omega = \frac{\rho}{a_c}\frac{\sin\alpha_0}{\sin i_c} \quad (5.14)$$

We can also solve for $\delta\omega$ from Eqn.(5.12), which enforces zero bias in the along-track direction.

$$\delta\omega = -\delta M - \delta\Omega \cos i_c \quad (5.15)$$

Table.(5.1) gives the six elemental differences that characterize the desired Hill's periodic solution. Once established all the above differences are constant. They are analogous to the six integration constants of Hill's equations. The relative orbits

Table 5.1 Orbital element differences as a function of disc size $\rho$ and phase angle $\alpha_0$

| | |
|---|---|
| $\delta a$ | $0$ |
| $\delta e$ | $-\frac{\rho}{2a_c}[\sin(\omega_c + \alpha_0) - 2e_c \sin(M_c + \omega_c + \alpha_0)]$ |
| $\delta i$ | $\frac{\rho}{a_c} \cos \alpha_0$ |
| $\delta \Omega$ | $\frac{\rho}{a_c} \frac{\sin \alpha_0}{\sin i_c}$ |
| $\delta \omega$ | $-\delta M - \delta \Omega \cos i_c$ |
| $\delta M$ | $\frac{\rho}{2a_c e_c} \cos(\omega_c + \alpha_0)$ |

obtained with the above choice of elemental differences are shown in figures (5.2) and (5.3), for the $\alpha_0 = 0^o$ and the $\alpha_0 = 90^o$ deputies, respectively.

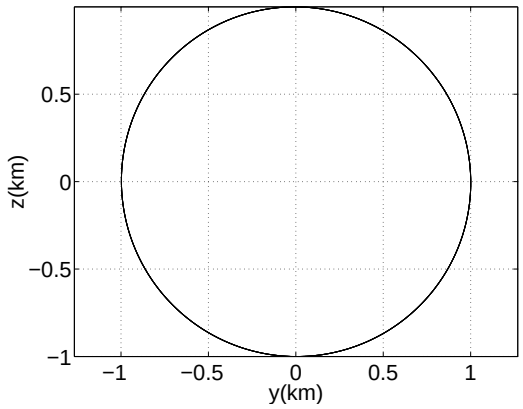


**Fig. 5.2:** Relative orbit obtained with $\alpha_0 = 0^o$

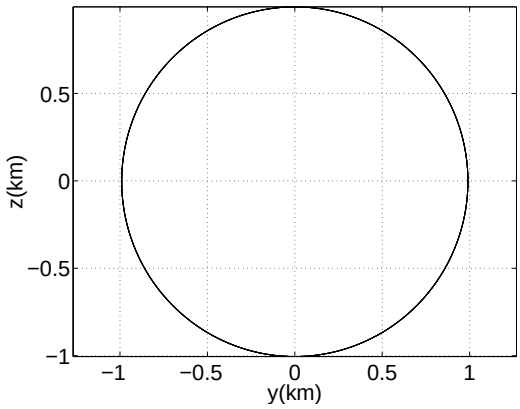


**Fig. 5.3:** Relative orbit obtained with $\alpha_0 = 90^o$

## 5.4 Gauss's Variational Equations

In the previous section, we prescribed a desired set of elemental differences to obtain the projected circular orbit. In this section we analyze the utility of Gauss's varia-

tional equations in establishing the desired elemental differences, utilizing impulsive thrust. Gauss's variational equations can be written as follows:

$$\frac{di}{dt} = \frac{r\cos\theta}{h}u_h \tag{5.16}$$

$$\frac{d\Omega}{dt} = \frac{rsin\theta}{h\sin i}u_h \tag{5.17}$$

$$\frac{da}{dt} = \frac{2a^2}{h}(e\sin f u_r + \frac{p}{r}u_\theta) \tag{5.18}$$

$$\frac{de}{dt} = \frac{1}{h}(p\sin f u_r + [(p+r)\cos f + re]u_\theta) \tag{5.19}$$

$$\frac{d\omega}{dt} = \frac{1}{he}[-p\cos f u_r + (p+r)\sin f u_\theta] - \frac{r\sin\theta\cos i}{h\sin i}u_h \tag{5.20}$$

$$\frac{dM}{dt} = n + \frac{\eta}{he}[(p\cos f - 2re)u_r - (p+r)\sin f u_\theta] \tag{5.21}$$

where $u_r, u_t$ and $u_h$ are the external accelerations in the radial, tangential and out of plane directions, respectively. The first order elemental differences obtained by firing the thrusters impulsively, are given as follows:

$$\delta i \approx \frac{r\cos\theta}{h}\Delta V_h \tag{5.22}$$

$$\delta\Omega \approx \frac{rsin\theta}{h\sin i}\Delta V_h \tag{5.23}$$

$$\delta a \approx \frac{2a^2}{h}(e\sin f\Delta V_r + \frac{p}{r}\Delta V_\theta) \tag{5.24}$$

$$\delta e \approx \frac{1}{h}(p \sin f \Delta V_r + [(p+r)\cos f + re]\Delta V_\theta) \tag{5.25}$$

$$\delta \omega \approx \frac{1}{he}[-p \cos f \Delta V_r + (p+r)\sin f \Delta V_\theta] - \frac{r \sin\theta \cos i}{h \sin i}\Delta V_h \tag{5.26}$$

$$\delta M \approx \frac{\eta}{he}[(p \cos f - 2re)\Delta V_r - (p+r)\sin f \Delta V_\theta] \tag{5.27}$$

where $\Delta V_r, \Delta V_t$ and $\Delta V_h$ are the magnitudes of the impulse components in the radial, tangential and out of plane directions, respectively.

The above equations relate the components of the impulse to the corresponding elemental differences created, for a single impulse. The equations offer four degrees of freedom, they are: 1) the choice of the magnitudes of the three impulse components and 2) the choice of the impulse location $f$. The projected circular orbit formation is characterized by the six orbital element differences. Therefore, at least two impulses are necessary to create these desired differences. Two impulses have six degrees of freedom and the location of the impulses offer two extra degrees of freedom. The locations can be chosen to minimize the fuel consumption. The following assumptions are found to be useful in determining these degrees of freedom.

**Assumptions**: 1. The out of plane cost constitutes a larger portion of the overall cost. 2. Hence, the locations of the two impulses are to be based on minimizing the out of plane cost.

The above assumptions are based on the results of certain numerical experiments and

they stand validated by the optimization results. They are useful in determining a structure to the optimal solution. The out-of-plane cost refers to the cost of creating the desired inclination and the desired nodal differences, and the in-plane cost refers to the cost of creating the remaining four elemental differences. The inclination and the node are effected by the out-of-plane thrust alone. Also, the desired inclination difference and the node difference can be obtained by one impulse, suitably located at the following latitude angle:

$$\theta_c = atan2(\delta\Omega \sin i, \delta i) \tag{5.28}$$

The corresponding $\Delta V_h$ is computed as follows:

$$\Delta V_h = \frac{h}{r}\sqrt{\delta i^2 + \delta\Omega^2 \sin^2 i} \tag{5.29}$$

The above scheme is optimal for creating a given $\delta i$ and $\delta\Omega$ using a single impulse. It can be shown that a $k$-impulse scheme can utmost perform as good as a single impulse used at the appropriate location, $\theta = \theta_c$.

Let $\theta = \theta_1, \theta_2, ...\theta_k$ be the latitude angle locations for the impulses $\Delta V_{h_1}, \Delta V_{h_2}, .....\Delta V_{h_k}$, respectively. The differences $\delta i$ and $\delta\Omega$ created by such a sequence of impulses are given by

$$\delta i = \frac{r\cos\theta_1}{h}\Delta V_{h_1} + \frac{r\cos\theta_2}{h}\Delta V_{h_2} + ..... + \frac{r\cos\theta_k}{h}\Delta V_{h_k} \tag{5.30}$$

and

$$\delta\Omega = \frac{r\sin\theta_1}{h\sin i}\Delta V_{h_1} + \frac{r\sin\theta_2}{h\sin i}\Delta V_{h_2} + ..... + \frac{r\sin\theta_k}{h\sin i}\Delta V_{h_k} \tag{5.31}$$

Since we are dealing with near-circular orbits, we hold $r$ constant. By using the triangle inequality, we obtain the following results :

$$|\delta i| \leq |\frac{r\cos\theta_1}{h}||\Delta V_{h_1}| + |\frac{r\cos\theta_2}{h}||\Delta V_{h_2}| + ..... + |\frac{r\cos\theta_k}{h}||\Delta V_{h_k}| \tag{5.32}$$

$$|\delta\Omega| \leq |\frac{r\sin\theta_1}{h\sin i}||\Delta V_{h_1}| + |\frac{r\sin\theta_2}{h\sin i}||\Delta V_{h_2}| + ..... + |\frac{r\sin\theta_k}{h\sin i}||\Delta V_{h_k}| \tag{5.33}$$

The magnitude of $\Delta V_h$ for a single impulse at $\theta = \theta_c$, is given by

$$\Delta V_h = \frac{h}{r}\sqrt{\delta i^2 + \delta\Omega^2 \sin^2 i} \tag{5.34}$$

Substituting equations (5.32) and (5.33) in Eqn.(5.34) we obtain the following relation:

$$\begin{aligned}\Delta V_h \leq \frac{h}{r}[(|\frac{r\cos\theta_1}{h}||\Delta V_{h_1}| + |\frac{r\cos\theta_2}{h}||\Delta V_{h_2}| + ..... + |\frac{r\cos\theta_k}{h}||\Delta V_{h_k}|)^2 \\ +(|\frac{r\sin\theta_1}{h\sin i}||\Delta V_{h_1}| + |\frac{r\sin\theta_2}{h\sin i}||\Delta V_{h_2}| + ..... + |\frac{r\sin\theta_k}{h\sin i}||\Delta V_{h_k}|)^2]^{\frac{1}{2}}\end{aligned} \tag{5.35}$$

$$\begin{aligned}\leq [(\cos^2\theta_1 + \sin^2\theta_1){\Delta V_{h_1}}^2 + (\cos^2\theta_2 + \sin^2\theta_2){\Delta V_{h_2}}^2 + .....(\cos^2\theta_k + \sin^2\theta_k){\Delta V_{h_k}}^2 + \\ 2\sum_{l,m=1}^{k}(|\cos\theta_l||\cos\theta_m| + |\sin\theta_l||\sin\theta_m|)|\Delta V_l||\Delta V_m|]^{\frac{1}{2}}\end{aligned} \tag{5.36}$$

The maximum value of $(|\cos\theta_l||\cos\theta_m| + |\sin\theta_l||\sin\theta_m|)$ is 1. Therefore,

$$|\Delta V_h| \leq [{\Delta V_{h_1}}^2 + \Delta V_{h_2}^2 + ..... + {\Delta V_{h_k}}^2 + 2\sum_{l,m=1}^{k}|\Delta V_l||\Delta V_m|]^{\frac{1}{2}} \tag{5.37}$$

$$\Rightarrow |\Delta V_h| \leq |\Delta V_{h_1}| + |\Delta V_{h_2}| + ..... + |\Delta V_{h_k}| \tag{5.38}$$

which proves that a single impulse at $\theta = \theta_c$ is the optimal $\Delta V_h$ to create the desired $\delta i$ and $\delta\Omega$. But it should be noted that the optimal one impulse $\Delta V_h$ given by Eqn.(5.29), also creates a $\delta\omega$ given by

$$\delta\omega = -\frac{r \sin\theta \cos i}{h \sin i}\Delta V_h = -\cos i \delta\Omega \tag{5.39}$$

This $\delta\omega$ must be corrected at a later time.

As per the second assumption, the optimal location of the two out-of-plane impulses is to be decided based on the out-of- plane cost alone. But we have already proved that a desired $\delta i$ and $\delta\Omega$, can be achieved optimally with one impulse alone, at $\theta = \theta_c$. However, this can be split up into two impulses, achieving the same $\delta i$ and $\delta\Omega$ without any additional cost. The two locations are $\theta = \theta_c$ and $\theta = \theta_c + \pi$, and the corresponding $\Delta V_{h_1}$ and $\Delta V_{h_2}$ can be obtained as follows:

$$\Delta V_{h_1} = \frac{1}{2}\frac{h}{r}\sqrt{\delta i^2 + \delta\Omega^2 \sin^2 i} \tag{5.40}$$

$$\Delta V_{h_2} = -\frac{1}{2}\frac{h}{r}\sqrt{\delta i^2 + \delta\Omega^2 \sin^2 i} \tag{5.41}$$

$\Delta V_{h_2}$ has a negative sign because $\cos(\theta_c+\pi) = -\cos\theta_c$ and $\sin(\theta_c+\pi) = -\sin\theta_c$. The two-out-of plane impulses $\Delta V_{h_1}$ and $\Delta V_{h_2}$, each create half of the desired corrections: $\frac{\delta i}{2}$ and $\frac{\delta\Omega}{2}$ with each impulse. Also, the total cost incurred is the same as that due to a single impulse at $\theta = \theta_c$.

$$|\Delta V_{h_1}| + |\Delta V_{h_2}| = \frac{h}{r}\sqrt{\delta i^2 + \delta\Omega^2 \sin^2 i} \tag{5.42}$$

Therefore, the choice of the two out of plane impulse components as well as the locations of the two impulses, is determined. There are still four degrees of freedom left,

which are the two radial and two tangential components of the two impulses. These degrees of freedom can be used to achieve the remaining four elemental differences.

$$\delta a = \frac{2a^2}{h}(e \sin f_1 \Delta V_{r_1} + \frac{p}{r_1}\Delta V_{\theta_1}) + \frac{2a^2}{h}(e \sin f_2 \Delta V_{r_2} + \frac{p}{r_2}\Delta V_{\theta_2}) \tag{5.43}$$

$$\begin{aligned}\delta e = &\frac{1}{h}(p \sin f_1 \Delta V_{r_1} + [(p + r_1)\cos f_1 + r_1 e]\Delta V_{\theta_1}) \\ &+\frac{1}{h}(p \sin f_2 \Delta V_{r_2} + [(p + r_2)\cos f_2 + r_2 e]\Delta V_{\theta_2})\end{aligned} \tag{5.44}$$

$$\begin{aligned}\delta\omega = &\frac{1}{he}[-p\cos f_1 \Delta V_{r_1} + (p + r_1)\sin f_1 \Delta V_{\theta_1}] - \frac{r_1 \sin\theta_1 \cos i}{h \sin i}\Delta V_{h_1} \\ &+\frac{1}{he}[-p\cos f_2 \Delta V_{r_2} + (p + r_2)\sin f_2 \Delta V_{\theta_2}] - \frac{r_2 \sin\theta_2 \cos i}{h \sin i}\Delta V_{h_2}\end{aligned} \tag{5.45}$$

The effect of out of plane impulse components on $\delta\omega$ has been computed earlier to be $-\cos i\delta\Omega$. Therefore, we can rewrite the above equation as follows:

$$\begin{aligned}\delta\omega + \cos i\delta\Omega = &\frac{1}{he}[-p\cos f_1 \Delta V_{r_1} + (p + r_1)\sin f_1 \Delta V_{\theta_1}] \\ &+\frac{1}{he}[-p\cos f_2 \Delta V_{r_2} + (p + r_2)\sin f_2 \Delta V_{\theta_2}]\end{aligned} \tag{5.46}$$

$$\begin{aligned}\delta M = \delta n_1(t_2 - t_1) + &\frac{\eta}{he}[(p\cos f_1 - 2r_1 e)\Delta V_{r_1} - (p + r_1)\sin f_1 \Delta V_{\theta_1}] \\ &+\frac{\eta}{he}[(p\cos f_2 - 2r_2 e)\Delta V_{r_2} - (p + r_2)\sin f_2 \Delta V_{\theta_2}]\end{aligned} \tag{5.47}$$

where $\delta n_1(t_2 - t_1)$ is the drift that occurs due to the change in the semi-major axis that is created by the first impulse. The times $t_1$ and $t_2$ are, respectively, the times of application of the first and second impulse. At the end of the second impulse, $\delta a$ will

be equal to zero and hence $\delta n$ will also be equal to zero. Once, $\delta n = 0$ is established $\delta M$ remains a constant. $\delta n_1$ can be related to the first impulse components as follows:

$$n = \sqrt{\frac{\mu}{a^3}} \tag{5.48}$$

$$\delta n_1 = -\frac{3n}{2a}\delta a_1 \tag{5.49}$$

where $\delta a_1$ is the semi-major axis difference that is created after the first impulse, which can be written as

$$\delta a_1 = \frac{2a^2}{h}(e \sin f_1 \Delta V_{r_1} + \frac{p}{r_1}\Delta V_{\theta_1}) \tag{5.50}$$

$$\Rightarrow \delta n_1 = -\frac{3n}{2a}[\frac{2a^2}{h}(e \sin f_1 \Delta V_{r_1} + \frac{p}{r_1}\Delta V_{\theta_1})] \tag{5.51}$$

The impulse application times $t_1$ and $t_2$, are separated by one half period. Hence $t_2 - t_1 = \frac{T_p}{2} = \frac{\pi}{n}$ where $n$ is the mean motion and $T_p$, the time period of the satellite's orbit. Therefore, the drift due to the change in semi-major axis resulting form the first impulse can be written as follows:

$$\delta n_1(t_2 - t_1) = -\frac{3n}{2a}[\frac{2a^2}{h}(e \sin f_1 \Delta V_{r_1} + \frac{p}{r_1}\Delta V_{\theta_1})]\frac{\pi}{n} \tag{5.52}$$

$$\delta n_1(t_2 - t_1) = -\frac{3\pi a}{h}(e \sin f_1 \Delta V_{r_1} + \frac{p}{r_1}\Delta V_{\theta_1}) \tag{5.53}$$

$$\begin{aligned}\delta M = &-\frac{3\pi a}{h}(e \sin f_1 \Delta V_{r_1} + \frac{p}{r_1}\Delta V_{\theta_1}) \\ &+\frac{\eta}{he}[(p \cos f_1 - 2r_1 e)\Delta V_{r_1} - (p + r_1)\sin f_1 \Delta V_{\theta_1}] \\ &+\frac{\eta}{he}[(p \cos f_2 - 2r_2 e)\Delta V_{r_2} - (p + r_2)\sin f_2 \Delta V_{\theta_2}]\end{aligned} \tag{5.54}$$

$$\delta M = [\frac{\eta}{he}(p\cos f_1 - 2r_1 e) - \frac{3\pi a}{h} e \sin f_1]\Delta V_{r_1} - [\frac{\eta}{he}(p + r_1)\sin f_1 + \frac{3\pi ap}{hr_1}]\Delta V_{\theta_1} + \frac{\eta}{he}[(p\cos f_2 - 2r_2 e)\Delta V_{r_2} - (p + r_2)\sin f_2 \Delta V_{\theta_2}] \quad (5.55)$$

The above equations can be encapsulated in the following form:

$$\delta \mathbf{e} = \mathbf{A}\boldsymbol{\Delta}\mathbf{V} \quad (5.56)$$

where $\delta \mathbf{e} = [\delta a \ \delta e \ \delta w + \cos i \delta\Omega \ \delta M]^T$ and $\boldsymbol{\Delta}\mathbf{V} = [\Delta V_{r_1} \ \Delta V_{t_1} \ \Delta V_{r_2} \Delta V_{t_2}]^T$ and the matrix $\mathbf{A}$ is given as follows:

$$\mathbf{A}(:, 1:2) = \begin{bmatrix} \frac{2a^2 e}{h}\sin f_1 & \frac{2a^2}{h}(1 + e\cos f_1) \\ \frac{p\sin f_1}{h} & \frac{p}{h}[\frac{2+e\cos f_1}{1+e\cos f_1}\cos f_1 + \frac{e}{1+e\cos f_1}] \\ \frac{-p\cos f_1}{he} & \frac{p}{he}[\frac{2+e\cos f_1}{1+e\cos f_1}\sin f_1] \\ \frac{\eta}{he}(p\cos f_1 - 2r_1 e) - \frac{3\pi a}{h} e\sin f_1 & -\frac{\eta}{he}(p + r_1)\sin f_1 - \frac{3\pi ap}{hr_1} \end{bmatrix} \quad (5.57)$$

$$\mathbf{A}(:,3:4) = \begin{bmatrix} \frac{2a^2e}{h}\sin f_2 & \frac{2a^2}{h}(1+e\cos f_2) \\ \frac{p\sin f_2}{h} & \frac{p}{h}[\frac{2+e\cos f_2}{1+e\cos f_2}\cos f_2 + \frac{e}{1+e\cos f_2}] \\ \frac{-p\cos f_2}{he} & \frac{p}{he}[\frac{2+e\cos f_2}{1+e\cos f_2}\sin f_2] \\ \frac{\eta}{he}(p\cos f_2 - 2r_2e) & -\frac{\eta}{he}(p+r_2)\sin f_2 \end{bmatrix} \tag{5.58}$$

The $\mathbf{\Delta V}$ vector can be obtained by inverting the $\mathbf{A}$ matrix.

$$\mathbf{\Delta V} = \mathbf{A}^{-1}\delta\mathbf{e} \tag{5.59}$$

The total impulse magnitude $\Delta V$ for the two impulses is

$$\Delta V = \sqrt{{\Delta V_{r_1}}^2 + {\Delta V_{t_1}}^2 + {\Delta V_{h_1}}^2} + \sqrt{{\Delta V_{r_2}}^2 + {\Delta V_{t_2}}^2 + {\Delta V_{h_2}}^2} \tag{5.60}$$

The two impulse scheme has been used to establish the elemental difference given by equations (5.10), (5.11), (5.13), (5.14), (5.15) and (5.1), for a projected circular orbit. Unlike the reconfiguration problem which involves a transfer from one orbit to another, herein, we try to establish a single projected orbit. The relative orbits thus established, with the two impulse scheme, are shown in figures (5.4) and (5.5), for the $\alpha_0 = 0^o$ and the $\alpha_0 = 90^o$ deputies, respectively. The chief and the deputy are initially coincident. Hence, the relative orbit starts from origin.

The location of the impulses can be calculated as follows:

$$\theta_c = atan2(\delta\Omega\sin i, \delta i) \tag{5.61}$$

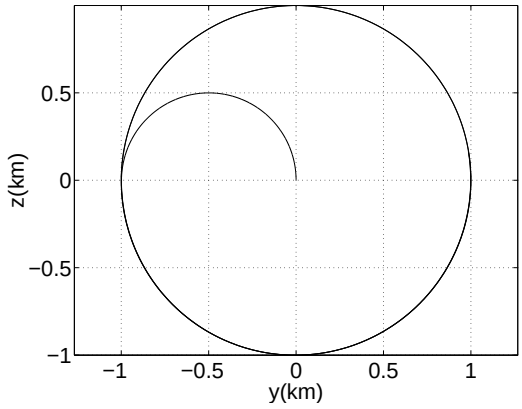


**Fig. 5.4:** Relative orbit established with the two impulse solution for the $\alpha_0 = 0^o$ deputy

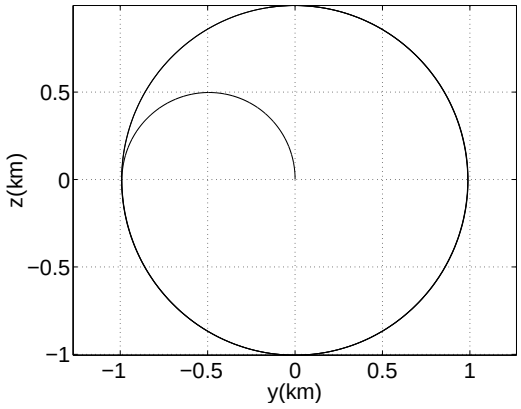


**Fig. 5.5:** Relative orbit established with the two impulse solution for the $\alpha_0 = 90^o$ deputy

Substituting $\delta\Omega$ and $\delta i$ from equations (5.13) and (5.14) we obtain the following:

$$\theta_c = atan2(\frac{\rho \sin\alpha_0}{a \sin i} \sin i, \frac{\rho \cos\alpha_0}{a}) = \alpha_0 \tag{5.62}$$

$$\Rightarrow f_c = \theta_c - \omega = \alpha_0 - \omega \tag{5.63}$$

$$\Rightarrow f_1 = \alpha_0 - \omega \tag{5.64}$$

and

$$f_2 = f_1 + \pi = \alpha_0 - \omega + \pi \tag{5.65}$$

## 5.5 Reconfiguration

In the previous section we have developed a two-impulse scheme for optimally establishing the projected circular relative orbit, for different deputies in a formation. In this section, we will study the reconfiguration problem, which involves resizing the

radius of the projected circular orbit from $\rho_i$ to $\rho_f$. The subscripts $i$ and $f$, stand for "initial" and "final" respectively. Let there be $k$ satellites, evenly distributed on the initial relative orbit, with phase angles starting at $0^o$ and differing by $\frac{2\pi}{k}$. Therefore, $\alpha_{0_i}$ takes the following values:

$$\alpha_{0_i} = 0^o, \frac{2\pi}{k}, 2\frac{2\pi}{k}, ...., (k-1)\frac{2\pi}{k} \tag{5.66}$$

$\alpha_{0_f}$ can also assume different values as follows:

$$\alpha_{0_f} = \phi, \phi + \frac{2\pi}{k}, \phi + 2\frac{2\pi}{k}, ...., \phi + (k-1)\frac{2\pi}{k} \tag{5.67}$$

where $\phi$ is an additional optimization parameter. $\phi$ indicates the angle by which the entire formation is to be rotated on the final relative orbit. The reconfiguration problem involves two optimization problems:(i) The problem of optimally transferring the satellite from a given location on the initial relative orbit to a given location on the final relative orbit and (ii) The problem of deciding for each satellite on the initial relative orbit, the optimal location on the final relative orbit. The first optimization problem can be solved by the two impulse analytical solution derived in the previous section. The desired elemental differences are given by equations (5.68) - (5.73). Therefore, the two impulse analytical solution discussed in the previous section can be used to establish them. The required elemental differences are:

$$\delta a = 0 \tag{5.68}$$

$$\delta e = -\frac{\rho_f}{2a_0}[\sin(\omega_0+\alpha_{0_f})-2e_0\sin(M_0+\omega_0+\alpha_{0_f})]+\frac{\rho_i}{2a_0}[\sin(\omega_0+\alpha_{0_i})-2e_0\sin(M_0+\omega_0+\alpha_{0_i})] \tag{5.69}$$

$$\delta i = \frac{\rho_f}{a_0}\cos\alpha_{0_f} - \frac{\rho_i}{a_0}\cos\alpha_{0_i} \tag{5.70}$$

$$\delta\Omega = \frac{\rho_f}{a_0}\frac{\sin\alpha_{0_f}}{\sin i_0} - \frac{\rho_i}{a_0}\frac{\sin\alpha_{0_i}}{\sin i_0} \tag{5.71}$$

$$\delta\omega = -\delta M - \delta\Omega\cos i_0 \tag{5.72}$$

$$\delta M = \frac{\rho_f}{2a_0e_0}\cos(\omega_0+\alpha_{0_f}) - \frac{\rho_i}{2a_0e_0}\cos(\omega_0+\alpha_{0_i}) \tag{5.73}$$

where $\alpha_{0_i}$ and $\alpha_{0_f}$ are the phase angles of the deputy on the initial and final relative orbits respectively.

Figures (5.6) and (5.7) show two examples of the reconfiguration problem, using the analytical two -impulse scheme.

The optimal solution to the reconfiguration problem also involves determining $\phi$ and pairing for each $\alpha_{0_i}$ given by Eqn.(5.66) on the initial relative orbit, to an $\alpha_{0_f}$ given by Eqn.(5.67) on the final relative orbit, such that the overall fuel consumption is minimized. Since there are $k$ satellites in the initial relative orbit, $k$ slots are required in the final relative orbit, for a unique pairing. There is an infinite number of families of evenly spaced slots, each characterized the parameter $\phi$, as per Eqn.(5.67). The overall fuel consumption is proportional to $\sum_{l=1}^{k}\Delta V_l$. The cost associated with each

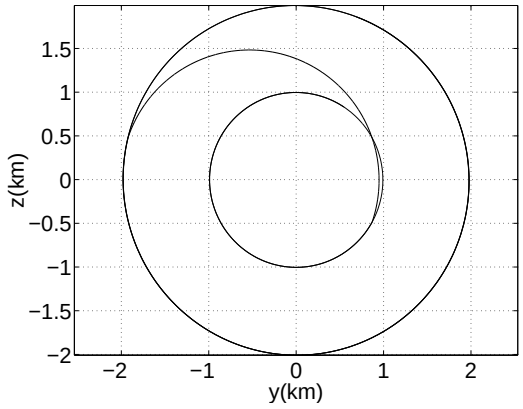


**Fig. 5.6:** Reconfiguring the $\alpha_{0_i} = 45^o$ deputy on the disc $\rho_i = 1$km to the $\alpha_{0_f} = 60^o$ location on the disc $\rho_f = 2$km with the two impulse analytical solution

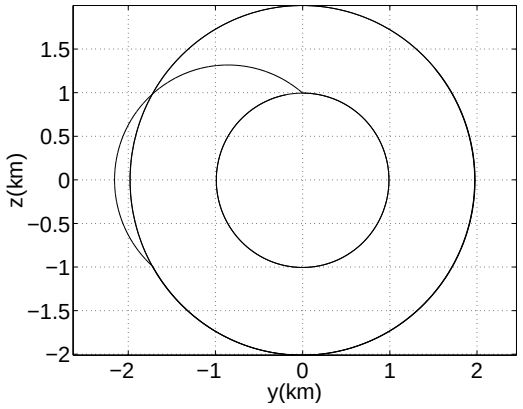


**Fig. 5.7:** Reconfiguring the $\alpha_{0_i} = 90^o$ deputy on the disc $\rho_i = 1$km to the $\alpha_{0_f} = 30^o$ location on the disc $\rho_f = 2$km with the two impulse analytical solution

pair can be computed apriori, using the two-impulse analytical scheme. Figure (5.8) shows the cost curves for a formation of six satellites.

It generates very useful insight into the solution of the pairing problem. The figure shows the cost plots for transferring from different values of $\alpha_{0_i}$ to different values of $\alpha_{0_f}$. The minima for each $\alpha_{0_i}$ curve occurs at a value of $\alpha_{0_f} = \alpha_{0_i}$. This clearly demonstrates that there is no conflict for slots, i.e., each satellite has a unique target slot of minimum fuel consumption. Pairing each individual satellite to its minimum fuel slot also minimizes the overall fuel consumption. Therefore, the optimal pairing assignment is $\alpha_{0_i} = \alpha_{0_f}$, which also implies that $\phi = 0$. Figure (5.8) also shows that the cost for each optimal pair is the same which results in a homogenous fuel consumption for the reconfiguration. These two inferences can also be derived ana-

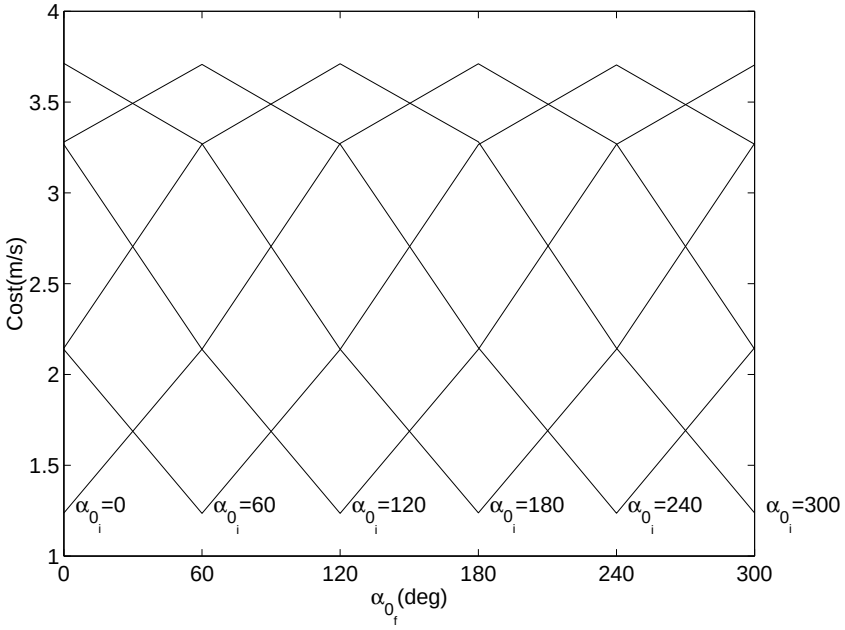


**Fig. 5.8:** Cost for different pairs of $\alpha_{0_i}$ and $\alpha_{0_f}$

lytically based on the out of plane cost computation as follows:

$$\Delta V_h = \frac{h}{r}\sqrt{\delta i^2 + \delta\Omega^2 \sin^2 i} \tag{5.74}$$

$$\delta i = \frac{\rho_f \cos\alpha_{0_f}}{a_0} - \frac{\rho_i \cos\alpha_{0_i}}{a_0} \tag{5.75}$$

$$\delta\Omega = \frac{\rho_f \sin\alpha_{0_f}}{a_0 \sin i} - \frac{\rho_i \sin\alpha_{0_i}}{a_0 \sin i} \tag{5.76}$$

Therefore,

$$\delta i^2 + \delta\Omega^2 \sin^2 i = \frac{{\rho_i}^2 + {\rho_f}^2 - 2\rho_i\rho_f \cos(\alpha_{0_i} - \alpha_{0_f})}{a_0^2} \tag{5.77}$$

Clearly, the above expression attains its minimum value at $\alpha_{0_i} = \alpha_{0_f}$. Also, the minimum value is given by

$$\Delta V_h = \frac{h|(\rho_f - \rho_i)|}{ra_0} \tag{5.78}$$

It should be noted that the above expression is free of $\alpha_{0_i}$ and $\alpha_{0_f}$. Hence different satellites with different values of $\alpha_{0_i}$, consume the same fuel to reach their optimal target slots, $\alpha_{0_f} = \alpha_{0_i}$. Hence the homogeneous fuel consumption for different satellites in the formation.

## 5.6 Extension to the $J_2$ problem

In the previous sections we have studied the two impulse analytical scheme for establishing formations in the absence of $J_2$. The scheme can be extended to establish formations in the presence of $J_2$ as well. However we first need to characterize the formations in terms of orbital elemental differences. In the presence of $J_2$, the standard orbital elements are no more constant. But a new set of orbital elements, called mean elements, can be defined using Brouwer's theory. The mean semi-major axis, mean eccentricity and mean inclination of each satellite are constant. The mean ascending node, mean argument of perigee and the "mean" mean anomaly vary linearly with time. Their rates are constant and functions of the mean semi-major axis, mean eccentricity and mean inclination only.

$$\dot{\Omega} = -1.5J_2(\frac{R_e}{p})^2 n \cos i \tag{5.79}$$

$$\dot{\omega} = 0.75J_2(\frac{R_e}{p})^2 n(5\cos^2 i - 1) \tag{5.80}$$

$$\dot{M} = n + 0.75J_2(\frac{R_e}{p})^2 n(3\cos^2 i - 1) \tag{5.81}$$

We characterize the formations in terms of the mean element differences. For the rest of the chapter all orbital elements will be assumed to be mean orbital elements. The mean elemental differences for all the elements, except the semi-major axis, are the same as those given by Eqns.(5.10) - (5.15). Matching the periods of the two satellites is crucial for bounded relative orbits in the absence of $J_2$. Hence, the semi-major axes difference is desired to be zero. However, this does not hold in the presence of $J_2$, as the inertial orbits are not periodic anymore. A rate-matching condition can be developed for the $J_2$ problem, which minimizes the secular growth in the along track direction. The rate matching condition is a condition for matching the mean angular velocities of the chief and the deputy. It can be written as follows:

$$\delta\dot{\omega} + \delta\dot{M} + \delta\dot{\Omega}\cos i = 0 \tag{5.82}$$

Substituting Eqns.(5.79) - (5.81) into Eqn.(5.82) we obtain the following:

$$\frac{\delta a}{a} = -\frac{J_2}{2}(\frac{R_e}{a})^2\frac{3\eta+4}{\eta^4}[(1-3\cos^2 i)\frac{e\delta e}{\eta^2} + \sin 2i\delta i] \tag{5.83}$$

Therefore, the difference in the mean semi-major axis depends on the difference in the mean inclination and mean eccentricity. The difference in mean eccentricity and inclination are chosen according to Eqn.(5.10) and Eqn.(5.13), respectively, by substituting the mean orbital elements on the right hand side of the equations.

Now, we need a scheme to establish these desired mean element differences. Gauss's equations have been derived for osculating elements. But Schaub and Alfriend[32] showed that the same equations can be used to approximately create mean element differences as well, by using mean elements on the right hand side of those equations. Therefore, we use the two-impulse analytical solution derived earlier with two modifi-

cations: (i) We use mean elements on the right hand side of the equations and (ii) We use the known mean drift rates of $\Omega$, $\omega$ and $M$, to predictively correct for them. The out of plane impulse components are computed according to Eqs.(5.40) and (5.41), by using the following correction for $\delta\Omega$:

$$\delta\Omega = \delta\Omega_{desired} - \Delta\dot{\Omega}\frac{T_p}{2} \tag{5.84}$$

where $\Delta\dot{\Omega} = \dot{\Omega}_{deputy} - \dot{\Omega}_{chief}$.

Similarly, the remaining four in-plane impulse components can be computed using Eqn.(5.59) with a corrected version of the $\delta\mathbf{e}$ obtained as follows:

$$\delta\mathbf{e} = [\delta a_{desired},\ \delta e_{desired},\ \delta w_{desired} + \cos i\delta\Omega - \Delta\dot{\omega}\frac{T_p}{2},\ \delta M_{desired} - \Delta\dot{M}_{J_2}\frac{T_p}{2}]^T \tag{5.85}$$

where

$$\Delta\dot{\omega} = \dot{\omega}_{deputy} - \dot{\omega}_{chief} \tag{5.86}$$

$$\dot{M}_{J_2} = 0.75J_2(\frac{R_e}{p})^2 n(3\cos^2 i - 1) \tag{5.87}$$

$$\Delta\dot{M}_{J_2} = \dot{M}_{J_2 deputy} - \dot{M}_{J_2 chief} \tag{5.88}$$

Figures (5.9) and (5.10) show two examples of the reconfiguration problem using the analytical two impulse scheme, in the presence of $J_2$.

## 5.7 Optimality of the Analytical Solution

Hitherto we studied the application of the analytical two impulse solution to establish and reconfigure formations. Though the out of plane cost was shown to be optimal, the optimality of the overall scheme has not been verified. In this section,

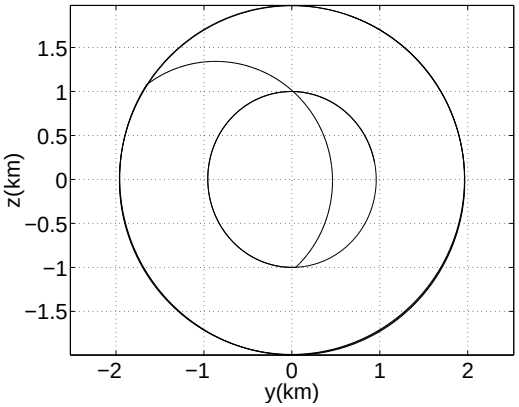


**Fig. 5.9:** Reconfiguring the $\alpha_{0_i} = 0^o$ deputy on the disc $\rho_i = 1km$ to the $\alpha_{0_f} = 60^o$ location on the disc $\rho_f = 2km$ with the two impulse analytical solution, in the presence of $J_2$

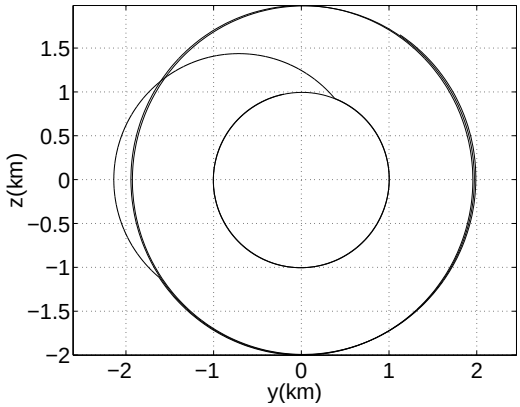


**Fig. 5.10:** Reconfiguring the $\alpha_{0_i} = 90^o$ deputy on the disc $\rho_i = 1km$ to the $\alpha_{0_f} = 45^o$ location on the disc $\rho_f = 2km$ with the two impulse analytical solution, in the presence of $J_2$

we compare the cost incurred with the analytical solution to the cost incurred by an optimized two-impulse solution. A two-impulse solution is obtained by minimizing the total $\Delta V$. The optimization parameters are the six impulse components and the two times of application. The constraints are set up to obtain the six desired orbital element differences. The optimization was performed with a numerical software called "NPOPT". Figures (5.11) and (5.12) compare the costs incurred with the analytical scheme and the optimized solution for the $\alpha_0 = 0^o$ satellite and the $\alpha_0 = 90^o$ satellite, respectively. The analytical solution is given as an initial guess to the optimizer. It could be seen from the Figures that optimal cost is close to that obtained using the analytical solution. The optimal cost is slightly higher, because the optimizer enforces the constraints to a higher accuracy. It should also be noted that the qual-

itative dependence of the cost on $\alpha_{0_f}$, remains the same, i.e., the minimum cost for the $\alpha_{0_i} = 0^o$ satellite is achieved at $\alpha_{0_f} = 0^o$ and similarly, for the $\alpha_{0_i} = 90^o$ satellite, it is at $\alpha_{0_f} = 90^o$. Therefore, irrespective of the choice of either of the two solutions the choice of the target $\alpha_0$ remains the same. It should also be noted that the times of the impulse application remained unchanged from their initial guesses. Therefore, the assumption of basing the impulse locations on the out-of-plane cost alone, seems to be justified. Also, the out-of-plane cost constitutes around 70% of the total cost using the analytical solution or the optimal solution.

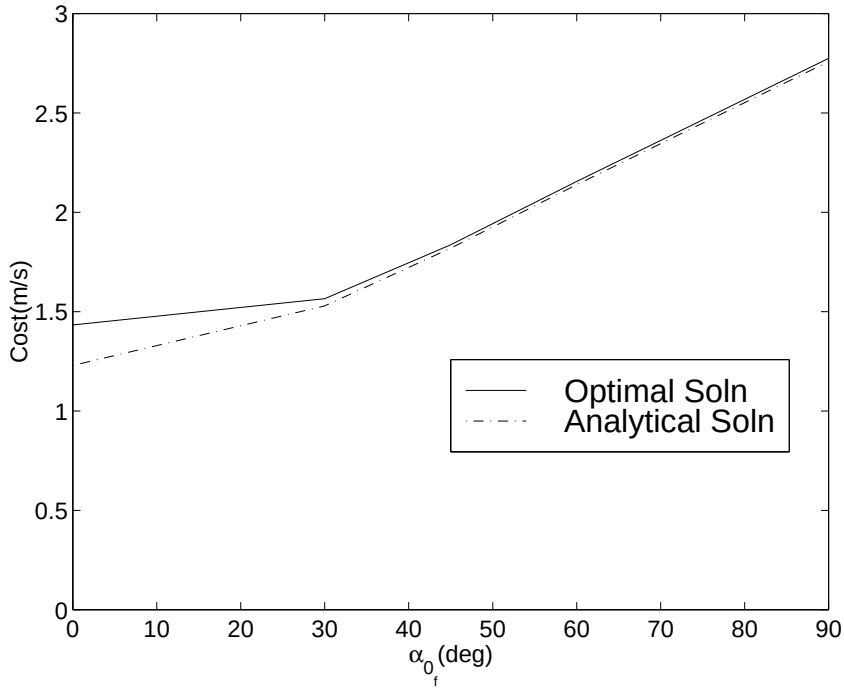


**Fig. 5.11:** Cost comparison of the analytical solution and the optimal solution for the $\alpha_0 = 0^o$ satellite

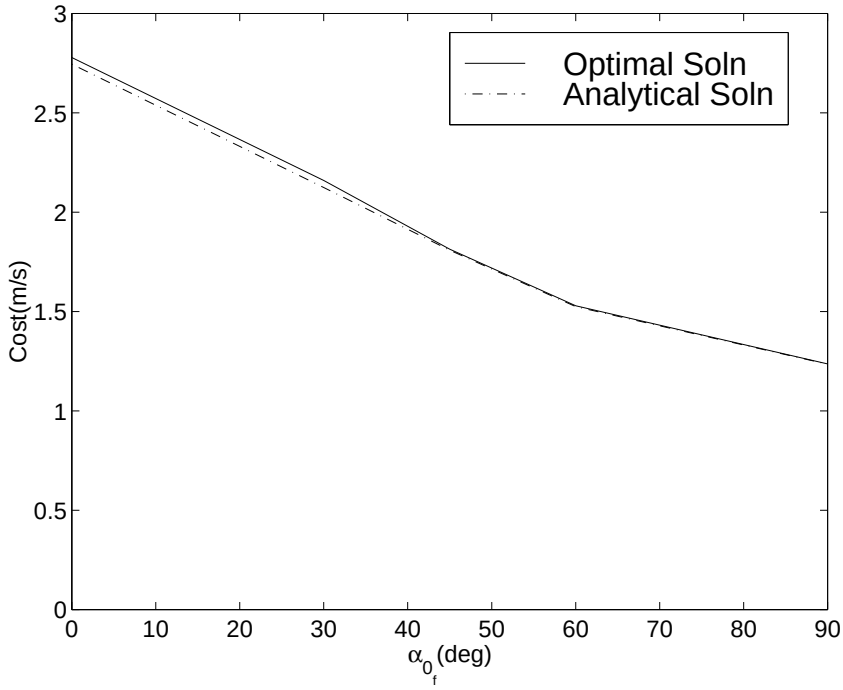


**Fig. 5.12:** Cost comparison of the analytical solution and the optimal solution for the $\alpha_0 = 90^o$ satellite

# CHAPTER VI

## SUMMARY

This dissertation dealt at length, various approaches to modelling relative orbits between two satellites, relevant to enabling formation establishment, maintenance, and reconfiguration. Differential equation models based on Newton's laws and geometric models based on orbital mechanics understanding, have been used extensively. HCW equations and solutions have received lot of attention in the literature for addressing formation flying problems. In this dissertation, more sophisticated models were developed and analyzed to obtain bounded relative orbit solutions that are more realistic then the HCW solutions. A perturbation method approach has been used to study the effect of quadratic nonlinearities on the breakdown of HCW solutions. The approach lead to a small correction in the initial conditions to prevent the breakdown of HCW solutions due to nonlinear effects. A geometric approach has been used to derive a similar correction to initial conditions, to counter the breakdown, resulting from the eccentricity of the chief orbit. The effect of the oblate Earth perturbation on the secular growth in the along-track direction and the out-of-plane direction has been modelled using mean elements. The analysis culminated in a methodology for obtaining initial conditions for relative motion, that lead to bounded relative orbits.

Formation maintenance problem has been addressed by developing different controllers that stabilize the formation in the presence of disturbances and initial condition errors. A cost comparison was made between a standard Lyapunov controller and a LQR controller. Results show that the LQR controller consumes lesser fuel in tracking the desired trajectories, than the Lyapunov controller, which explicitly

cancels the nonlinearities. It was analytically shown that the LQR controller has a region of attraction of 150km around the chief satellite. An innovative controller named period-matching controller has been developed in this dissertation. Unlike the Lyapunov and LQR controllers, which track a given reference trajectory, the period matching controller forces the relative motion dynamics to a certain desired manifolds. The controls required for maintaining the relative orbits on these manifolds is zero. Though the period-matching controller does not guarantee the tracking of a particular relative orbit, it guarantees zero steady controls. A hybrid approach of using the Lyapunov and period-matching controllers, has been proposed and implemented to obtain the desired trajectories at zero steady state cost. A disturbance accommodating controller has been proposed for preventing the controller from fighting short and long period oscillations resulting from different perturbations. The controller has been extensively tested on a sophisticated model, for satisfactory results.

An impulsive control scheme has been developed for establishing and reconfiguring formations. Geometric models map the LVLH cartesian coordinates to orbital element differences between the chief and the deputy satellite. This mapping has been used to characterize the desired formations in terms of orbital element differences. A sub-optimal control scheme has been proposed to establish the desired elemental differences. Gauss's equations have been used to design the necessary impulses. The control scheme has been compared to a control scheme obtained through numerical optimization. Results indicate that the structure of the optimal solution proposed remains the same for the numerically obtained solutions as well. Also, the cost incurred by the proposed control scheme is close to that incurred by the optimized solutions.

## REFERENCES

[1] Anthony, M. L. and Sasaki, F. T., "Rendezvous Problem for Nearly Circular Orbits," *AIAA Journal*, Vol. 3, No. 9, September 1965, pp. 1666–1673.

[2] London, H. S., "Second Approximation to the Solution of Rendezvous Equations," *AIAA Journal*, Vol. 1, No. 7, September 1965, pp. 1691–1693.

[3] Kechichian, J. A., "Motion in General Elliptical Orbit with Respect to a Dragging and Precessing Coordinate Frame," *Journal of Astronautical Sciences*, Vol. 46, No. 1, 1998, pp. 25–46.

[4] Prussing, J. E. and Conway, B. A., *Orbital Mechanics*. Oxford University Press, New York, 1996.

[5] deVries, J. P., "Elliptic Elements in Terms of Small Increments of Position and Velocity Components," *AIAA Journal*, Vol. 1, No. 11, September 1965, pp. 2626–2629.

[6] Broucke, R. A., "A Solution to the Elliptic Rendezvous Problem with Time as the Independent Variable," *Proceedings of the AAS/AIAA Space Flight Mechanics Meeting*, San Antonio, TX, January 2002.

[7] Yamanaka, K. and Ankersen, F., "New State Transition Matrix for Relative Motion on an Arbitrary Elliptical Orbit," *AIAA, Journal of Guidance, Control and Dynamics*, Vol. 25, No. 1, January-February 2002, pp. 60–67.

[8] Carter, T. E., "State Transition Matrices for Terminal Rendezvous Studies : Brief Survey and New Example," *AIAA, Journal of Guidance, Control and Dynamics*, Vol. 21, No. 1, January-February 1998, pp. 1468–155.

[9] Tschauner, J. and Hempel, P., "Rendezvous zu einem in elliptischer Bahn umlaufenden Ziel," *Astronautica Acta*, Vol. 11, 1965.

[10] Carter, T. E. and Humi, M., "Fuel-Optimal Rendezvous Near a Point in General Keplerian Orbit," *AIAA, Journal of Guidance, Control and Dynamics*, Vol. 10, No. 6, November-December 1997.

[11] Inalhan, G., Tillerson, M., and How, J. P., "Relative Dynamics and Control of Spacecraft Formations in Eccentric Orbits," *AIAA, Journal of Guidance, Control and Dynamics*, Vol. 25, No. 1, January 2002, pp. 48–59.

[12] Melton, R. G., "Time Explicit Representation of Relative Motion Between Elliptical Orbits," *AIAA, Journal of Guidance, Control and Dynamics*, Vol. 23, No. 4, July-August 2000, pp. 604–610.

[13] Knollman, G. C. and Pyron, B. O., "Relative Trajectories of Objects Ejected from a Near Satellite," *AIAA Journal*, Vol. 1, No. 2, September 1965, pp. 1666–1673.

[14] Karlgaard, C. D. and Lutze, F. H., "Second-Order Relative Motion Equations," *Proceedings of the 2001 Astrodynamics Specialist Conference*, Quebec City, Canada, July-Aug 2001.

[15] Schweighart, S. A. and Sedwick, R. J., "High Fidelity Linearized Model for Satellite Formation Flight," *AIAA, Journal of Guidance, Control and Dynamics*, Vol. 25, No. 6, November-December 2002.

[16] Vadali, S. R., Alfriend, K. T., and Vaddi, S., "Hill's Equations, Mean Orbital Elements and Formation Flying of Satellites," *The Richard H. Battin Astrodynamics Symposium*, College Station, TX, AAS 00-258, March 2000.

[17] Brouwer, D., "Solution of the Problem of Arificial Satellite Theory Without Drag," *The Astronomical Journal*, No. 1274, 1959, pp. 378–397.

[18] Schaub, H. and Alfriend, K. T., "J2 Invariant Relative Orbits for Formation Flying," *International Journal of Celestial Mechanics and Dynamical Astronomy*, Vol. 79, 2001, pp. 77–95.

[19] Alfriend, K. T., Schaub, H., and Gim, D. W., "Gravitational Perturbations, Nonlinearity and Circular Orbit Assumption Effects on Formation Flying Control Strategies," *Proceedings of the* $23^{rd}$ *Annual AAS Guidance and Control Conference*, Breckenridge, CO, AAS 00-012, February 2000.

[20] Gim, D. W. and Alfriend, K. T., "The State Transition Matrix of Relative Motion for the Perturbed Non-Circular Reference Orbit," *Proceedings of the AAS/AIAA Space Flight Mechanics Meeting*, Santa Barbara, CA, AAS 01-222, February 2001.

[21] Alfriend, K. T., Gim, D. W., and Vadali, S. R., "The Characterization of Formation Flying Satellite Relative Motion Orbits," *Proceedings of the AAS/AIAA Space Flight Mechanics Meeting*, San Antonio, TX, AAS 02-143, January 2002.

[22] Vadali, S. R., "An Analytical Solution for Relative Motion of Satellites," *The DCSSS Conference*, Cranfield, UK, July 2002.

[23] Schaub, H. and Alfriend, K. T., "Hybrid Cartesian and Orbit Element Feedback Law for Formation Flying Spacecraft," *AIAA, Journal of Guidance, Control and Dynamics*, Vol. 25, No.2, March-April 2002.

[24] Yedavalli, R. K. and Sparks, A., "Spacecraft Formation Flying Maneuvers Using Linear Quadratic Regulation with No Radial Axis Inputs," *Proceedings of the*

*2001 AIAA Guidance, Navigation and Control Conference and Exhibit*, Montreal, Canada, August 2001.

[25] Starin, S. R., Yedavalli, R. K., and Sparks, A. G., "Spacecraft Formation Flying Maneuvers Using Linear Quadratic Regulation with No Radial Axis Inputs," *Proceedings of the 2001 AIAA Guidance, Navigation and Control Conference and Exhibit*, Montreal, Canada, August 2001.

[26] Mitchell, J. W. and Richardson, D. L., "Maintaining Periodic Trajectories with the First-Order Nonlinear Hill's Equations," *Proceedings of the 2001 Astrodynamics Specialist Conference*, Quebec City, Canada, July-August 2001.

[27] Queiroz, M. S.d., Kapila, V., and Yan, Q., "Adaptive Nonlinear Control of Multiple Spacecraft Formation Flying," *AIAA, Journal of Guidance, Control and Dynamics*, Vol. 23, No.3, May-June 2000.

[28] Naasz, B. J., Karlgaard, C. D., and Hall, C. D., "Application of Several Control Techniques for the Ionospheric Observation Nanosatellite Formation," *Proceedings of the 2002 AAS/AIAA Space Flight Mechanics Meeting*, San Antonio, TX, January 2002.

[29] Middour, J. W., "Along Track Formation Keeping for Satellites with Low Eccentricity," *Journal of Astronautical Sciences*, Vol. 41, No. 1, January-March 1993.

[30] Zhang, F. and Krishnaprasad, P. S., "Formation Dynamics Under a Class of Control Laws," *Proceedings of the American Control Conference*, No. ACC02-AIAA1052, Anchorage, AK, July-August 2002.

[31] Vadali, S. R. and Vaddi, S. S., "Large-Angle Kinematics for the Control of

Satellite Relative Motion," *AIAA Guigance, Navigation and Control Conference*, Monterey, CA, AAS 00-258, August 2002.

[32] Schaub, H. and Alfriend, K. T., "Impulsive Feedback Control to Establish Specific Mean Orbit Elements of Spacecraft Formations," *AIAA, Journal of Guidance, Control and Dynamics*, Vol. 24, No. 4, July-August 2001.

[33] Vadali, S. R., Schaub, H., and Alfriend, K. T., "Initial Conditions and Fuel Optimal Control for Formation Flying of Satellites," *Proceedings of the 1999 AIAA GNC Conference*, Portland, OR, July-August 1999.

[34] Ahn, Y. T. and Spencer, D. B., "Optimal Reconfiguration of a Formation Flying Satellite Constellation," *Proceedings of the 53 International Astronautical Congress. The World Space Congress - 2002*, October 2002.

[35] Tillerson, M., Inalhan, G., and How, J. P., "Co-ordination and Control of Distributed Spacecraft Systems Using Convex Optimization Techniques," *International Journal of Robust and Nonlinear Control*, Vol. 12, 2002.

[36] Ioannou, P. A. and Sun, J., *Robust Adaptive Control*. PTR Prentice Hall, Upper Saddle River, NJ, 1996.

[37] Vadali, S. R., Vaddi, S. S., and Alfriend, K. T., "An Intelligent Control Concept for Formation Flying Satellites," *International Journal of Robust and Nonlinear Control*, No. 12, 2002, pp. 97–115.

# VITA

Veera Venkata Sesha Sai Vaddi was born in Andhra Pradesh, India on August 20, 1974. He received his baccalaureate degree in mechanical engineering from Regional Engineering College, Calicut, India in August 1996. He received his master's degree from the Indian Institute of Science, Bangalore, India also in mechanical engineering in August, 1999. In the same month, he joined the aerospace engineering department of Texas A&M University for his graduate studies. While at Texas A&M University, he worked with Dr. Srinivas R. Vadali and Dr. Kyle T. Alfriend. His doctoral work focussed on formation flying spacecraft.

He can be reached at 309 Ball Street, 2006, College Station, TX-77840 or by contacting Dr. Srinivas R. Vadali, Department of Aerospace Engineering, Texas A&M University, College Station, TX-77843.

This document was typed by Veera Venkata Sesha Sai Vaddi.